Feasibility of microfluidic routes to monitor protein stability as a tool for bioprocessing

A thesis submitted to University College London

for the degree of

Doctor of Philosophy

by

Nina Remtulla

September 2009

The Advanced Centre for Biochemical Engineering

Department of Biochemical Engineering

University College London

Torrington Place

London WC1E 7JE

Abstract

During the bioprocessing of therapeutics, proteins may become damaged leading to modifications and changes in stability. This may, as a consequence, cause serious and potentially fatal side effects when administered to patients making damage assessment crucial. High throughput determination of protein stability has become an important factor in many different areas such as protein engineering, formulation and manufacturing. Microfluidics, defined as micro-scale fluid flow systems, can be used to create high throughput methods to monitor these effects, while reducing reagent consumption without compromising sensitivity. Protein denaturation can be measured in many ways however, fluorescence spectroscopy is thought to be the most adaptable to use with microfluidics. In this thesis the feasibility of using microfluidics to detect protein denaturation using this fluorescence method of analysis adapted from a microplate format assay is examined. Protein unfolding transitions were monitored by detecting tryptophan fluorescence at 340nm upon excitation at 266nm. A laser-excited detection system was optimised to detect minimum concentrations of protein, in both the native and denatured states. The range and limitations of this system were assessed and compared to that of the established microplate reader method. The minimum protein concentration detectable in microfluidics was higher than that of the microplate reader, with a reduction in volume leading to a reduction in reagent consumption (10^5 molecules) while increasing throughput by 50%. Three representative proteins were assessed in an array of process relevant conditions. The 3D protein response surfaces obtained were characterized by global fitting to provide parameters for assessment of protein stability and assist in the determination of processing conditions.

Acknowledgements

I would first and foremost like to thank my supervisors Dr Daniel G. Bracewell and Professor Quentin A. Pankhurst for their support, guidance and knowledge in the project. I would like to thank the BBSRC for funding this project.

I would like to extend my thanks to the people who worked on the BRIC project. Dr Matthieu Gaudet for his help and wisdom in the microfluidic section of this thesis. I would also like to thank the supervisors on this project Dr Paul. A. Dalby and Professor Gabriel Aeppli for their insight and continual input. Working together has made this project possible.

I thank Simon Edwards-Parton for his help on the computation side of this project and his broad knowledge in Biochemical Engineering. I would like to acknowledge all my colleagues in the Biochemical Engineering department at UCL and LCN for their help when I came to them with no knowledge about a great number of techniques.

I would like to thank my mother, Shainul, my father, Gulam and sister, Salimah, for supporting me in my times of need and anger. I would also like to thank William Nicklin for putting up with me while I was going through this difficult process and for not giving up on me.

'I, Nina Remtulla, confirm that the work presented in this thesis is my own. Where information has been derived from other sources, I confirm that this has been indicated in the thesis.'

Table of Contents

List of Figures

List of Tables

Chapter 1:

Introduction

1.1. Development of biopharmaceuticals

In recent years, the growth of the biopharmaceutical industry has gained momentum due multiple advances in technology, leading to a 25% share of the total pharmaceutical industry (Lawrence and Lahteenmaki 2008). Drug discovery and development are expensive, with only a small number of compounds approved for market. This highlights a growing need for a reduction in costs and production time. One way in which this can be done is by a drastic improvement of process design in the manufacturing of these biopharmaceuticals. There is a heavy investment needed in pre clinical development, clinical trials and safety monitoring to start the procedure of bringing a drug to market. New chemical entities (NCEs) often fail half way through this process incurring large costs with no return revenue. Cost and time to market of an NCE is thought to have risen to $802 million in 2001 over a period of 8-12 years (DiMasi, Hansen et al. 2003). Patent lifetimes on a product mean the speed of development is critical to take full advantage of this lifetime and hence maximise profit to counteract the large investment.

One way costs can be reduced is by increasing throughput and decreasing reagent use, however quality and stability of the product produced should not be compromised. For this reason, monitoring product condition throughout the development and maintenance of a process is very important (DiMasi, Hansen et al. 2003). If quality is compromised and the product is deemed unfit for market in the early stages of process design, investment into development can be halted. This assessment of a product's manufacturability determines a faster rate of failure reducing failure costs. During the preliminary stages of process and product design protein quantities are limited, hence stability testing must assessed with a minimal protein consumption assay with a high degree of accuracy.

1.1.1. Protein stability and bioprocessing

The term bioprocessing is a broad term that includes not only production but also preformulation and formulation of pharmaceuticals. Formulation entails the use of various chemicals to create a product that is both stable and efficacious for a patient after storage, shipping and administration. This stability can be an important indicator to the protein condition when prepared with various chemical formulations. Optimisation of formulation can be monitored by assessing protein stability as a measure of protein condition. In production and formulation there are many areas for improvement, making optimisation of these areas, one of the largest challenges for successful commercialisation (Patro, Freund et al. 2002).

During production, a biopharmaceutical can encounter many different conditions (such as temperature or pH changes), which may be detrimental to the quality of the product. It is important to know the impact of these factors on the protein condition, by assessing damage at each stage of a process. In process development, understanding protein stability is a crucial part of any process design. This is also the case for formulation and preformulation whereby characteristics and properties of a pharmaceutical must be known before, after and during each stage. During preformulation, the characterisation of a drug's specific physical, chemical and mechanical properties can be used to choose which additives should be used when a preparation is formed. Understanding the behaviour of a given protein under a variety of stress conditions such as pH, concentration and temperature variations allows the identification and hence reduction of mechanisms of degradation. Conditions must be developed to ensure product stability in the final preparation. This avoids product inactivity and hence invalidation of clinical trials due to unknown active dosage. It is important to assess the condition of a pharmaceutical quickly and often throughout the development and running of a process.

This assessment method should be low cost using simple inexpensive equipment with minimal product consumption.

1.2. Protein properties

In it's simplest form a protein can be described as a molecule made up of a chain of linked amino acids. These amino acids are ordered in a specific way coded by a gene's DNA sequence. Each protein has it's own unique function that is determined by structure and has many roles such as transport, storage and regulation (Lesk 2004).

1.2.1. Protein structure

The pharmaceutical industry has over the past decade become a primary user and contributor to protein structure databases, as understanding key features in a protein structure is imperative when looking at protein stability. Knowledge of protein stability allows optimisation of protein condition and production in processing and formulation (Branden 1999). Proteins make up a class of bio macromolecules, which also include lipids, polysaccharides and nucleic acids. These macromolecules form the main constituents of biological organisms (Hames and Hooper 2000) making them vital for survival. Proteins perform a large range of functions such as structural (scaffolding in cell membranes), mechanical, storage or transport roles (of various ligands). Proteins known as enzymes can also play a major role in the catalysis of chemical reactions. To carry out their functions each protein has a specific structure, composed of four aspects of protein configuration known as primary, secondary, tertiary and quaternary structures (Figure 1.1) A loss in any of these structures is known as denaturation. In nature it has been found that proteins can evolve under selective pressure to perform specific functions by structural alterations. (Branden 1999). Functional properties are seen to

depend on the structure of a protein. For this reason protein structural investigations can increase knowledge of functionality and stability of a protein. Protein structures are formed by linear polypeptide amino acids chain arranged folded to generate compact domains with specific 3D structures. These structures cannot be determined by polypeptide chains sequence due to complicity of folding involving many different interactions, which cannot be reliably predicted. For this reason 3D structures are determined by various experimental methods such as X-ray crystallography, electron crystallography and nuclear magnetic resonance (NMR).

1.2.2. Primary structure

Primary structure is made up of a chain of amino acids, joined end to end in protein synthesis by peptide bonds, forming specific amino acid sequences that are the basis of protein structure. This sequence is made up of a combination of 20 types of amino acids each with differing side chains conferring various properties. The sequence and properties of these amino acid side chains determine the uniqueness of a particular protein. This includes biological function and specific three-dimensional structure (Fersht. 1999), determined by genetic code. The propensity of a protein to denature or aggregate is determined by the primary structure. Any alterations or mutations to this sequence can increase or decrease the stability of a protein when influenced by environmental factors (Wang 2005).

1.2.3. Secondary structure

This is defined as the characteristic 3D structure formed by the arrangement of one or more primary chains of amino acids in space in relation to other amino acids (Schulz 1996). Hydrogen bonding forms highly patterned sub structures such as α helices, β-

sheets and random coils to create a thermodynamically stable configuration. This secondary structure can be further arranged into supersecondary structures or motifs.

1.2.4. Tertiary structure

The tertiary structure of a protein molecule is the arrangement of all its amino acids in space, independent of its relationship with neighbouring molecules or subunits. The main driving force for the folding of proteins appears to be the burying and clustering of hydrophobic side chains to minimise contact with water. This characteristic can be exploited for determination of stability.

1.2.5. Quaternary structure

The quaternary structure of protein molecules is the arrangement of its subunits in space and the collection of the intersubunit interactions known as non-covalent associations, which are independent of the internal geometry of the subunits. The structure of each subunit is still referred to as its tertiary structure (Schulz 1996).

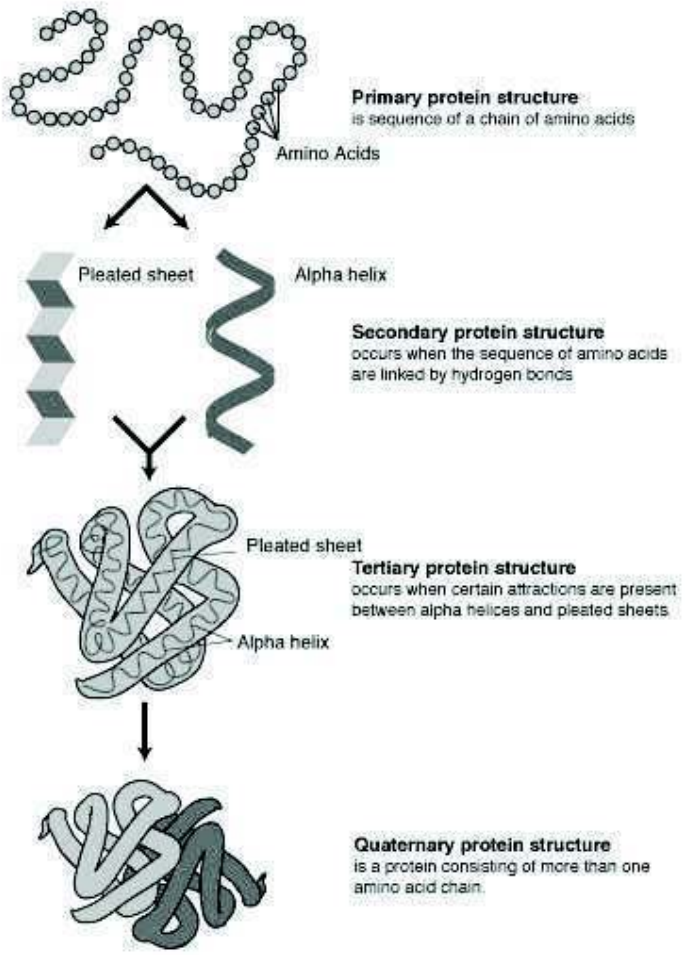

Figure 1.1. Diagrammatic representation of primary, secondary, tertiary and quaternary structure

This diagram shows a summary of the layers of structure present in a protein, from the polypeptide chain to the folded protein. These various layers of structure allow a protein to be carry out a function with a high degree of specificity (Adapted from National Human Genome Research Institute NHGRI)

1.2.6. Protein folding

Many interactions affect protein folding, resulting in a change in protein stability. These include backbone hydrogen bonds, Van der Waals interactions, hydrophobic forces,

conformation entropy and polar side chains. Hydrogen bonds allow polar backbone groups to be buried within the core of a protein while Van der Waals interactions are dispersion forces that favour packing. Hydrophobic forces allow the formation of a hydrophobic protein core by using the repulsion of the non-polar amino acid side chains to water. This in turn energetically favours burying of the side chains into the core of the protein away from the contact of water. Conformational entropy is an opposing force to folding as it allows the flexible polypeptides to be held in a fixed place upon folding. Polar side chains allow hydrogen bonds and electrostatic bond formation at the protein surface and are a key factor in function through the active site structure, which is crucial in enzyme catalysis. These interactions form the main structural components allowing function with a high degree of specificity. This indicates the importance of monitor changes in protein structure when looking at function. Changes in structure can be measured and quantified to reveal changes in energy between native and denatured protein types (Figure 1.2).

1.2.7. Protein function and activity

The biological function of proteins is dependant on the folded state and the stability of the protein involved. A small change in protein structure can have a large consequence on the function and toxicity (Gruebele 2002). This is seen in disease conditions whereby the cause is the stability of protein variants (Dobson 1999) such as Alzheimer's disease, Parkinson's disease and CJD among many others.

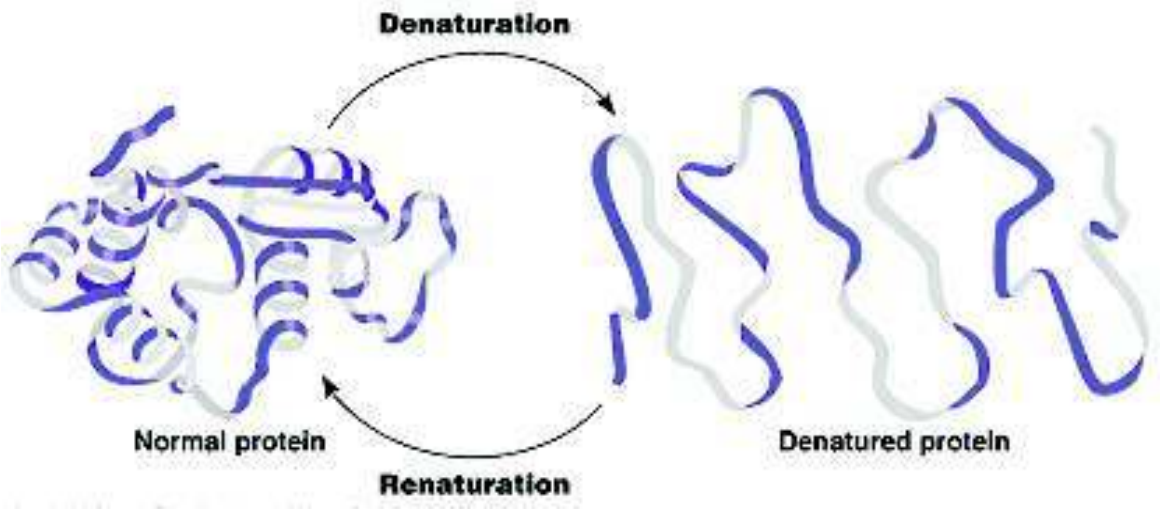

Figure 1.2. Schematic showing a protein in both the native and denatured states

This diagram shows the process of denaturation showing a loss in structure of the protein. This may or may not be reversible reforming the polypeptide chain to their original structure. (Adapted from Pearson Education Inc. publishing as Benjamin Cummings).

The extent to which a protein is denatured can be measured by a loss or reduction of biological activity or function. There are many assays for protein function such as enzymatic assays (in the case of enzymes) and activity and binding assays (in the case of antibodies). These assays determine reaction specifics and functional parameters related to the protein. Denaturation can affect many reaction criteria such as rate of reaction, affinity for substrate, pH optimum, temperature optimum and specificity of reaction. This may not always be the case however as a small alteration in structure may not be translated to large effect on biological activity. For this reason functional assays may not by the optimum assessment of structural changes.

Spectroscopic methods such as absorbance, fluorescence and calorimetry are available to monitor the denaturation of protein as well as track the folding and unfolding

equilibriums. Applications of fluorescence are growing rapidly indicating it to be a major research tool in basic as well as applied research and highly applicable to scale down.

1.3. Mechanisms and consequences of protein damage

The extent to which a protein's denaturation can be determined is dependant on the observation method. Denaturation can be observed by a number of methods for example loss of solubility, increased proteolysis, loss of biological activity and spectroscopic methods. To obtain a detailed analysis of structural changes in a protein it might be beneficial to use several of these methods. A single analysis method can be used to indicate a change in structure as a precursor to further analysis. Proteins can be denatured in many ways including proteolysis, use of a denaturant or alteration of pH. Various methods of denaturation can be tested to gather information about the stability of a protein. By looking at the condition in which a protein is most stable the optimum operating conditions for use during bioprocessing can be determined.

Native proteins are highly resistance to denaturation. Conditions that alter protein structure can mean that denaturation is more likely to occur indicating of protein damage. In this way estimation of protein denaturation pathways can be determined by the exposure of various portions of the protein to varyingly intensive treatments together with a knowledge of tertiary structure (Tanford 1968) or by protein engineering.

During manufacturing, there are many processes in which a protein can experience many potentially hazardous conditions such as freeze thaw during formulation (Patro, Freund et al. 2002), centrifugation, adsorption and desorption processes, fermentation

and filtration. These processes can have a detrimental effect on protein structure triggering aggregation or loss of solubility as a consequence.

1.3.1. Aggregation

Aggregation is a significant problem in bioprocessing occurring under various different conditions and at several stages in a process, for example during fermentation (Finke, Roy et al. 2000), refolding (Nguyen and Hall 2002), shearing or shaking (Katakam, Bell et al. 1995), freeze thawing (Kreilgaard, Frokjaer et al. 1998), drying or storage. It occurs by protein contact or formation of a new covalent bond (Wang 2005) causing the direct crosslinking of proteins or alteration of the aggregation tendency of the original protein. Aggregates can be soluble or insoluble depending on conditions, protein involved and protein damage. Damaging a protein exposes patches of contiguous hydrophobic groups initiating the aggregation process. When chemically denatured the protein is more likely to aggregate, due to the local molecular flexibility of the protein's amino acids. For this reason rates of reaction and kinetics may appear higher in denatured states. Native states of a protein may be less susceptible to damage or chemically degradation than a denatured form of a protein (Wang 2005).

Physical protein aggregates may be resolubilised by adjustments in environmental properties such as pH, temperature and addition of chemical denaturant however this relies on the reversibility of the aggregation process. In a process it is thought if protein damage has occurred to the extent of aggregation, the product is no longer viable due to the possibility of increased toxicity (Rosenberg 2006; Carpenter, Randolph et al. 2009). Early detection of protein damage and stability can allow optimisation of process design reducing extensive protein damage and hence aggregation.

1.3.2. Loss of solubility

Loss of solubility is not a true indication of protein denaturation and is considered a consequence of denaturation rather than a measure. Loss of solubility does not show the full extent of protein denaturation as partial protein denaturation can occur before the protein become insoluble. Resistance to loss of solubility varies greatly from protein to protein and is dependant on the denaturing procedure. For this reason solubility is considered an indication of denaturation and not a measure of denaturation.

1.3.3. Protein stability

The past two decades has seen an explosive growth in the biopharmaceutical industry. With this growth there becomes a need to increase the sensitivity and throughput of techniques involved including the characterisation of protein stability throughout a process. There are many pathways in almost all phases of protein drug development that physical and chemical denaturation can occur to a protein, potentially leading to aggregation (Biddlecombe, Craig et al. 2007). Successful control of both the physical and chemical stability of a protein in bioprocessing is needed to deliver and manufacture a protein product that is stable enough to meet the stringent requirements stipulated by regulatory agencies. Understanding the structure of a protein is fundamental to understand how a process can affect stability.

Protein stability can broadly be defined as the propensity of the protein to unfold and alter its conformation. As protein aggregation and solubility are not a true indication of protein denaturation it is thought that the direct assessment of protein stability may give a greater idea of protein condition. The assessment of protein stability is essential for distinguishing and monitoring protein function. The direct determination of protein stability has many applications and can be used to assess the condition of a protein in

protein engineering, proteomics, bioprocessing and formulation (Aucamp, Cosme et al. 2005). Each of these applications requires different variety of parameters to assess stability depending on the output needed, including unfolding transition midpoint or free energy of unfolding. All these applications do however need a high throughput assay to determine the stability of a protein. Examples of difficulties in protein engineering and formulation are described. In protein engineering, one library can contain thousands of mutants, each to be screened for efficacy and stability, which can be time consuming and labour intensive. There are many therapeutic proteins requiring optimal formulation, to improve their shelf life during storage and drug delivery to decrease degradation and hence toxicity. Optimum excipient combinations can be tested using small amounts of protein in multiple conditions at high throughput.

High throughput analysis of protein stability has often been carried out by looking at aggregation (Won. C.M. 1998) or activity assays (Giver, Gershenson et al. 1998) however both of these methods require the inactivation of the protein for assay. This can be misleading as proteins can renature if conditions are altered. Large structural change may not always lead to a large change in the activity or toxicity of the protein creating an inaccurate assessment of protein stability. Directly looking at stability of a protein by investigating structural changes allows more accurate assessment of damage. High throughput methods include DSC which can promote a sample rate of 50 samples per day (Weber and Salemme 2003) or H/D exchange and MALDI MS exchange(Ghaemmaghami, Fitzgerald et al. 2000) which produce a sample rate of 1000 samples per day. However it is thought that the throughput of protein analysis can be greatly increased with a reduction in protein sampling (Aucamp, Cosme et al. 2005). Protein stability has also been assessed using spectrophotometry, which will be discussed later in the chapter.

1.4. Methods of protein denaturation

Protein denaturation can be defined as a non-covalent change in protein structure (Navon, Ittah et al. 2001). This can be caused through alterations in primary, secondary, tertiary or quaternary structure. Monitoring these alterations is very important, as a small degree of denaturation may have a dramatic effect on protein function or visa versa.

Protein denaturation can occur by various methods such as thermal, pH or chemical denaturation, changes in dielectric constant, denaturation at interfaces and ionic strength. These each have a different effect on the protein as discussed below.

1.4.1. Thermal denaturation

During bioprocessing, proteins can experience a wide fluctuation in temperature. The optimum temperature for each stage of the process may vary, as may the stability of the protein itself. Two examples of this are viral inactivation and sample storage. During viral inactivation in protein purification, a heat treatment of 60 degrees centigrade is needed to inactivate viral proteins. The storage of a protein after processing can involve the reduction of the temperature to –20 degrees centigrade. There are many factors or conditions that may destabilise the folded state, stabilise the unfolded states or favour formation of intermediates. Temperature is the most prevalent of these (Wang 2005). Proteins unfold at various temperatures depending on primary sequence and stability. Upon heating secondary sequence of a protein may change, altering denaturation and aggregation behaviour. Initially during mild heating, there can be a weakening of the bonds involved in the tertiary structure, known to play a part in long-range interactions allowing the protein to take on a flexible structure that is easily reversible. When heating is continued, the helical structure is weakened causing the interaction of solvent

with the destabilized hydrogen bonds. This in turn weakens the structure further, leading to exposure of hydrophobic groups to the solvent. This is highly unfavourable for the protein, resulting in these residues being buried in the core of protein hence exposing polar groups to the solvent. During this process, the protein will take on a new structure, different from that of the native protein. Aggregation may occur due to bonds formation between denatured protein molecules reducing solvent exposure. Refolding to the native structure is unfavourable upon cooling as newly formed bonds must be broken, which is kinetically unlikely due to a potential large energy barrier. Although a change in temperature maybe unfavourable during a process, temperature may be used to assess the stability of a protein. By increasing the temperature of the protein environment, a profile of denaturation can be determined for specific proteins and conditions allowing direct comparison for process optimisation.

1.4.2 Chemical denaturation

Two routinely used strong chemical denaturants are urea and guanidine hydrochloride (GdHCl). Urea and GdHCl act as chaotropes in low concentrations by disrupting covalent bonds involved in water interaction with the protein to allow solubilisation of even hydrophobic proteins. They can be used as protein denaturants altering the 3D structure of the protein sometimes irreversibly upon interaction, causing loss of function. Chemical denaturants can also be used to solubilise inclusion bodies, allowing refolding of denatured proteins (Wingfield, Palmer et al. 2001; Mannall, Myers et al. 2008). High concentrations (6 to 8M) of these chemical denaturants break hydrogen bonds, which hold the protein in its unique structure, leading to the denaturation. They may also disrupt hydrophobic interactions by promoting the solubility of hydrophobic residues in aqueous solutions (Dittrich and Manz 2006). Aggregation can also occur in

high concentration protein solutions due to the protein being fully denatured and unable to stay in solution. Chemical denaturant can be used to assay denaturation by titrating the denaturant at various concentrations to produce a denaturation curve. This denaturation curve can be used to assess specific parameters, unique to each protein. If the protein is damaged, chemical denaturation can be used as a way of detecting and monitoring the protein stability.

1.4.3 pH denaturation

pH is a measure of acidity or basicity of a solution and is known to be a function of the log of hydrogen ion activity in an aqueous solution. pH denaturation of a protein is dependant on the isoelectric point, defined as the pH at which the protein has no net charge. At physiological pH, most proteins are above their isoelectric points having a net negative charge, however when the pH is taken below this point, there is a net positive charge. At the isoelectric point, most proteins will precipitate due to the charge repulsion of similar molecules being at a minimum, caused by the protonation of ionised side chains. The effects of increasing the pH on the protein solution are similar to those of decreasing the pH potentially leading to aggregation. Aggregation does occur by the effect of repulsion of like charged proteins but by the repulsion of like charges within the molecule, which in turn expose hydrophobic groups. This can lead to irreversible protein unfolding caused by acid labile groups (Tanford 1968; Yang, Yang et al. 2007).

During processing, a protein can experience a number of treatments that involved the use of alkaline pHs, which may cause chemical modifications in the proteins. This exposure should be minimised, as this may lead to an alteration of protein structure. If exposure does occur, assessment of potential damage to the product is crucial.

1.4.4 Solid-liquid denaturation

Shear strain forces can occur during many stages of the manufacturing process. It is important to assess the exposure to shear in bioprocessing, as it can cause decreases in protein stability and lead to aggregation rendering a product unfit for use. High shear can also occur in various stages throughout a process for example, centrifugation, pumping, mixing, filtration, fill-finish operations formulation, protein drug delivery (Lengsfeld and Anchordoquy 2002) and cell lysis (Maa and Hsu 1996). Freezing and thawing of the purified bulk, formulation, sterile filtration and freeze drying (Patro, Freund et al. 2002) have all been seen to have a negative effect on the stability of a protein increasing susceptibility to solid-liquid denaturation. Denaturation at physical interfaces may occur due to a shear stress or shear rate (Chisti 2001). Shear is the stress state in which the shape of a material tends to change without particular volume change. This occurs due to the motion of fluids upon surfaces causing a change in velocity between the surface fluid and the body of fluid. This causes a stress on the liquid and the protein contained in it (Biddlecombe, Craig et al. 2007). An analysis of 2IgG4 human monoclonal antibodies found that exposure to a high shear stress over a period of 7 hours can lead to a 90% reduction of the monomer (Biddlecombe, Craig et al. 2007). For this reason, it is important to consider shear as a form of denaturation. Microfluidics devices allow the production of controlled solid liquid interfaces that can be computationally modelled to quantify stresses experienced. These stresses can be accurately controlled using flow rate and long flow vessels (Kang. K. 2005) to mimic conditions in processing.

1.4.5 Air-liquid interfaces for denaturation

Denaturation can occur at a number of interfaces such as air-liquid interfaces and liquid-liquid interfaces as well as physical interfaces. A protein experiences conditions at the interface that can cause unfolding due to the flexibility of tertiary structure of the protein. The extent of unfolding at an interface is greatly dependant on the rigidity of the 3D protein structure, which in turn is dependant on the number and location of hydrophobic groups (Maa and Hsu 1997). Hydrophobic residues in a protein can associate in air causing the protein to unfold. This can occur when a system is not air tight causing bubbling or foaming occurs. Detection of foaming or bubbling may not be possible in a closed unit such as a centrifuge, hence determine the protein stability after each stage of the process becomes crucial. Air liquid interfaces can easily produced in microfluidics due to the airtight continous flow systems. This allows the incorporation of controlled amounts of air possible, creating an ideal sealed system for air liquid interface analysis (Atencia and Beebe 2005).

1.5. Measurement of protein denaturation

As previously mentioned, spectroscopy has been used to produce a high throughput method of monitoring protein stability. A high sensitivity of detection with a high accuracy allows the possibility for scale down of detection. The type of spectroscopy used in the analysis of a protein is dependent on the parameters needed to be determined. For the means of this thesis we will discuss two methods of spectroscopy and the adaptation and relevance to scale down to microfluidics.

1.5.1. Absorbance

Absorbance is defined as the amount of light absorbed by a sample at a given wavelength. Absorbance is commonly used to measure protein concentrations and protein condition, for example aggregation can be measured at absorbance at 600nm. This can be carried out using a spectrophotometer, a colorimetric or spectrophotometric assay. Colorimetry assays use a dye bound to the protein to measure its absorbivity. An example of this is Coomasie Blue in the Bradford protein assay to assess protein concentration. Absorbance can also be used to monitor protein structure by looking at absorbance at 280nm. This is, however, only gives a quantitative method of structural analysis with no information given about these changes. The wide spread use of such methods as NMR, CD and fluorescence have left UV absorbance spectroscopy outdated to the point that that it is only used for simple concentration determination, enzymatic assays and occasionally in protein structural studies. (Mach, Volkin et al. 1995). UV absorption can also be particularly complicated for larger proteins due to the large number of groups that can absorb at any given wavelength. It is thought that UV fluorescence of particular amino acids offers an increasingly sensitive measurement that is dependant on the local environment of the amino acid, offering more information than absorbance. For this reason only the use of fluorescence spectroscopy will be considered further.

1.5.2. Fluorescence

There have been a variety of methods developed to measure the interaction of electromagnetic radiation with molecules such as fluorescence spectroscopy. Fluorescence can be used to assess the dynamic properties of proteins, membranes and nucleic acids on a nanosecond timescale (Lakowicz 1980). Fluorescence is an optical

phenomenon, in which the molecular absorption of a photon triggers the emission of a lower-energy photon with a longer wavelength. The energy difference between the absorbed and emitted photons is released as molecular vibrations or heat. Usually the absorbed photon is in the ultraviolet range, and the emitted light is in the visible range, but this is dependant on the absorbance curve and Stokes shift of the particular fluorophore (Lakowicz 2000). Emission depends solely on the conformation of groups involved in the structure of the protein. These groups can act a fluorophores, which can be defined as fluorescent components of a molecule.

1.5.3. Protein fluorescence

Fluorescence in proteins can be divided into two classes, intrinsic and extrinsic. Intrinsic fluorophores occur naturally within a protein, whereas extrinsic fluorophores are added to the sample to display the desired spectral properties. Examples of these are tryptophan fluorescence and 1-Anilino-8-Naphthalene (ANS) fluorescence respectively. The advantages and disadvantages of both must be discussed to decide which is most applicable to function.

1.5.4. Intrinsic fluorescence

Tryptophan fluorescence is widely used to monitor changes in protein conformation (Lakowicz 1999). Three aromatic amino acids residues that act as natural fluorophore are widely found in most proteins. Changes in intrinsic fluorescence displayed by these residues can be used to determine the structural changes in protein folding (Turoverov and Kuznetsova 1998). The average fluorescence exhibited by these aromatic residues is relative to their environments, hence it to be used as a measure of perturbation of structure. Most emissions are due to the excitation of trytophan residues, with a small

proportion of emissions due to tyrosine and phenylalanine caused by the higher quantum efficiency of trytophan. A protein may possess one or more tryptophan residues (generally present at 1% in proteins) and this must be known for interpretation of structural data (Matulis, Baumann et al. 1999).

Tryptophan is very sensitive to its local environment shown by the intensity, quantum yield, wavelength or fluorescence maximum changes in emission. It is possible to see changes in emission spectra in response to many factors such as conformational changes, substrate binding, and denaturation. Tryptophan fluorescence is dependent on the residue's exposure to water and it's proximity to other residues. For this reason a change in local environment causes a change in the overall fluorescence. Tryptophan residues buried in the core of the protein can have spectra that are shifted 10 to 20nm compared to that of a tryptophan on the protein surface. Tryptophan residues can be selectively excited at 280-305nm to avoid excitation of tyrosine residues with emission detectable at 330-350nm.

Fluorescence of these aromatic residues can increase or decrease when comparing folded protein and unfolded protein at a certain wavelength. Average fluorescence can be used as an indicator of structural change, creating a better understanding of the protein by monitoring the wavelength and spectrum of emitted light.

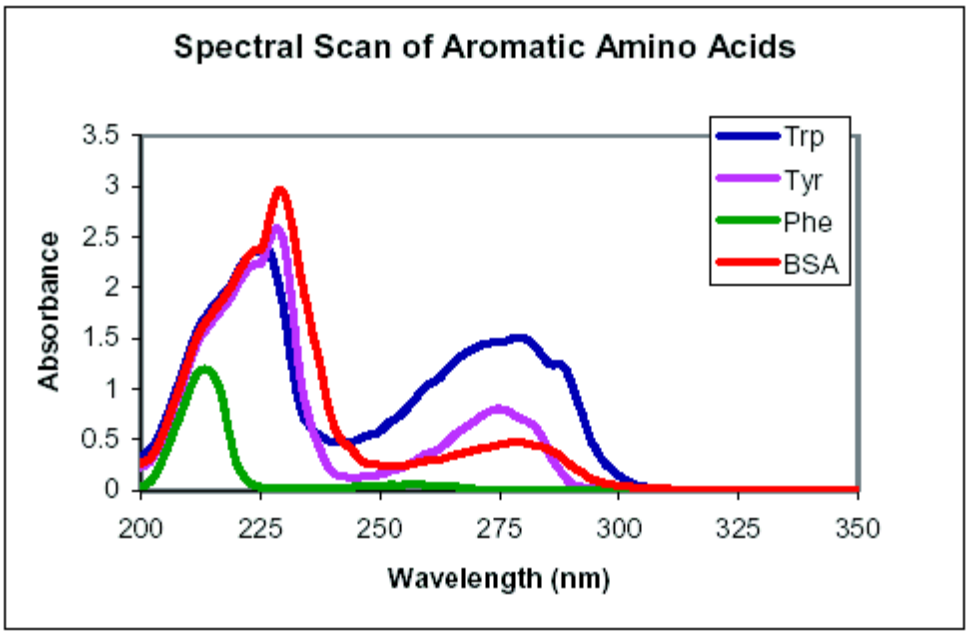

Figure 1.3. Spectral Scan of Aromatic Amino Acids

Spectral scan of a range of wavelengths of aromatic amino acids and BSA. It can be seen that BSA spectra shows a combination of amino acid spectra (Adapted from Biotek, UK).

When decreasing the scale of detection, natural fluorescence may be undetectable due to the low intensity and UV wavelength of the emitted fluorescence. If this is the case an extrinsic fluorophore can be used to produce a fluorescent protein conjugate.

1.5.5. Advantages and disadvantages of intrinsic fluorescence

Internal fluorescence is a measure of unperturbed protein as the signal is emitted from amino acids that naturally occur within the protein. The signal and parameters measured are solely emitted by the protein and not by a protein conjugate complex. By conjugating an external fluorophore to the protein, stabilisation or destabilisation of the protein may occur, changing the stability parameters measured. The quantum efficiency

of natural fluorescence is very low leading to a low fluorescence signal emitted in the UV range. This makes the detection of intrinsic fluorescence difficult, as equipment must be very sensitive in the UV range.

1.5.6. External fluorophore fluorescence

Proteins that do not contain fluorescent aromatic amino acids can be fluorescently labelled by covalently bonding to an extrinsic fluorophore. The wavelength of emission and excitation is dependant on the external fluorophore used. ANS has been used in the past as a hydrophobic probe for visualisation of protein folding. ANS is a fluorescent amphipathic dye quenched by water allowing utilisation to determine protein damage. Upon addition to the protein it binds to the exposed non-polar hydrophobic groups in the protein by its naphthalene phenyl groups and charged sulphonate groups with increasing intensity. In the fully native state the proteins inner hydrophobic regions are shielded from the ANS. Upon protein unfolding these hydrophobic residues can allow the ANS to bind, shielding the fluorophore from the water hence fluorescence is increased (Aucamp, Cosme et al. 2005).

1.5.7. Advantages and disadvantages of external fluorophore fluorescence

The addition of an external fluorophore to a protein solution allows the fluorescent labelling of a protein that does not contain any fluorescent residues. It also allows the fluorescent wavelength to be determined by the fluorophore conjugate chosen allowing an increase in wavelength to the visible range. The quantum efficiency of the fluorophore is much higher than that of an aromatic amino acid leading to an increased signal. This means that the equipment involved will need to be less sensitive and does

not need to be adapted to UV specifications. By binding to the protein an external fluorophore interacts with it, causing changes in protein stability. This can create a bias that may not be seen when using internal fluorescence.

1.6. Microfluidics for measurement of protein denaturation

1.6.1. Microfluidics measurement

Microfluidics is a term that refers to any experimental or theoretical research of liquid streams generated in microsized channels (Kim, Kang et al. 2005). These channels have a typical scale of microns with nanolitres or in some cases femtolitres liquid volume, while still allowing high sensitivity of detection. Microfluidic chips can be defined as small platforms comprising of channel systems connected to liquid reservoirs by tubing. They can involve any experimental or theoretical research of liquid, gases, fluidised solids or particles streams generated in chips comprising microsized channels. Microfluidic chips have emerged as a means to improve throughput, resolution and fidelity of measurements in many biological applications. These applications can include capillary electrophoresis (Uchiyama, Nakajima et al. 2004), isoelectric focusing (Macounova, Cabrera et al. 2001), immunoassays (Hatch, Kamholz et al. 2001), flow cytometry (Sohn, Saleh et al. 2000), PCR amplification (Khandurina, McKnight et al. 2000) and chemical gradient formation among others.

There are many advantages of microfluidic devices that make them clinically useful and versatile including simple and inexpensive fabrication to make highly elaborate, multiplexed devices, which are mass producible. These devices also improve thermal and mass transfer by decreasing effective rates of thermal dissipation and effective diffusion. Microfluidics use small reaction volumes reducing sample utilization without evaporation (Dittrich and Manz 2006) (a problem experienced in other scale down

methods) due to the use of a sealed flow vessel. This allows parallelisation of detection with multiple channels on one chip due to the reduction of scale with rapid methods of analysis due to continuous flow conditions (Dittrich and Manz 2005). Heat transfer can be easily facilitated and accurately regulated due to a high surface to volume ratio. Microfluidic devices can be used to obtain many different measurements, for example molecular diffusion coefficients (Costin, Olund et al. 2003), fluid viscosity (Macounova, Cabrera et al. 2000), pH (Hadd, Raymond et al. 1997), chemical binding coefficients (Costin, Olund et al. 2003) and enzyme kinetics (Vivian and Callis 2001). The small size of the devices creates the need for adequate, highly sensitive detection techniques to measure these desired parameters.

A key application for microfluidics is the miniaturisation of previously devised analytical techniques. In this project this application is being used to mimic conditions that can cause protein damage during bioprocessing of therapeutics in the form of proteins. It is currently known that damage can occur in bioprocessing via many different mechanisms and it is important to monitor this using a high throughput method without compromising accuracy. At the development stage of a process, product is valuable and testing on this small amount must be vigorous. Microfluidics offer the potential to achieve all these criteria.

1.6.2. Laminar flow and reynolds number

In microfluidics, it is important to understand the fluid flow inside the channel considering microfluidic system design. Fluid behaviour at microfluidic scale is increasingly influenced by viscosity rather than inertia, resulting in a laminar flow (Atencia and Beebe 2005). This fluid flow can be characterised by the Reynolds number which is related the ratio of inertial to viscous flow. Viscosity is defined as the internal

friction of fluid that produces a resistance to shear. Inertia is the tendency of a body in motion to retain its initial motion resulting in turbulent flow. Laminar flow is the tendency of the fluid to move in parallel layers. Reynolds number **(Re)** can be calculated as:

$$Re = \frac{aV}{v} \qquad \textit{Equation 1.1}$$

Where **V** is the velocity scale of the fluid, **a** is the characteristic distance of the system and **v** is the kinetimatic viscosity of the fluid. Due to the small dimensions of microchannels, Re is usually less than 100 leading to a laminar flow with no turbulence. Transition to turbulent flow generally occurs around 1500-2000 (Nam-Trung Nguyen 2002). Characterising laminar flow is important to govern and predict the conditions within the channel. By knowing the conditions inside a microfluidic channel it allows conditions to be modelled to replicate a process and to assess that the readings received during analysis are not due to turbulent flow. By keeping flow inside the microfluidic channel laminar, ensuring the protein experiences minimal stress due to flow, shear or mixing.

1.6.3. Continuous flow microfluidics

The use of continuous flow microfluidics allows an increase in throughput in comparison to stop flow methods. In protein engineering libraries large numbers of compounds can be screened for specific characteristics, allowing the assessment of many samples in a short time. The conventional methods of using microwells for high throughput assessment can be miniaturised by both increasing plate size and decreasing

well size requiring robotic systems to pipette with speed and accuracy (Aucamp, Cosme et al. 2005). There is however a limit at which further scale down is no longer possible, due to pipetting inaccuracies and evaporation (Atencia and Beebe 2005). For this reason a continuous flow method of analysis is beneficial. Microfluidic systems forms sealed continuous flow reaction system while still reducing reaction volumes with minimum human error associated.

1.6.4. Microfluidics uses

Microfluidics can be used for many applications including the use of fuel cells, DNA analysis, proteomics and characterisation assays (such as kinetic assays, fluorescence assays and structural assays). These can use many different components such as particles, capillaries, gels and microfluidic chips or involve the use of "Lab on a Chip" devices (Atencia and Beebe 2005). Lab on Chip devices integrate one or several laboratory functions on a single chip. There are many different applications of microfluidics due to the number of systems that have been developed e.g. microheat exchanger, micromixers, microreactors, microchannel electrochemical reactors and microadsorbers. Microfluidic components have the potential to control critical parameters (such as temperature and concentration) to mimic each component of a process in parallel or in procession (Figure 1.4) mimicking the complete process of drug discovery.

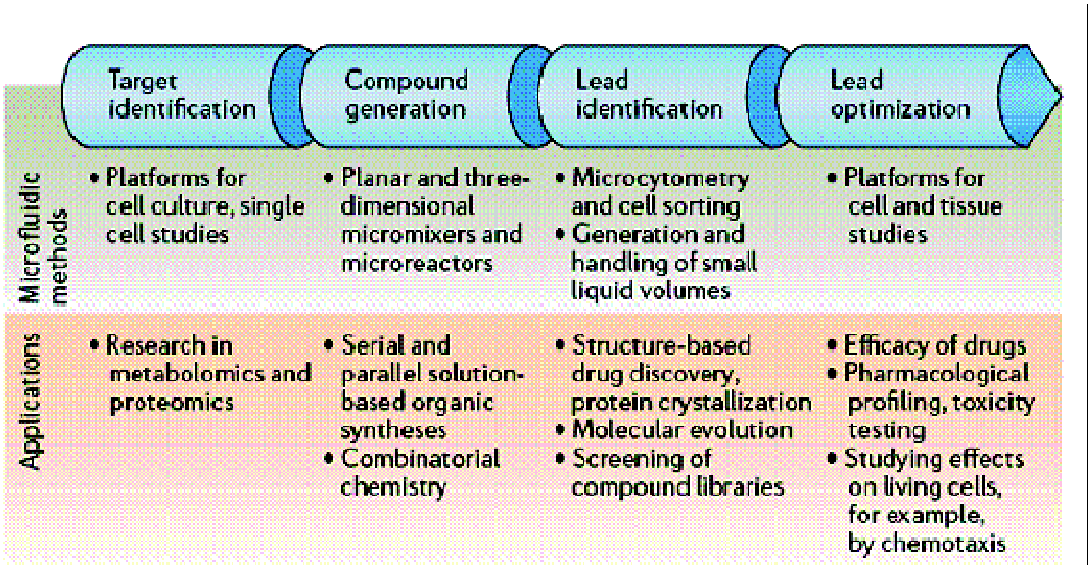

Figure 1.4. Illustrate multiple uses of microfluidics in an upstream process

This diagram shows the potential of use of microfluidics in upstream processing to reduce processing time and reagent use (Adapted from Dittrich and Manz 2006).

1.6.5. Microfluidic fabrication

Microfluidics devices can be made out of a number of materials depending on the required system characteristics. Commonly used materials include glass and silicon. These materials possess several advantages such as excellent surface stability, solvent compatibility and optical properties (important in spectroscopy) (Chovan and Guttman 2002). More recently polymers based material such as polydimethylsiloxane (PDMS), plastics and teflon have been increasingly used to increase throughput and decrease costs (Pihl, Karlsson et al. 2005). Fabrication of these devices can be carried out by various methods depending on the features and characteristics of the resulting devices needed. Methods include wet and dry etching, micromachining and lithography among many others. Once these features have been fabricated onto the chip, surfaces can be modified by oxidation or salinatisation to decrease the fouling potential of the chip. A

glass slide can be anodically bonded to the channels to form a sealed system to allow continuous flow without evaporation. There are various different designs for microfluidic devices ranging from capillary tubing to the more complex chip with various features included. When designing a system it is important to begin with a simple design that is more adept for use in the system it is needed for despite the complex systems available.

1.6.6. Advantages and commercial aspects of microfluidic scale down

With the recent achievements regarding the Human Genome Project and the potential of biotechnology, microfluidics promises to be a huge commercial success. Industry interest shows the commercial value of microfluidic devices for practical applications. From the traditional microfluidic devices (inkjet print heads) a much broader microfluidic market is emerging. An increasing number of microfluidic devices have recently been created and marketed, showing the need for the scale down that microfluidics can offer (Figure 1.5).

There have been major applications for microfluidics in many areas such as medical diagnostic, genetic sequencing, chemistry production, drug discovery and proteomics. It is said that microfluidics has had a similar effect on analysis to that of integrated circuits on computers and electronics (Dittrich and Manz 2006). Microfluidic devices have changed the way companies market to their customers opening a mass market of cheap disposable devices instead of a few expensive items. Microfluidics has revolutionised chemical screening power allowing the pharmaceutical industry to rapidly screen combinatorial libraries using smaller quantities of material. Fast analysis is enabled by parallel analysis of multiple channels on the same chip. This in turn makes microfluidics applicable in multiple disciplines due to the number of potential

applications. New effects, new chemical reactions and new microinstruments lead to new applications in chemistry and bioengineering not possible in traditional devices.

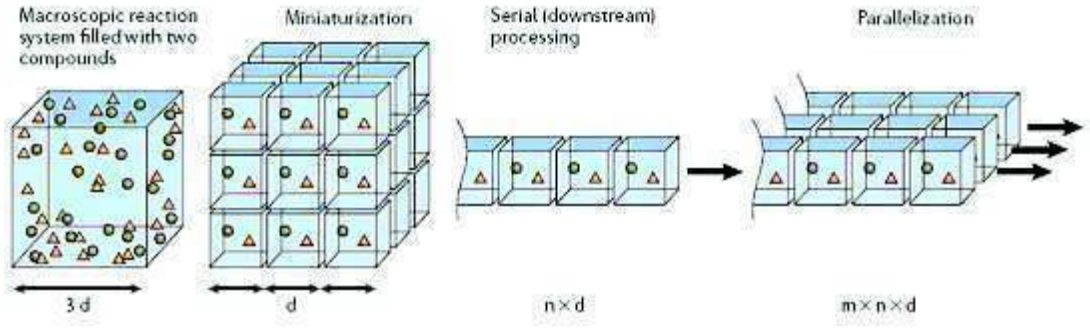

Figure 1.5. Comparison of microfluidics to conventional methods

Diagram showing parallelisation and serialisation of microfluidic devices compared to macroscopic analysis systems. By offering the potential to scale and use various systems together microfluidics offers the potential of a large scale down effect (Adapted from Dittrich and Manz 2006).

Current methods of protein stability assessment use large amount of reagents to yield relatively small amounts of information regarding the protein. Microfluidics offers many advantages of scale such as a decrease in reagent consumption, increased surface to volume ratios, high throughput analysis, increased thermal conductivity, low fabrication costs and increased sensitivity. This makes it ideal for scale down of biological and chemical processes

1.6.7. Adaptation to microfluidics for scale down potential

In the past small scale devices have been used to successfully assess products for market, however the increase in growth and hence competition has lead to the need for further scale down and throughput. The development of high throughput techniques in

other areas, such as protein engineering, has meant that there are high demands on biophysical characterisation. The use of directed evolution can look at variants of proteins, however this technique does not give information on parameters such as activity, structure, stability and ligand binding affinity, which are important for the development of therapeutics. Tagged protein purification and high throughput automation has allowed the modification of many processes to investigate physiochemical properties in protein however there is still a bottleneck in the characterisation of biophysical properties. This includes the stability assessment of new protein therapeutics, such as enzymes, used in biocatalytic processes at high temperatures or in organic solvents. Protein denaturation and stability has previously been detected in many other high throughput fluorescence methods. One of these methods uses a 96 well microtitre plate system, read by a fluorescence microplate reader (Aucamp, Cosme et al. 2005) forming a direct method of determining protein stability. Using this method, protein unfolding transitions can be monitored using tryptophan fluorescence and ANS with chemical denaturant. This assay, although already proven to be high throughput with the use of robotics, is thought to be scalable to produce a continuous flow assay with a large reduction in cost and reagent using microfluidics. The parameters used to test this method must be carefully chosen for optimum adaptation to microfluidics.

Fluorescence spectroscopy offers a high sensitivity of detection allowing the use of low amounts of analyte to be involved in microfluidic analysis. The high temporal resolution offered by fluorescence enables real time measurements, allowing assays to be handled insitu or with continuous flow analysis. The sensitivity of fluorescence spectroscopy allows a decrease in sample volume as well as a decrease in background signal from impurities, Rayleigh stray light, Raman scattering. For detection of this small number of

molecules, it is important to design an experimental system to adequately detect the fluorescence from the sample while reducing the background signal.

1.7. Thesis objectives

Measurement of the impact of process conditions on protein stability throughout the various stages of formulation and bioprocessing are critical to the production of biologics. Currently analysis is carried out using methods that are labour and reagent intensive leading to high turnaround times in optimisation.

In research and development expenditure can be greatly reduced by decreasing this unnecessary cost, placing time limitations on optimisation. Increasing the throughput of protein stability analysis is becoming increasingly important throughout process development, as this allows faster process design decreasing costs.

The goal of this thesis is to develop a microfluidic approach to rapid analysis of protein stability during process design. This would in turn produce large sets of data to allow a thorough investigation of protein condition while dramatically reducing analysis time and amount of reagent used. This will give rise to improved process understanding enabling better process design and operation than with current methods.

The study has several aims that are addressed in three experimental chapters as follows:

Chapter 3 covers the use of a fluorescence protein stability assay across an array of process relevant conditions. This was carried out at microwell scale, and used for comparison to the microfluidic optical system. Various different conditions are investigated as an assessment of protein stability.

Chapter 4 covers the development of equipment for high throughput screening. This includes an assessment of feasibility of scale down initially. The development of a fluorescence system to increase the throughput of screening protein stability is then

described. Development of this system is then shown to achieve reliable results for low protein concentrations with a high signal to noise ratio. Finally results from the microfluidic system are compared to those at microwell to look at reliability of the system.

Chapter 5 will covers the analysis of protein from the fluorescence stability assay. This will include the 3D analysis of protein landscapes to reveal how the benefits of a high throughput microfluidic system can be used to understand protein stability across the range of process relevant conditions and hence directly help process design.

Chapter 2:

Materials and Methods

2.1. Protein preparation

All chemicals were purchased from Sigma Aldrich (Dorset, UK). 98% albumin from bovine serum (BSA), α-chymotrypsin from bovine pancreas and 98% ribonuclease A (RNase A) from bovine pancreas Type XII-A were tested. The protein stock solution concentrations were determined from absorbance measurements in a spectrophotometer using the molar absorption coefficients values of $43890M^{-1}cm^{-1}$ at 280nm for BSA (Pace et al. 1995) and $9800M^{-1}cm^{-1}$ at 278nm for RNase A (Sela et al. 1957) and $51000M^{-1}cm^{-1}$ for α-chymotrypsin (Bru et al. 1991). All spectrophotometric measurements were made using an ATI UniCam UV2 spectrophotometer from Unicam Ltd (Cambridge, UK). Buffers used were 50mM TRIS and 60mM sodium phosphate, 1M sodium bicarbonate, phosphate saline buffer (PBS) and deionised water (H_2O). The denaturant stock solutions were made up in various buffers to 9M urea and 7M guanidine hydrochloride.

2.1.1. High-throughput microwell fluorescence measurement

Microwell protein unfolding measurements were measured using 96 well microtiter plates. Readings were taken using a fluorescence microplate reader, BMG FLUOstar Optima (BMG Labtechnologies Ltd, Bucks, UK). Detection was carried out using a 280nm ±10nm excitation filter and a 340±10nm emission window filter for intrinsic tryptophan fluorescence. Excitation and emission measurements were set to read from both the top and bottom of each well by changing the optic fibre positions. Gain was set to measure 90% of the maximum fluorescence value. Protein measurements were carried out using the fixed volume denaturation method (Aucamp et al. 2005). Blanks measured were empty wells, buffer and stock chemical denaturant. Outer wells of the plate were not used due to

variations in fluorescence readings for these wells (Aucamp et al. 2005). 20µL stock protein solutions were added to each microwell in the plate in triplicate. Wells were filled with various volumes of buffer containing denaturant to produce a denaturation curve of fluorescence against denaturant concentration.

2.1.2. Selection of microwell plate type (baseline and stability)

Non-treated black microplate (Nunc, VWR International, Darmstadt, Germany), and non sterile 96 well clear flat bottom UV-transparent acrylic microplate (3635, Corning, MA, USA) were tested to identify baseline and stability variability throughout the microplates. Baseline variability was compared by filling each well with 280µL of 60mM sodium phosphate buffer pH 7.4. Plates were read using a BMG FLUOstar plate reader with excitation at 280nm and emission detected at 340nm. Detection was carried out in each well with excitation and emission from both top and bottom of the microplates. Fixed volume urea denaturations of BSA 1.43mg/ml (21µM) were carried out in 96 well plate format in 60mM sodium phosphate buffer.

2.1.3. Fixed volume denaturation

Varying concentrations of BSA or BSA plus ANS in 20µL of 60mM sodium phosphate buffer were loaded into each well of a 96-well microtitre plate to detect the limits of the BMG plate reader. Wells were filled with various volumes of buffer containing 0 to 8.4M urea and 0 to 6.5M GdHCl to a final volume of 280µL. ANS was used in a ratio of 1:1 with BSA and left to incubate at ambient temperature for 15 minutes to ensure binding. Upon addition of chemical denaturant each sample was left to reach equilibrium with time

dependant on protein. Samples were prepared and read in triplicate using the BMG FLUOstar plate reader. Intrinsic tryptophan fluorescence was read using excitation at 280nm with emission at 340nm. ANS was excited at 340nm and emission at 470±12nm. Fluorescence signals were plotted against denaturant concentrations. Fluorescence curves were analysed using non-linear least squares regression fitting in SigmaPlot 9.0.

2.1.4. Characterisation of thermal increase in plate reader

280µL of 60mM sodium phosphate buffer pH 7.4 was added to one well in the 96 well microplate. A thermocouple (Digitron 2022T) was secured in place ensuring the well was not covered and thermocouple probe was fully submersed in sample. BMG FLUOstar plate reader has an integrated thermal heating system comprising of thermal heating plates above and below the 96 well microplate. Heating plates were set at 60˚C and well temperature readings were taken every two minutes. This was repeated in various positions across the plate to characterise the variation of heat transfer to the liquid.

2.1.5. Thermal denaturation studies

Samples were prepared in various buffers and plated to a final well volume of 280µL. All sample were prepared and read in triplicate. Thermal heating plates were set to 60˚C ensuring a start temperature of 24.7˚C using a thermocouple. Fluorescence and absorbance reading were taken every 2 minutes up to 30 minutes and every 5 minutes there after. Fluorescence was read at 280nm excitation and 340nm emission with absorbance at 600nm. Initial and final temperature readings were taken of the samples to ensure that heating has

occurred as profiled. Fluorescence and absorbance were plotted as a function of temperature.

2.1.6. SDS PAGE gel analysis

SDS PAGE gels were carried out using the Mini-PROTEAN II electrophoresis kit (BioRad Laboratories Inc., Hercules, CA, USA). Gels consisted of 12% separating and 4% stacking gel. Samples were heated with 1:1 SDS reducing buffer for five minutes. 20µL of sample was loaded onto the gel. Gel was run using in running buffer prepared according to the Mini-PROTEAN 11 electrophoresis cell instruction manual at 100V for 60 minutes. Markers used were PageRuler Prestained Protein Ladder (Fermantas Life Sciences) and Precision Plus marker (BioRad). Gels were stained for 30 minutes using Coomassie Blue stain made of 0.1% (w/v) Coomassie Blue R-250, 40% (v/v) methanol and 10% (v/v) acetic acid. Gels were destained using 40% (v/v) methanol and 10% acetic acid overnight and imaged using a UV transilluminator.

2.1.7. pH denaturation of proteins

Samples were made in TRIS buffer prepared in pH range 3 to 10. Proteins were left to incubate at ambient temperature for 15 minutes to ensure equilibrium is reached. A well volume of 280µL of sample was read with excitation at 280nm and emission at 340nm. Concentration of proteins used: RNase A 1.43mg/ml (0.1mM), Chymotrypsin 0.71mg/ml (27µM) and BSA 0.71mg/ml (10µM). Fluorescence was plotted as a function of pH.

2.1.8. Long term denaturation effects

Samples of BSA at 20mg/ml (0.3mM) were prepared in 60mM sodium phosphate buffer pH 7.4. Samples were continuously stirred while heating using a thermal hotplate (Halogen, UK). Temperature was kept at a constant at 70˚C for up to 140 minutes, measured using a thermocouple to ensure minimum variation of temperature during heating. Samples were allowed to cool and treated using a fixed volume urea denaturation. Final BSA concentrations after denaturation were 1.43mg/ml (21μM). Samples were left to reach equilibrium and fluorescence was read at 280nm excitation with emission at 340nm.

2.1.9. Buffer unfolding studies

BSA formulated in various buffers and tested using the fixed volume urea denaturation method as specified above. Buffers used were 60mM sodium phosphate buffer (pH 7.4), phosphate buffered saline (PBS) (pH 7), 50mM TRIS buffer (pH 7), 1M sodium bicarbonate (pH 7.95) and deionised H_2O. Chemical denaturant and proteins were made up in the specific buffer for each test. Final protein concentrations were 1.43mg/ml (21μM). Samples were read at 280nm emission and 340nm excitation as above.

2.2. Microfluidics optical detection system

2.2.1. Feasibility study

A stock solution of 1M fluorescein (pH 7.4) was diluted by serial dilution to concentrations 5nM to 50nm. In optimisation studies it was found that the optimum ratio of BSA and ANS was 1:1 BSA/ANS. Samples of BSA/ANS were made up to 5μM to 27μM. BSA solutions were made to 5μM to 108μM and all samples were plated onto 96 well UV transparent

microplates. Samples were plated at various concentrations and read at the same gain. Blanks were empty wells and 280μL of buffer. Plates were read three times using various filters to compare fluorescence. Fluorescein was detected with excitation at 490nm and emission at 514nm. BSA was detected with excitation at 280nm and emission at 340nm. ANS was excited at 340nm and emission at 470± 12nm. All solutions were made in 60mM sodium phosphate buffer pH 7.4. Fluorescence readings were measured using the BMG FLUOstar plate reader with equal gain for each plate reading.

2.2.2. Well volume determination

BSA at 20mg/ml (0.3mM) was made up in 60mM sodium phosphate buffer pH 7.4. Samples were plated at varying volumes in wells around the plate. Each sample was prepared and read in triplicate. Gain was set on 280μL volume well and kept constant for each sample.

2.2.3. Capillary preparations

Fused silica tubing (Presearch, Hampshire, UK) FS-110 with an internal diameter (ID) of 100μm and an outer diameter (OD) of 360μm. Capillary consists of a fused silica tube coated in a standard polyimide coating. Fluorescent coating of capillary was removed by heating in a blue flame followed by piranha cleaning. Ethanol was used to clean the capillary and remove any residue. The procedure was repeated until all coating was removed. Capillary was piranha cleaned over night inside and outside to remove organic residue and remains of the outer coating. Piranha clean consists of a mixture of sulphuric acid (H_2SO_4) and hydrogen peroxide (H_2O_2) in a ratio of 7:3. Piranha clean was handled

according to the Lawrence Berkeley National Laboratory safe operating procedure. Due to the hazards involved all solutions were handled in a fume hood with adequate personal protective equipment. Piranha solution is an exothermic violent reaction that should be handled with care. Piranha cleaning solution was left for 24 hours in the capillary to ensure the reaction was inactive when water was added. Capillary was rinsed in RO water at high flow rate to remove piranha clean. Capillary was handled with care due to the brittleness caused by removal of the coating.

Capillaries were cleaned between readings with 2% Helmanex detergent (Helma, Germany) for 2 passes at 20ul/min and rinsed with RO water for 5 passes or until background reading is reached.

2.2.4. SEM of capillaries

Carl Zeiss XB1540 “Cross-Beam” focussed-ion-beam microscope equipped with an in situ field-emission scanning electron microscope for gallium-free imaging was used to image capillaries treated in various ways. Outer coating of capillaries was removed by burning only, piranha cleaning only, and a mixture of burning and piranha cleaning. Images were imaged to look at removal of outer coating

2.2.5. Capillary 3D imaging

Fused silica capillary was cleaned and stripped as above. FEP green PEEK tubing sleeves 1/16 x 0.0155 (Presearch, Hampshire, UK) were attached to a clean glass microscope slide. Capillary was held in tubing to ensure movement was minimal during reading. Capillary was filled with samples using a syringe. To ensure there was no movement of fluid, syringe

was kept in place during reading. Samples of 60mM sodium phosphate buffer (pH 7.4) and 200mg/ml BSA in 60mM sodium phosphate buffer (pH 7.4) were measured using confocal microscopy. Leica TCS SP confocal microscope with functions as a 3-colour, UV and visible confocal microscope in one system, utilizing fiber coupled UV, VIS and IR lasers. Microscope recorded 28 z images over the capillary depth. Pinhole size was taken to 1.4a with a PMT gain of 123V using a DAPI stain filter. Image J software was used to render the pictures into a 3 dimensional image. Fluorescence readings were taken over a region of interest on the capillary to determine if detection was viable.

2.2.6. Concentration viscosity investigation

BSA was made up in various concentrations in the range of 0.1 to 500mg/ml (1.5μM to 7.5mM) in 60mM sodium phosphate buffer at pH 7.4. Rheological measurements were carried out using a Rheomat 115 rotational viscometer (Contraves AG, Zurich, Switzerland) with a plug in 7/7 module operating system and a concentric cylinder (MS-0/115) measuring unit with quick release coupling. Measurements of shear stress and shear rate of the liquid were converted to the corresponding viscosity measurements. Visocity measurements were converted via Pouseille's Law to pressure.

2.2.7. Spectral scan of BSA

Spectral scanning of BSA (50μg/ml) in 60mM sodium phosphate buffer pH 7.4 was carried out using Perkin Elmer LS30 luminescence spectrophotometer (PerkinElmer UK, Buckinghamshire, UK) to carry out spectral scans of both excitation and emission wavelength. Samples were excited at a range of 260nm to 385nm and emission was

measured over a range of 300nm to 600nm. To ensure a stable detection of fluorescence signal protein solutions were pumped into the fluorescence flow cell for 15 seconds before data capture. Emission wavelength was plotted as a function of excitation wavelength.

2.2.8. Spectral scan of BSA with urea

BSA 10mg/ml (0.15mM) in sodium phosphate buffer (pH 7.4) with and without urea (8.4M) scanned using Tecan Sapphire II Fluorometric plate reader (Tecan UK Ltd, Reading, UK). Scanning was carried out in UV transparent plates with a final well volume of 280µL. Samples were excited at 280nm and emission range was scanned over a range of 280nm-850nm. Fluorescence was plotted as a function of emission wavelength.

2.3. Microfluidic detection apparatus

2.3.1. Pump apparatus

Two KDS 210p syringe pumps (KD Scientific, MA, USA) were daisy chained using an RS232 interface. Using LabVIEW 8.0 (National Instruments, Austin, TX, USA) these syringe pumps were programmed to create a controlled automated flow with an accuracy of ±1% and a reproducibility of ±0.1%. Gas tight syringes were used to dispense a controlled amount of liquid (Hamilton, GR, Switzerland). Syringes were directly attached to the capillary using fittings to form an airtight seal around the capillary (Presearch, Hampshire, UK). Samples were flowed into a nanomixer (Presearch, Hampshire, UK) from each syringe pump to mix flows to one constant mixed stream of fluid.

2.3.2. Bench top configuration

Output capillary was held using FEP green PEEK tubing 1/16 x 0.0155 (Presearch, Hampshire, UK). Tubing was held by a purpose made stand to ensure minimum movement of the capillary during detection. This stand was held on a xyz platform (561 UltraAlign precision linear stage) to allow precision placement of the capillary detection area. All equipment was fixed to an optical bench to allow minimum vibrations from outside sources and encased in a matt black box to ensure background readings were emitted.

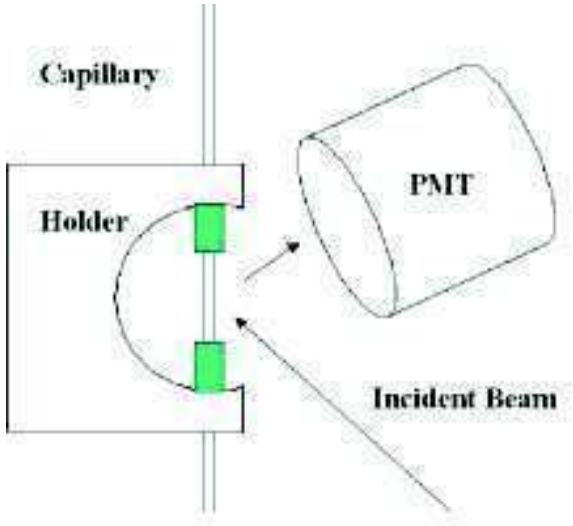

Figure 2.1. Capillary holder configuration

Schematic of capillary holder configuration showing capillary held by PEEK tubing and secured with holder. Conical holder allows minimal interference with incident and emission beams.

2.3.3. Laser and excitation filters

266 nm Nd:YAG ultra-compact diode-pumped Q-switched laser (Crystal Laser) was positioned so the incident beam was at 135 degrees to the PMT and 90 degrees to the flow of the capillary. Capillary was positioned in the beam to ensure the entire capillary was illuminated by the beam. Laser frequency was kept at 1.1kHz with a pulse width of 20 nanoseconds. Laser beam was filtered using a UG5 bandpass filter (Schott, Stafford, UK) to remove harmonics produced by the laser and to ensure a high transmission (97%) at 266nm only. Laser intensity was also reduced using optical density filters to allow 10% of the laser beam to reach the capillary, reducing high intensity laser heating of the sample.

2.3.4. PMT and emission filters

Photomutiplier tube R1166 (PMT) (Hamamatsu, Hertfordshire, UK) was powered by a high voltage power supply C9525 (Hamamatsu, Hertfordshire, UK) at 1000V. The PMT was sensitive to UV fluorescence in the range of 300nm to 650nm with a head diameter of 19mm. PMT was covering in a cone to reduce scattering from the capillary and placed 5mm from capillary to reduce unwanted light while allowing detection of emission light. PMT signal was also filtered using a Nd:YAG, high energy laser mirror to reflect high intensity 266nm wavelengths (CVI, Melles Griot, Cambridge, UK) and 340 ± 2 nm biomedical band pass filter DFS-001844 (Newport, Oxford, UK) to remove the incident beam. PMT was positioned at 135 degrees to the incident beam to reduce detection of scatter from the laser. PMT signal was inputted into the NI PXI chassis, PXI-1033 with integrated MXI-Express Controller. This in turn was connected to the NI express card 8360 to allow data collection via LabVIEW 8.0 (National Instruments, Austin, TX, USA) to

produce an average fluorescence signal. Average fluorescence was calculated by measuring 200 data points on each signal curve to calculate the area beneath this curve. Standard deviation of curve area over time is also calculated.

2.3.5. Sample detection using microfluidic apparatus

Blanks were taken of empty capillary and capillary with buffer over a period of five minutes. Samples were prepared in 60mM sodium phosphate buffer pH 7.4. Syringes are filled with premixed samples and flowed at a rate of 20μL/min through capillary ensuring there is no air in the mixture. Samples were degassed using the syringe to remove air from the samples by retraction. In-situ mixing entailed two syringes of desired degassed samples flowed at 20μL/min ensuring there is no air in the sample.

2.3.6. Protein fluorescence detection

Protein solutions were prepared in buffer with and without urea to a final concentration of 9M. Solutions were place in syringes and pumped through the capillary at varying flow rates using syringe pumps. Syringe pumps were programmed using NI LabVIEW to produce controllable gradients of solutions. Solutions were pumped through a length of capillary with a predetermined flow rate to allow residence time to be equal to that of the protein equilibrium time. Flow rate were kept at 10 to 20uL/min dependant on calculated residence times.

2.4. Multivariant denaturation of proteins

2.4.1. pH and thermal denaturation

Thermal and pH denaturation of BSA, chymotrypsin and RNase A was carried out in 96 well microtitre plates. Samples were made up in 50mM TRIS buffer at various pHs (6 to 9). Thermal denaturation was carried out using the BMG FLUOstar thermal heating plates set to 60˚C. Fluorescence and absorbance reading were taken every 2 minutes up to 30 minutes and every 5 minutes there after. Fluorescence was read at 280nm excitation and 340nm emission with absorbance at 600nm. Initial and final temperature readings were taken of the samples to ensure that heating has occurred as profiled. Fluorescence and absorbance were plotted as a function of temperature and pH.

2.4.2. pH and chemical denaturation

GdHCl and pH denaturation was carried out in 96 well microtitre plates. Samples of RNase A, chymotrypsin and BSA were formulated in 50mM TRIS buffer at various pHs (6 to 9). Proteins and GdHCl samples were made up in the desired pH and concentration for each sample. Upon addition of chemical denaturant each sample was left to reach equilibrium with time dependant on protein. Each sample was prepared and read in triplicate using the BMG FLUOstar plate reader. Natural tryptophan fluorescence was read using excitation at 280nm with emission at 340nm.

2.4.3. Thermal and chemical denaturation

Thermal and chemical denaturation of BSA, RNase A and chymotrypsin was carried out in 50mM TRIS buffer. GdHCl was added to each sample in a range of 0 to 6.5M. Samples

were left to equilibrate before thermal denaturation. Thermal denaturation was carried out using the BMG FLUOstar thermal heating plates set to 60˚C. Fluorescence readings were taken every 2 minutes up to 30 minutes and every 5 minutes there after, at 280nm excitation and 340nm emission. Initial and final temperature readings were taken of the samples to ensure that heating has occurred as profiled. Fluorescence and absorbance were plotted as a function of temperature.

2.4.4. Surface fitting of denaturation

Fluorescence was measured over 180 different combinations of temperature and guanidine concentrations. The two dimensional surface defined by this data set was fitted to Equations 5.8, 5.9 and 5.10. The fitting was done using a nonlinear least-squares optimisation procedure, lsqcurvefit, in MATLAB (The Mathworks Inc, Natick, Massachusetts, USA) with the goal of the optimisation to reduce the sum of the square errors between the model and the experimental data through adjustment of the model coefficients. There were a total of 11 adjustable parameters of which seven defined the upper and lower baselines used for the fit (a, b, c, d, e, f and g defined by *Equations 5.9, 5.10*). ΔH (at 25˚C), ΔS (at 25˚C), ΔCp and m could all be determined using this fit.

Chapter 3:

Fluorescence determination of protein stability: Microwell applications towards bioprocessing

3.1. Introduction and aims

In the development of a bioprocess, optimum operating conditions must be determined to allow production, purification and formulation of a product of marketable quality. Fluctuations in any parameters may have a detrimental effect on the quality and stability of the protein. These parameters can vary between process stages hence stability changes must be assessed. A large number of assays are available to detect the stability of a protein but it is preferable to use one assay to monitor a protein throughout a process. This assay must be assessed for reproducibility and accuracy in detecting small stability variations when environmental conditions of the protein are varied (Burton et al. 2002). The assay must also be able to function across the range of variable parameters involved in bioprocessing, such as pH and temperature, with a high throughput and sensitivity.

The main aim of this chapter is to assess a microwell high throughput unfolding assay (Aucamp et al. 2005) to investigate its potential to rapidly characterise protein stability as various parameters are altered. This method was optimised in microwells to detect UV fluorescence, using chemical denaturant to perturb the protein. Increasing concentrations of denaturant are titrated with protein samples, allowing stability assessment, with the potential to use robotics to increase accuracy and automation. This allows protein transition points in various conditions to be determined for each protein. Each protein's stability can be characterised by its response creating a profile that is unique for that protein. It is hypothesised that fluorescence measurements produced in the high throughput microwell method can allow estimation of optimum process parameters of protein stability when treated by temperature and pH in microwells. In this chapter the fluorescence assay is assessed in various conditions for its ability to detect protein stability. To characterise the

validity of this method various experiments were carried out to select such criteria as microwell plate type, natural versus external fluorophore fluorescence and chemical denaturation. Range and reproducibility of this assay were determined to allow characterisation of accuracy. Proteins were tested using parameters such as temperature, pH and buffer type to assess adaptability of this assay to mimic bioprocessing conditions.

3.2. Microwell protein denaturation and theoretical considerations

Microwell denaturation can be used to assess the stability of a protein in comparison to its native state. Denaturation is carried out in stepwise stages to produce stability graphs of fluorescence versus denaturant concentration. Experiments were carried out in 96 well plate format using the BMG FLUOstar plate reader, exciting at 280nm with detection at 340nm. 1.43 mg/ml BSA (21μM) was added to each well with varying concentrations 0 to 7M urea in 60mM sodium phosphate buffer. Samples were incubated at ambient temperature for 15 minutes to equilibrate, after which fluorescence could be read (Figure 3.1). Data was analysed to determine parameters associated with protein stability. For this reason it is important to understand the theoretical considerations involved.

3.2.1. Stability calculations for urea denaturation

Using the two state model of protein stability, parameters can be calculated from protein fluorescence denaturation data (Pace 1986; Fersht 1999). In this model it is assumed two populations are present with no unique native or denatured states and no population overlaps or intermediates. Transitions between native and denatured states must be thermodynamically reversible (Franks 1993). Detection of the denatured and native states

when a perturbing effect is experienced allows the calculation of stability (Ahmad et al. 1995).

Figure 3.1 shows that for BSA as urea concentration increases the average fluorescence decreases. Pre and post folding baselines of the native and denatured states are determined. These baselines are used to calculate the corrected values of 100% and 0% unfolded for each denaturant concentration accounting for the signal drift. Prefolding baseline can be represented by *Equation 3.1*.

$$F_{obs,N} = m_N[D] + F^{\circ}_N \qquad \textit{Equation 3.1}$$

When fluorescence **($F_{obs,N}$)** is plotted against denaturant concentration **([*D*])**, m_N is the gradient of the baseline **($dF_{obs,N}/d[D]$)** and F°_N is the fluorescence signal for the native state at 0M denaturant (Aucamp et al. 2005). Post folding baseline is represented by *Equation 3.2*.

$$F_{obs,U} = m_U[D] + F^{\circ}_U \qquad \textit{Equation 3.2}$$

whereby m_U is the gradient of the baseline **($dF_{obs,U}/d[D]$)** and F°_U is the fluorescence signal for the denatured state. These figures can be used to calculate percentage unfolded and can also be substituted into *Equation 3.3*.

$$F_{\text{obs}} = \frac{(\mathbf{F}^{\circ}_{\mathbf{N}} + \boldsymbol{m}_N[\boldsymbol{D}]) + e^{\left(\frac{\mathbf{m}_G[\mathbf{D}-\mathbf{C}_{1/2}]}{\mathbf{RT}}\right)}(\mathbf{F}^{\circ}_{\mathbf{U}} + \boldsymbol{m}_U[\boldsymbol{D}])}{e^{\left(\frac{\mathbf{m}_G[\mathbf{D}-\mathbf{C}_{1/2}]}{\mathbf{RT}}\right)} + 1} \qquad \textit{Equation 3.3}$$

Where **R** is the gas constant (1.987cal.mol^{-1}) and **T** is the absolute temperature (298K). Data is fitted using SigmaPlot 9.0 by non linear least squares extrapolation methods of pre transition and post transition regions to the transition region using *Equation 3.3*. By fitting the raw data to this equation the parameters $C_{1/2}$ and m_G can be estimated with errors. $\mathbf{C_{1/2}}$ (M) is the denaturant concentration whereby half the protein is in the unfolded state and $\mathbf{m_G}$ (kcal^{-1}.mol^{-1}.M^{-1}) is the change in free energy of unfolding with respect to the **[*D*]** (Santoro et al. 1988). An increase in $C_{1/2}$ indicated an increase in stability of the protein, as more chemical denaturant is needed to denature half the population of protein.

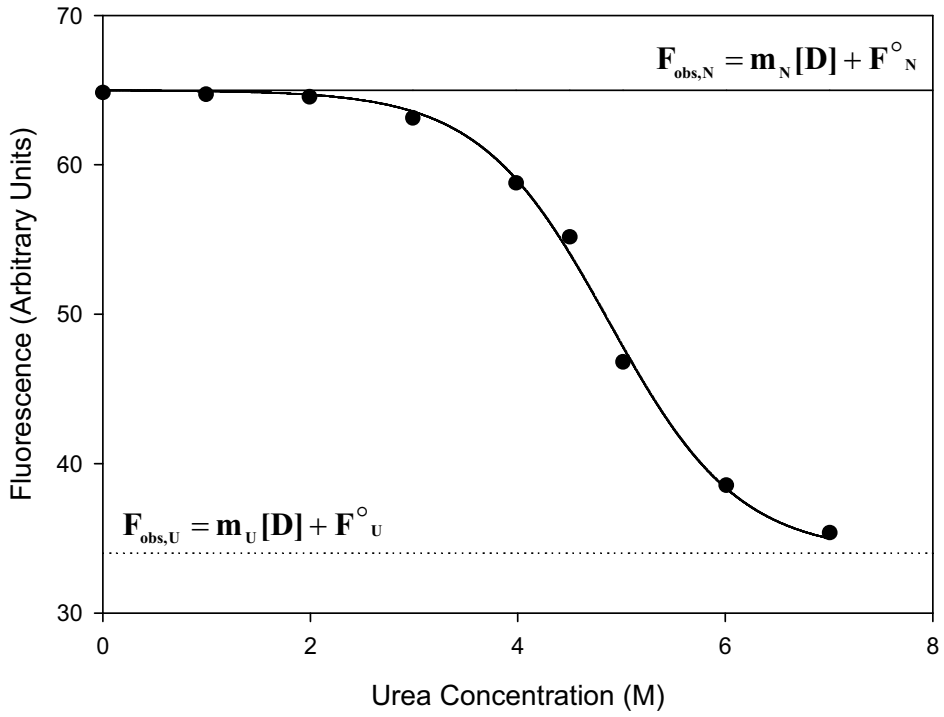

Figure 3.1. Baseline determination and linear fitting of BSA denaturation
1.43 mg/ml BSA denaturation (21μM) using urea (0 to 7M) in 60mM sodium phosphate buffer (pH 7.4). Fluorescence is plotted as a function of denaturant concentration (M). Upper and lower baselines determined to account for signal drift. Data was fitted using the linear extrapolation method to calculate percentage unfold and parameters $C_{½}$ and m_G to assess protein stability.

The free energy of protein unfolding **(ΔG)** can also be used to assess stability. This is calculated using the following equations (Pace 1986).

$$K_{obs} = \frac{F_{obs} - F_{obs,N}}{F_{obs,U} - F_{obs}} \qquad \textit{Equation 3.4}$$

$$\Delta G = -RT\ln K_{obs} \qquad \textit{Equation 3.5}$$

K_{obs} is a function of the intensity of the perturbing effect and is the fraction of molecules in each state (*Equation 3.4)*. F_{obs} is the fluorescence observed, $F_{obs,N}$ and $F_{obs,U}$ are the corrected fluorescence for the protein in it's native state as in *Equation 3.1* and *3.2* respectively. ΔG (kcal mol^{-1}) for each value can be plotted against concentration of denaturant. Using linear extrapolation (Pace 1986; Ahmad et al. 1994) ΔG_{H2O} (the free energy of the native protein in water) and m_G can be determined, seen in *Equation 3.6*.

$$\Delta G = \Delta G_{H20} - m_G[D] \qquad \textit{Equation 3.6}$$

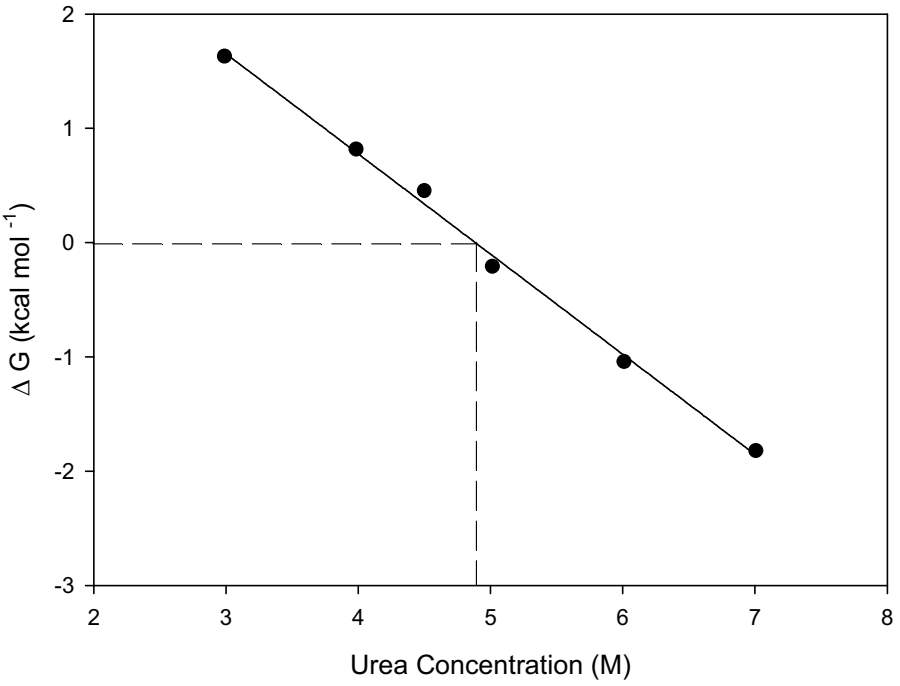

Figure 3.2. Linear extrapolation of ΔG as a function of denaturant concentration
BSA denaturation (0.3mM) using urea (0 to 7M) in 60mM sodium phosphate buffer (pH 7.4). The change in free energy observed (ΔG) is plotted against urea concentration (M). ΔG is found to decrease as urea concentration increases. The free energy of the native protein in water (ΔG_{H20}) can be found by linear extrapolation around the transition point to the y intercept. The $C_{½}$ is equal to the corresponding urea value as ΔG=0. m_G and ΔG_{H20} can also be calculated from this plot.

Extrapolation is carried out on values around the transition point to allow accurate representation of ΔG values. Error on this calculation is increased the higher the denaturant concentration needed to denature the protein, the smaller the data set and the steeper the gradient of this line (Franks 1993).

As denaturant concentration is increased, ΔG decreases linearly. $C_{1/2}$ is equal to the corresponding urea value at ΔG=0. The $C_{½}$ value obtained from both methods should be compared to increase accuracy. ΔG_{H2O} is the ΔG value of the native state of the protein in water and is seen at the y intercept in Figure 3.2. An increase in the ΔG_{H2O} signifies an

increased stability of the native state in water (Finkelstein et al. 2002). An increase in the m_G value signifies a rapid decrease in stability with denaturation concentration and a higher exposure of the unfolded state to solvent (Soulages 1998). These multiple methods should be used together to confer stability of the protein (Franks 1993).

3.3. Validation of method

To assess the validity of this method, model proteins were compared using various conditions to assess the accuracy of this method. Although there are many proteins that may be applicable and of greater interest in bioprocessing, it was thought that bovine serum albumin (BSA), chymotrypsin and ribonuclease A (RNase A) would be the most adaptable for this investigation. This is due to wide scale availability and susceptibility to denaturation.

3.3.1. Model proteins

BSA is a serum albumin protein with many uses in biochemistry due to its stability, water solubility, versatile binding affinity and reactivity. BSA has many uses including enzyme stabilisation during DNA digests and reducing adhesion to apparatus, blots and ELISAs. It is a byproduct of the cattle industry that is readily purified from bovine blood accounting for 60% of the total serum protein. It consists of a single polypeptide chain with three domains with no carbohydrates. The isoelectric point of BSA is 4.7 in solution and a molecular weight of 66.4kDa. At pH 5-7 BSA contains seventeen intrachain disulphide bridges and one sulfhydryl group. BSA has 583 residues with two tryptophan residues

(W135 and W214) making it an ideal protein for fluorescence spectroscopy (Gelamo et al. 2000).

Ribonuclease A (RNase A) is an endonuclease that cleaves single stranded RNA. In protein science, bovine pancreatic RNase A is thought of a classic model system. It has been used in many spectroscopic methods to look at structure and conformation, as it was one of the first proteins to be purified in large amounts. These methods include absorbance, circular dichroism and raman spectroscopy making it ideal for use with fluorescence. RNase A is a small monomeric enzyme with a molecular weight of 13.7kDa. The structure is made up of 124 amino acids containing four disulfide bonds. RNase A have an isoelectric point if 9.6 (Tanford 1956) with many positive charges. It is thought to have a condition dependant melting temperature of between 36-70°C (Ahmad 1983; Wang 1999)

α-chymotrypsin is a digestive proteolytic enzyme synthesised in the pancreas. It cleaves proteins at the carboxyl side of tyrosine, tryptophan, phenylalanine, leucine and methionine. It is made up of 189 amino acids with a molecular weight of 21.6kDa. An isoelectric point of 7.3 and a melting temperature of between 42-47°C makes it ideal for thermal and pH experiments (Wang 1999; De Diego et al. 2004).

3.3.2. Selection of microwell plate type

Due to the potential for further scale down, it is important to look at variable criteria in this assay to adapt it to the specific use in this thesis. As there are various methods of detection at this scale (such as absorbance or luminescence as well as fluorescence), a number of 96 well plates are available for microwell determination of stability. Fluorescence can then be read, either from the top or the bottom of the plate, using the BMG FLUOstar plate reader.

The type of plate most applicable to this method can be determined by assessing such parameters as variability of signal baseline and calculation of stability parameters. Clear and black 96 well plates were tested with a maximum well capacity of 280µL. Clear plates were made of a UV transparent acrylic and black plates contained entirely black wells. Signal detection of 60mM sodium phosphate in various positions on the plates was measured to assess variability. Two plates were compared each with the standard 96 well plate format with clear plates read from both the top and the bottom. It was seen that as the highest error around the background signal was seen in black plates (11%), then clear plates read from the top (9.1%) and with least error seen in clear plates read from the bottom (3.9%). Errors appeared high in each case due to the low signal. Signal to noise (S/N) percentages are also represented in Table 3.1. It can be seen that the lowest S/N (background signal of buffer and well) was seen in clear plates read at the bottom. This was closely followed by black plates with clear plates read from the top displaying the highest signal to noise ratio.

BSA denaturation curves were generated using the fixed volume method to compare both types of plate. Urea denaturation using 1.43mg/ml BSA (21µM) was carried out in 96 well plate format in 60mM sodium phosphate buffer at pH 7 in each case. Plates were read from the top and bottom (for clear plates) in these experiments to allow direct comparison between the clear and black plates (Figure 3.3). Excitation was carried out at 280nm and emission detected at 340nm. Results obtained using clear plates and black plates for $C_{1/2}$ and m_G were found to be similar as seen in Table 3.1. It appears that the error associated with the black plates is much higher than in the clear plates. It can be seen that the S/N percentage is higher in black plates than in clear plates read from both the top and the

bottom. It is also thought that using the clear welled plates reading from the bottom is more comparable to microfluidic systems (which will be carried out in a later chapter). Due to this, in future experiments UV transparent plates read from the bottom were used.

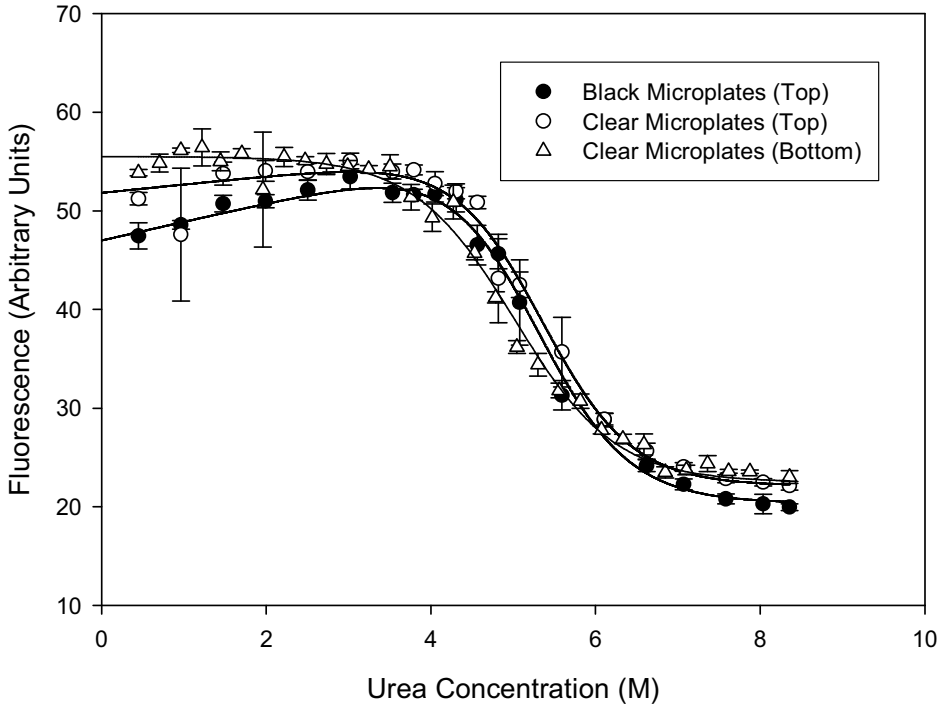

Figure 3.3. Accuracy of denaturation in clear and black microwell plates
Urea denaturation of BSA 1.43mg/ml (21μM) in 96 well plate format in 60mM sodium phosphate buffer (pH 7). Wells were read in the BMG FLUOstar with excitation (280nm) and emission (340nm) detected from the top and bottom. Fluorescence is plotted as a function of urea concentration (M) with error bars of one standard deviation shown. Clear and black plates have similar values for both m_G and $C_{1/2}$ as can be seen in Table 3.1. Error appears higher in black welled plates with irregularities in profiles.

Fluorescence	(% S/N)	$C_{1/2}$ (M)	m_G (kcal $mol^{-1}M^{-1}$)	ΔG_{H2O} (kcal mol^{-1})
Clear Plates(B)	1.70	5.10	1.01	5.15
Clear Plates (T)	7.58	5.12	1.01	5.18
Black Plates (T)	2.85	5.23	0.99	5.18

Table 3.1. Summary of clear and black plate comparison
Black plates and clear UV transparent plates were used to determine parameters and error associated. Plates showed consistent parameter determination of $C_{1/2}$ however errors associated with baseline values appears higher in black plates. Signal to noise ratios are also seen to be lower in black plates than clear plates.

3.3.3. Accuracy of natural tryptophan fluorescence versus external fluorophore fluorescence (ANS)

Variability of ANS and tryptophan fluorescence was assessed using the chemical denaturation method. Using an external fluorophore the denaturation method can be used to look at stability of proteins that have no aromatic residues and do not naturally fluoresce. It is preferable to use tryptophan fluorescence to reduce interaction with the natural state of the protein. ANS is an amphipathic dye that fluorescently labels proteins by binding to exposed non polar hydrophobic groups. By binding to the protein the fluorophore may alter its stability. Excitation occurs at 340nm and emission at 470nm, increasing detection wavelength beyond ultraviolet range. The quantum efficiency of ANS is higher than tryptophan producing a higher signal even at low concentrations. Results are compared between both the external fluorophore and internal fluorescence to see how both monitor the parameters involved in stability measurement (Figure 3.4 and Figure 3.5).

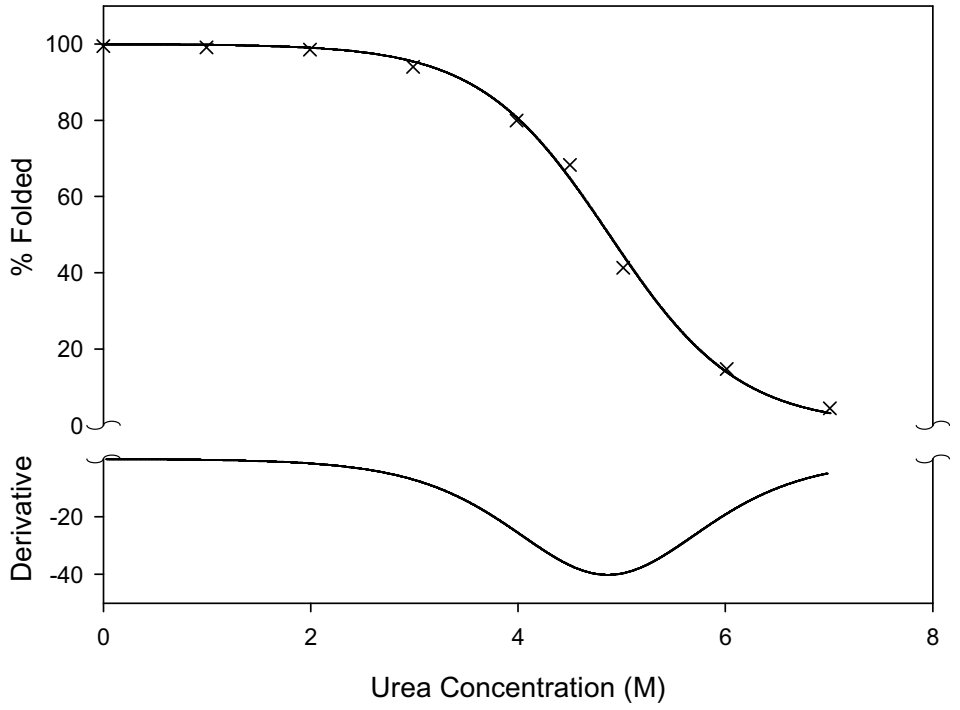

Figure 3.4. Chemical denaturation of BSA using intrinsic tryptophan fluorescence
Percentage unfolded variation with urea concentration using microwells (280µL). BSA (0.1mM) was denatured using urea (0 to 7M) using 60mM sodium phosphate buffer pH 7.4 Data was fitted using the two state model. Derivation of plot also shown to indicate $C_{1/2}$ (4.88M)

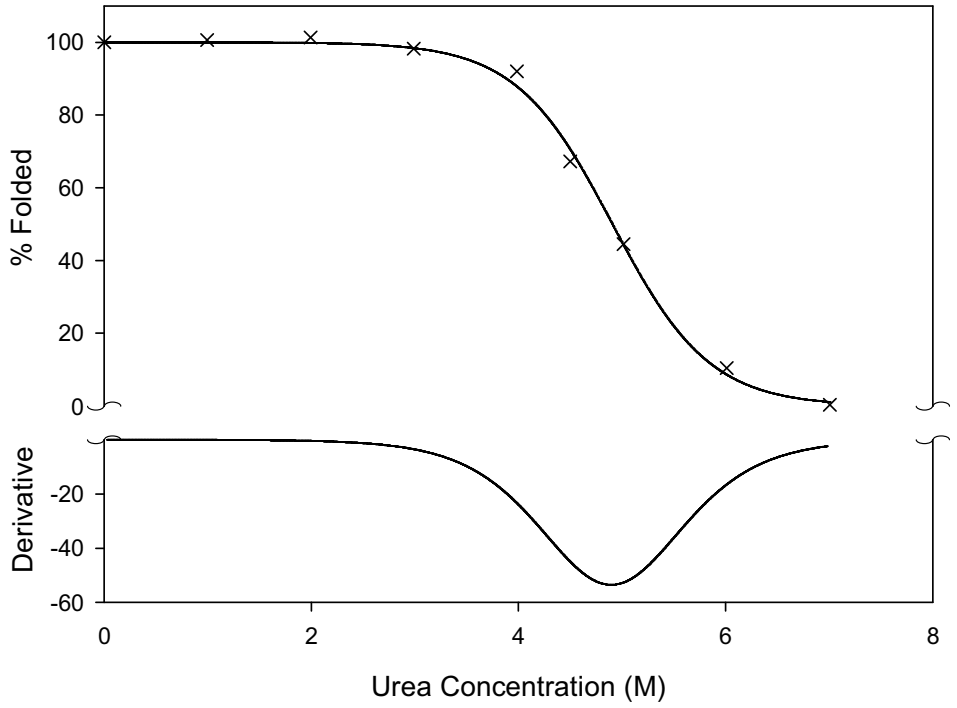

Figure 3.5. Chemical denaturation of BSA using external fluorophore (ANS)
BSA denaturation profile with addition of ANS (1:1 ratio). BSA/ANS was denatured using urea (0-7M) using 60mM sodium phosphate buffer (pH 7.4). Final reaction volume was 280µL. Percentage unfolded shown as a function of urea concentration (M). Derivation of plot also shown to indicate $C_{1/2}$ (4.90M).

Fluorescence	$C_{1/2}$ (M)	m_G (kcal $mol^{-1}M^{-1}$)	ΔG_{H2O} (kcal mol^{-1})
Tryptophan	4.88M	0.89	4.36
ANS	4.90M	1.30	6.46

Table 3.2. Summary of stability parameters determined using external fluorophore and intrinsic tryptophan fluorescence
The determination of these parameters show that the $C_{1/2}$ is constant between both methods of fluorescence analysis values for tryptophan and ANS fluorescence to be 4.88M and 4.90M respectively.

From the results in Table 3.2 it can be seen that both methods give consistent $C_{½}$ values. This indicates that both methods can be used to confer stability parameters. It is thought that unless necessary internal fluorescence should be used, due to the variation in conferred m_G and ΔG values. It can be seen in Table 3.2 that the tryptophan fluorescence parameters of m_G and ΔG are lower than for the ANS. It can be seen that ANS is binding to the protein conferring additional stability. The increased m_G may also be due to the binding of the ANS as m_G is proportional to the number of groups and size of the complex. This result indicates comparison of proteins treated in the same way is viable (using the same type of fluorescence) when determining stability.

3.3.4. Chemical denaturant selection

When treating more stable proteins, urea denaturation may not completely denature the protein hence difficulty in accurate post folding baseline determination may be found. For this reason, other denaturants such as guanidine hydrochloride (GdHCl) can be considered. It is necessary to characterise the GdHCl as a denaturant to see if it produces similar conformational transition curves to that of urea. BSA 1.43mg/ml (21μM) was formulated at

pH 7.4 in 60mM sodium phosphate buffer and denaturation was carried out using GdHCl to establish stability parameters (Figure 3.6).

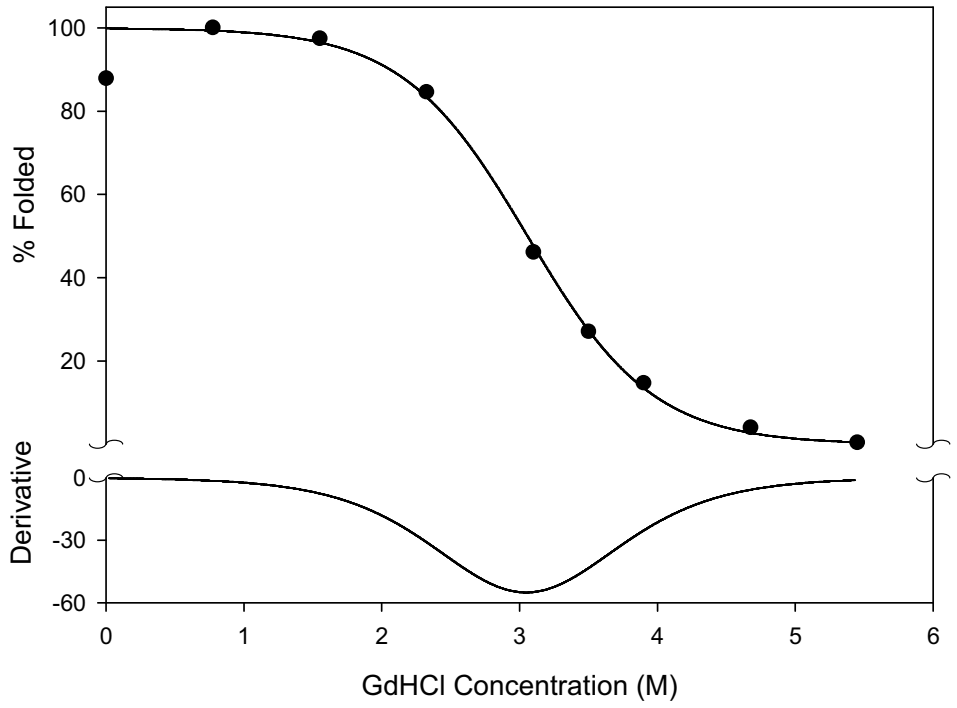

Figure 3.6. Guanidine denaturation of BSA measured by intrinsic tryptophan fluorescence

Microwell fluorescence denaturation profile with addition of GdHCl denaturant (0 to 5.5M). BSA 1.43 mg/ml (21μM) was formulated at pH 7.4 in 60mM sodium phosphate buffer. Data was fitted using non linear regression fitting. Lower graph shows the derivative of the fitted plot to indicate the maximum denaturation point believed to occur at $C_{(1/2)}$ *(3.00M).*

Denaturation Chemical	$C_{1/2}$ (M)	m_G (kcal $mol^{-1}M^{-1}$)	ΔG_{H2O} (kcal mol^{-1})
Guanidine	3.00	1.30	4.25
Urea	4.88	0.89	4.36

Table 3.3. Parameters for comparison of denaturation using various denaturants for stability curves
Parameter determination indicate guanidine is a stronger denaturant and can be used if protein is very stable and is not 100% denatured using urea. This is indicated by the decrease in $C_{1/2}$ and increase in m_G.

It can be seen from Figure 3.6 that GdHCl can be used as a denaturant to produce conformational transition curves. The curve can be accurately fitted with the derivative plotted to estimate parameters for this transition. From Table 3.3 it can be seen $C_{1/2}$ for GdHCl occurs at a much lower denaturant concentration than urea due to GdHCl being a stronger denaturant. For this reason proteins that are very stable can be tested using GdHCl, as they may be more likely to fully denature allowing accurate calculation of post folding baselines. It can be seen that the ΔG of both methods is similar with a difference in m_G. The m_G of GdHCl is higher than that of urea indicating that denaturation occurs much quicker (Figure 3.6) due to the strength of the denaturing agent. This indicates that parameters of stability can only be compared between proteins treated in a similar manner (using the same denaturant).

3.4. Conformational transition curves using chemical denaturation with BSA, RNase A, chymotrypsin

As the assay has been optimised for its application, it is important to investigate monitoring of stability as a function of various parameters seen in bioprocessing. This includes

assessing the lower limit and reproducibility of the plate reader and denaturation assay as well as its applicability. For this reason thermal denaturation, pH stabilisation, long-term denaturation effects and the effects of various buffers are investigated in this section.

3.4.1. Range and reproducibility of protein stability determination

It is necessary to assess the range and reproducibility of the microwell protein stability determination to establish the error and reliability of the results produced. In this section the reproducibility of plates read on different days were assessed. Various urea denaturations (0 to 7M) were plated using BSA 20mg/ml (20μM) in 60mM sodium phosphate buffer (pH 7.4) and compared. Average values of each concentration were plotted and one standard deviation of the error calculated. Values were averages of 16 replicates (Figure 3.7).

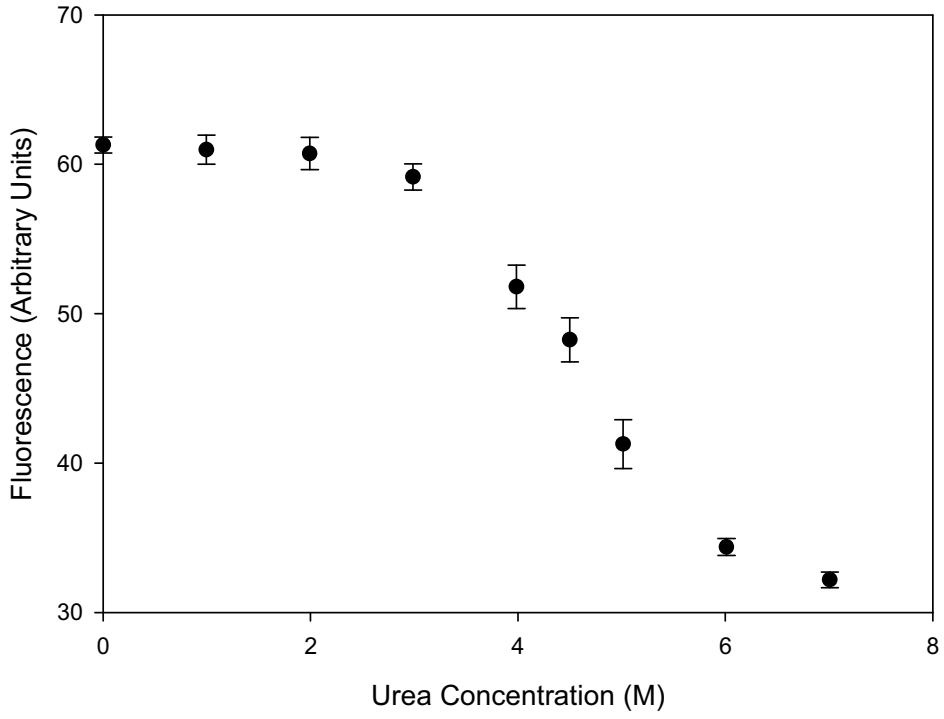

Figure 3.7. Assessment of reproducibility of assay
BSA (21μM) urea denaturation (0 to 7M) in 280μL was carried out in microwells in 60mM sodium phosphate buffer (pH 7.4). 16 replicates of each value were taken and spread was assessed to look at variability and reliability of each value. Error bars of one standard deviation are plotted. Largest errors are seen around the transition point of the graph

It appears that the largest errors are seen around the transition points. Errors of one standard deviation on values range from 0.9% to 4.0% of the overall value with the largest standard deviation seen at 4.5M urea concentration. This may be due to pipetting error, as the error is not seen throughout the profile (for example at the baselines). This indicates it may be optimal to increase the number of points around the transition point of denaturation to compensate for inaccuracies.

To investigate the lower range of detection, the concentration of BSA was decreased, so the equipment could no longer accurately detect a signal. In this case it was thought that it

would be more relevant to collect protein denaturation profiles at each concentration. The equipment may be able to detect lower values of protein concentration but at these low values may be unable to accurately detect a stability profile. This is due to the decrease in fluorescence as a function of denaturant concentration i.e. towards the higher concentrations of denaturant.

Gain of the equipment was taken to the maximum recommended by the manufacturer to allow detection of the lower concentrations. BSA was tested at concentration 2.6μM, 1.1μM and 0.5μM to characterise the limits of detection. It can be seen that a profile is produced at 2.5μM and 1.1μM that can be fitted using the two state model (Figure 3.8 a, b). This is not seen at 0.5μM as there is a large deviation in fit (Figure 3.8c). This fit does not give similar parameters with $C_{1/2}$ varying to 5.1M for a concentration of 1.1μM BSA. This may be due to the variability of results as denaturation begins (3 to 4M) causing an inaccurate fit. There is also an increase in error on values. At 0.5μM it can be seen that there is no determinable profile and fitting is not appropriate on this denaturation curve. Each value in this profile has large errors associated with each reading, with 7 out of the 9 readings having an associated error of one standard deviation over 3% with a maximum of 5.5% of the reading. For this reason it is advisable to take readings at concentrations above 1.1μM. For use with different proteins, concentrations should be used that have an equivalent fluorescence reading with this gain. It is necessary to know this range of detection as it allows calculation of number fluorescent detectable in a fluorescent system.

(a) ***(b)***

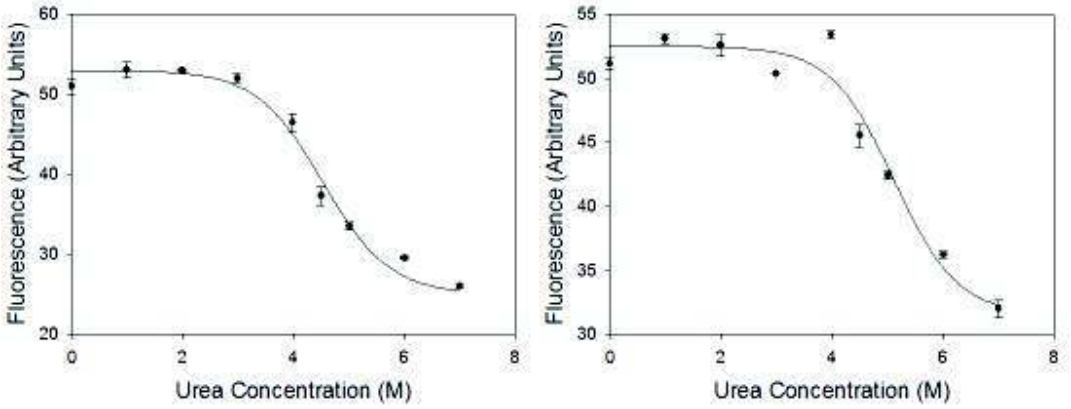

(c)

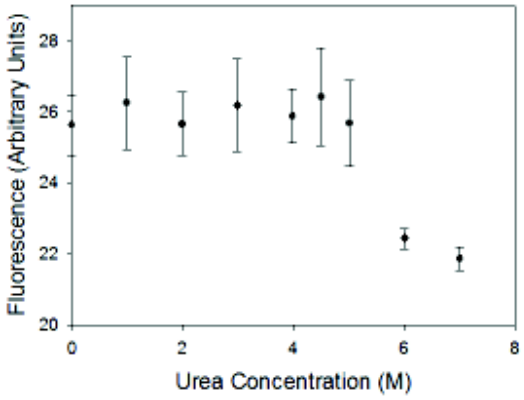

Figure 3.8. Limit of detection of plate reader
Protein denaturation was tested at various concentrations (2.6μM(a), 1.1μM(b) and 0.5μM(c) respectively) to characterise limits of detection. Standard deviations of results show that the limit of detection is reached at 1.1μM with errors of one standard deviation increasing as concentration is reduced to 0.5 μM. At 2.6μM curves can still be determined with errors of one standard deviation being low.

3.5. Protein denaturation using temperature

In bioprocessing optimum parameters for each stage can vary. This is particularly seen with temperature. Protein denaturation can occur with small variations in temperature. This may not always be seen by conventional methods such as aggregation studies. For this reason it is important to assess the ability of UV fluorescence to detect thermal denaturation. It is also important to see how thermal inactivity can affect chemical denaturation as an assessment of protein stability. To carry out thermal denaturation the plate reader must first be characterised for its heating profile.

3.5.1. Characterisation of thermal increase in plate reader

Heating in the BMG FLUOstar is carried out using a temperature control system that allows heating up to 60˚C. According to the manufacturers specifications the temperature stability is 0.2˚C. Stable and uniform incubation is carried out using temperature regulated heating plates above and below the entire microplate. Using this system it is important to characterise temperature increase in the system to allow accurate measurement of protein thermal denaturation as heating is not directly on the plate. A thermocouple placed in 280µL of 60mM sodium phosphate buffer in each well to measure heating across the plate taking care not to cover the well and to fully submerse the probe. The error on this measurement was characterised by looking at various well positions on the microplate to determine if distribution of heating is equal throughout the plate. As can be seen from Figure 3.9 a maximum temperature of 57.4˚C was reached. There appears to be a maximum standard deviation of 3.31 in this profile. However it is seen that the temperature at time

zero also has a standard deviation of 1.84. This could be the cause of the larger standard deviation on the later values. For this reason the starting temperature should be made kept constant (24.7˚C) allowing the average values of temperature to be accurate. It can be seen that there is a sigmoidal increase in temperature with time as expected with heating in microwells.

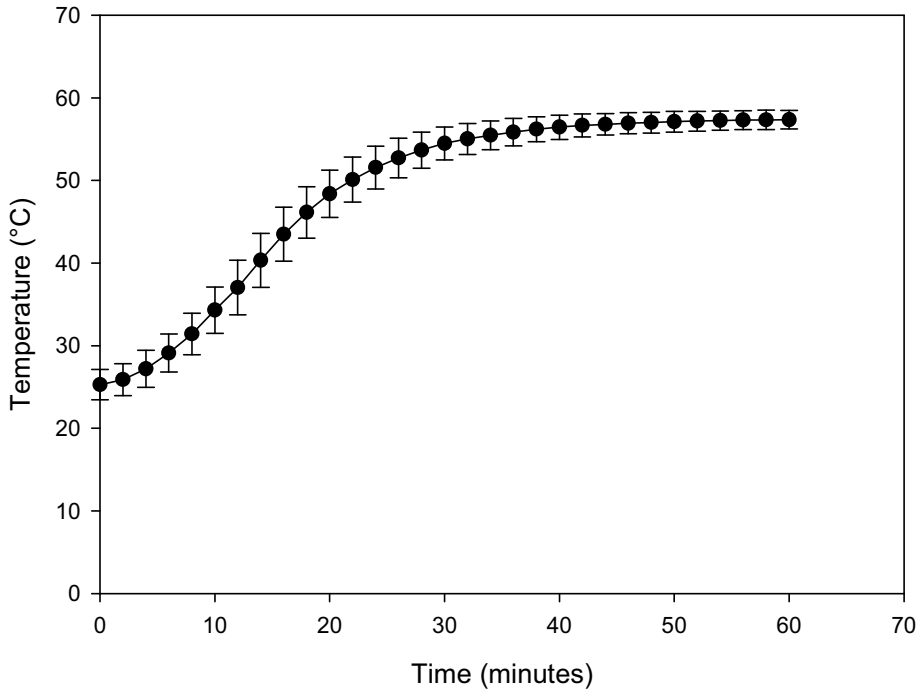

Figure 3.9. Profile of heating in BMG FLUOstar
280µL sodium phosphate buffer was heated in the BMG FLUOstar plate reader. Plate reader heating plates were set to 60˚C and well temperature was measured. A thermocouple was placed around the plate to determine variation around the well. Temperature reaches a maximum of 57.4˚C over 60 minutes. Errors are plotted as one standard deviation.

3.5.2. Thermal denaturation of BSA

Thermal denaturation was carried out using 1.43mg/ml of BSA in 50mM TRIS buffer at pH 7. Thermal heating plates were set to 60˚C and fluorescence readings were taken every 2 minutes for the first 30 minutes and every 5 minutes after. Fluorescence was plotted as a function of temperature. Temperature range was 24.7 to 57.4˚C (Figure 3.10).

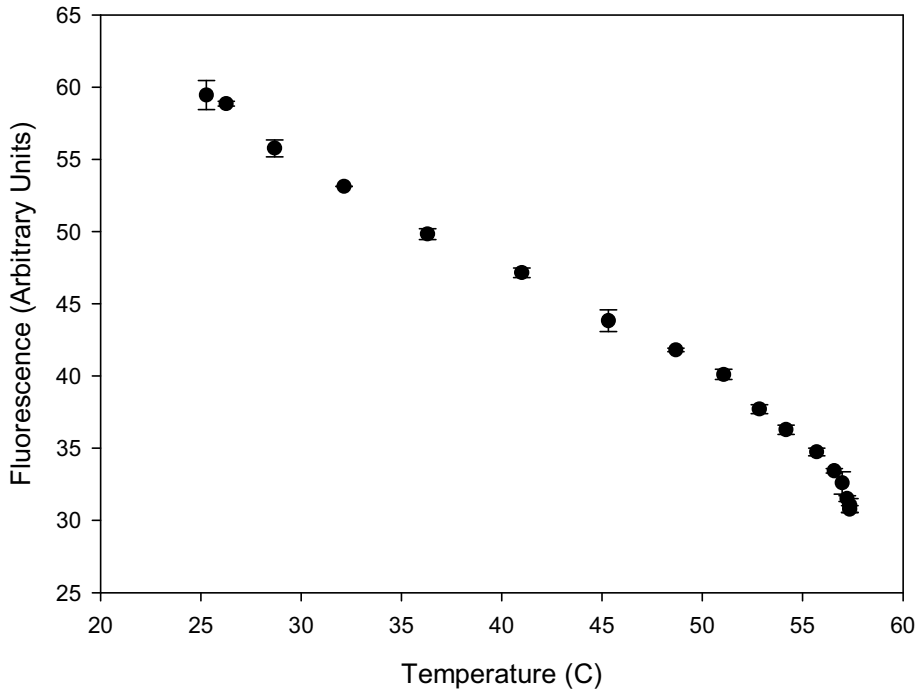

Figure 3.10. Thermal denaturation of BSA
20mg/ml BSA (0.3mM) in 60mM sodium phosphate buffer was heating using the BMG FLUOstar plate reader. A temperature range of 24.7 to 57.4˚C was used. Fluorescence is plotted as a function of temperature. Measurements were carried out in triplicate and standard deviation of fluorescence plotted. A decrease in fluorescence can be seen with temperature increase however profile is not sigmoidal as expected.

It can be seen that as temperature increases, a decrease in fluorescence is seen. The melting temperature of BSA is known to be 59˚C in 20mM TRIS buffer at pH 7.2 (Arakawa et al. 2000). It is thought that the experimental range of thermal denaturation is too narrow for accurate measurement of melting temperature. It can be seen however that a change in temperature causes a linear decrease in fluorescence, which maybe due the experimental range in the linear region of the sigmoidal curve of denaturation. For this reason it is thought that it is possible to detect a change in stability with thermal denaturation. By producing this profile it can be seen that BSA in this formulation is most stable at 24.7˚C. This can be compared to BSA in various other formulations to compare stability. Chemical denaturation can also be carried out in addition to thermal denaturation to assess the decrease in stability by parameters determined. It is thought that although thermal denaturation is not complete due to the limited experimental range, fluorescence can still be used to detect changes in stability due to thermal denaturation.

3.6. Protein denaturation in formulation

There are various conditions in manufacturing that need to be monitored, in both processing and formulation. In this section we look at effects such as pH on protein stability. Other conditions that are discussed are the effect of long-term denaturation (similar to shelf life) and buffers on urea denaturation. It is important to understand these conditions and their effect on the protein, by imitating formulation conditions allowing optimisation to increase shelf life.

3.6.1. pH effects

pH may have a dramatic effect on the stability of a protein. Although a large number of proteins are most stable at physiological pH 7 this is not always the case. It is thought that using this fluorescence technique can allow the prediction and optimisation of formulation without high reagent consumption. Proteins were treated with various pHs, to assess stability changes. All proteins were tested in 50mM TRIS pH range 3 to 10 (Figure 3.11).

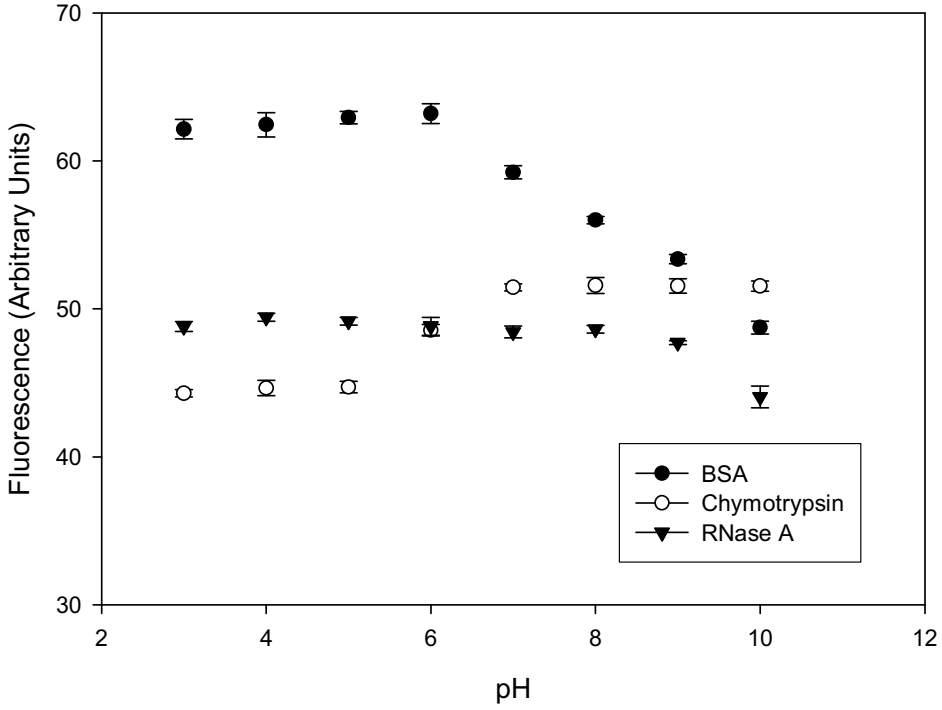

Figure 3.11. pH denaturation of various proteins
pH denaturation was carried out on BSA, chymotrypsin and RNase A. Denaturation was performed in 50mM TRIS buffer (pH 3 to 10) in 280µL. Proteins were used at 1.43mg/ml RNase A, 0.71mg/ml chymotrypsin and 0.71mg/ml BSA. RNase A shows a slight decrease in signal from pH 6 to 9. There is a dramatic decrease seen in signal at pH 10. Chymotrysin appears to increase in fluorescence with an increase in pH whereas BSA shows a decrease in fluorescence as pH is increased.

RNase A fluorescence decreases slightly with a increase in pH to pH 9. There is a dramatic decrease in fluorescence at pH 10. This indicates that RNase A increases in stability as pH increases. Chymotrypsin shows a 10% increase in fluorescence from pH 6 to 10. This may be due to the aggregation of the protein caused by pH. This is thought to cause complications when considering urea denaturation, as this aggregation will cause irregular denaturation profiles. It is known that the isoelectric points of chymotrypsin, RNase A and BSA are 7.4, 9.6 and 4.7 respectively. As a protein passes its isoelectric point a structural change maybe seen due to repulsive forces in the protein. This is consistent with data obtained in Figure 3.11 which shows a change in fluorescence as pH reaches the isoelectric point of chymotrypsin and RNase A.

3.6.2. Long term denaturation effects

It is important to establish whether this system can detect small changes in protein condition. It was thought that a protein should be tested that has been thermally treated for prolonged periods of time and then cooled to see if changes in stability can be detected using chemical denaturation. Although chemical denaturation is not used in many processes, in this case it can be used as an indicator of protein stability. BSA 20mg/ml (0.3mM) was heated at 70°C for between 20 to 140 minutes. Samples were allowed to cool and chemically denatured (0 to 7M). Heating and denaturation was carried out in 60mM sodium phosphate buffer. Each sample was carried out in triplicate in a volume of 280µL. From the results (Figure 3.12) it can be seen that there appears to be some irregularity in $C_{1/2}$ values (Table 3.4), showing some irregularities in protein stability. This may be due to the reversibility of thermal denaturation. There is however a general increase in m_G (Table

3.4), with prolonged heating. This implies that the denaturation of the protein occurs quicker as treatment time of BSA is increased. There is also a general increase in ΔG showing that protein stability in its physiological state appears higher as prolonged heating occurs however denaturation occurs more quickly. These erratic results indicate that this is not the ideal way to treat the protein to determine effect due to the reversibility of the thermal reaction. It may be more advantageous to carry out the urea denaturation and long term heating simultaneously to increase accuracy and decrease variability.

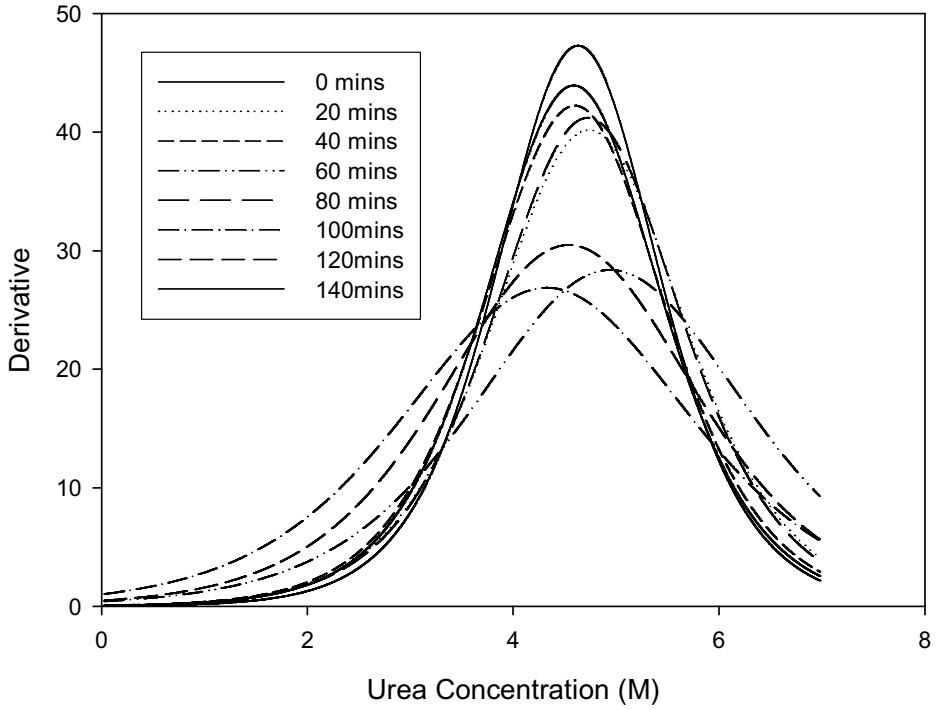

Figure 3.12. Urea denaturation after heating to 70°C
BSA 1.43mg/ml (0.3mM) was heating to 70°C for between 20 to 140 minutes. Samples were allowed to cool and chemically denatured using urea (0 to 7M). Heating and chemical denaturation was carried out in 60mM sodium phosphate buffer in triplicate. Heating was carried out on a hotplate. Derivative of fits are plotted as a function of urea concentration (M).

Time of Heating (minutes)	$C_{1/2}$ (M)	m_G (kcal $mol^{-1}M^{-1}$)	ΔG_{H2O} (kcal mol^{-1})
0	4.85	0.88	4.30
20	4.75	0.92	4.33
40	4.61	0.94	4.24
60	4.95	0.93	4.22
80	4.74	1.01	4.47
100	4.34	1.00	4.44
120	4.55	1.09	4.65
140	4.60	1.17	4.64

Table 3.4. Parameters determined from long term denaturation effects
Determination of $C_{1/2}$ shows no over all trend as temperature increases. m_G and ΔG_{H2O} increases as temperature increases indicating that denaturation occurs more quickly.

3.6.3. Denaturation using various buffers

To assess parameters for bioprocessing it was thought that buffer choice might cause a variation in protein stability. For this reason it is important to understand this stability to make a choice of the ideal buffer for a process or formulation. This was tested using various buffers and chemical denaturation with BSA.

Urea denaturation was carried out in the presence of various buffers to examine the effect of buffer formulation on protein stability. Each experiment was carried out with a final concentration of 21μM of BSA. Denaturation was carried out with a final urea concentration range of 0 to 7.4M. Buffers used were 60mM sodium phosphate buffer (pH 7.4), phosphate buffered saline (PBS) (pH 7.0), 50mM TRIS buffer (pH 7.0), 1M sodium bicarbonate (pH 7.95) In Figure 3.13, Table 3.5 it can be seen PBS confers the least stability with denaturation occurring quickly. The buffer that appears to confer the highest stability is TRIS buffer with slowest denaturation occurring in sodium phosphate buffer,

which may make it the best buffers for processing. This method gives an indication of optimal parameters in processing however the use of multiple methods of denaturation may be advantageous.

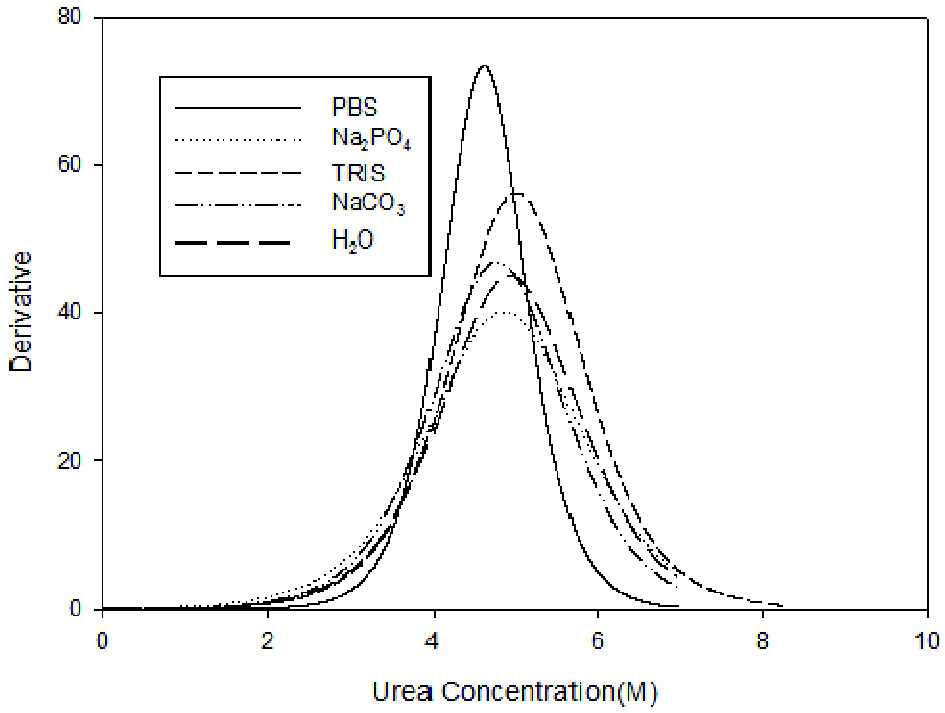

Figure 3.13. BSA denaturation using various buffers.
Urea denaturation was carried out in the presence of various buffers to confer the effect of buffer on protein stability. Each experiment was carried out with a final concentration of 0.2mM BSA. Denaturation was carried out with a final urea concentration range of 0 to 7.4M. Buffers used were 60mM sodium phosphate buffer (pH 7.4), phosphate buffered saline (PBS) (pH 7), 50mM TRIS buffer (pH 7.4), 1M sodium bicarbonate (pH 7.95) and water. It can be seen that various buffers confer different stabilities of BSA. This is summarised in the table below.

Buffer	$C_{1/2}$ (M)	m_G (kcal $mol^{-1}M^{-1}$)	ΔG_{H2O} (kcal mol^{-1})
PBS	4.58	1.21	5.66
Sodium Phosphate	4.87	0.88	4.29
H_2O	4.85	1.36	6.73
TRIS	5.60	1.26	7.00
$NaHCO_3$	4.76	1.31	5.42

Table 3.5. Summary of protein stability occurring in various buffers.
Results show variation in protein stability when using various buffers. It is found that TRIS confers the most stability of all the buffers with PBS conferring the least stability. Denaturation occur quickest is H_2O with slowest in sodium phosphate buffer.

3.7. Conclusion

In bioprocessing it is very important to monitor the condition and stability of a protein in protein engineering, formulation and processing. This can be done by various methods including fluorescence spectroscopy. Typically assays that involve fluorescence use reagents volumes in the order of millilitres, which can be expensive. Recent developments in bioprocessing have moved to testing in microlitres. For this reason it is important to characterise the adaptability of a fluorescence assay to perform in this range. This assay should be adaptable to bioprocessing conditions and scale down thereby increasing throughput and reducing reagent consumption.

The aims of this chapter were to assess the suitability of an established microwell assay by looking at variables relevant to bioprocessing and optimising this method towards this application. This included characterisation of the method assessing range and reproducibility to produce a route for high throughput protein stability screening. This can in turn allow optimisation of a process, screening of product condition, stability and quality

during processing and characterisation of optimum formulation to prolong shelf life. These results show that using clear plates to look at stability results gave a higher reproducibility than that of black plates. This in turn increased the average accuracy, reproducibility of results and signal to noise ratio. A comparison of external fluorophore to internal fluorescence determined that both could be used to investigate stability of the protein, however to minimise interaction with the protein natural fluorescence should be used if possible. The external fluorophore also allows a higher quantum efficiency, wavelength and testing of proteins without tryptophan residues.

This method is found to be sensitive enough to be used in microwells allowing a rapid screening of protein stability in conditions representing bioprocessing. This method can be used to monitor stability but does not interfere with protein structure to confer change in conformation. It can be used as a warning of a change in protein condition, which can then be followed by using other methods of characterisation such as circular dichroism or HPLC. This protein assay system has been shown to be adaptable to scale down and increased throughput both of which may have the potential of further improvement.

It is hypothesised that investigation of multiple conditions allows the production of 3D landscapes to characterise a protein's stability in various conditions. This would however need a large number of data points, for increased accuracy. For this reason it is thought that there is the potential for improvement of this assay detection with improved automation and scale down to microfluidics as discussed in the next chapter.

Chapter 4:

Fluorescence determination of protein stability: Development and operation of microfluidic apparatus

4.1. Introduction

There is currently a need in bioprocessing for an assay system to assess protein quality using inexpensive equipment, while reducing reagent consumption and decreasing labour costs. The potential for fluorescent protein stability detection has lead to a scale down to the microwell tryptophan fluorescence assaying (Aucamp et al. 2005). Although the microwell system, discussed in the previous section, has increased throughput while decreasing reagent consumption, it is thought that further scale down is possible incorporating automation and increasing analysis speed. However interest has turned to microfluidics to present a solution to this problem.

The aim of this chapter is to develop a high throughput, inexpensive method to assess stability of a protein using a fluorescence unfolding assay (Pace 1986). It is thought that microfluidics has the potential to do this however optimisation of fluorescence detection is needed at this scale. The small volumes used in microfluidics may make detection of natural fluorescence difficult due to the low quantum efficiency of tryptophan fluorescence. Hence it is important to assess the feasibility of using such small-scale devices by comparison to previously published data and use of known fluorophores at the microwell scale. UV detection in capillaries by confocal microscopy can also be used to assess feasibility.

Once feasibility had been determined, an optical system was designed; built and tested that was powerful enough to detect low intensity fluorescence. Each component was chosen for its high sensitivity and compatibility to this fluorescence system. The system was optimised and characterised for sensitivity and reproducibility.

Once the system had been developed, it was evaluated to show comparability to other methods such as the previously mentioned microwell method in the determination of stability parameters. The microfluidic apparatus was assessed by determining the lower limit of detection to establish the magnitude of scale down. This comparison was carried out to look at the range of detection of both concentration and protein stability curves. By assessing the range of detection, this allows users in the bioprocessing industry to quantify the concentrations to be used in this device. Some processes may not have the required concentration, especially in the developmental stages and is a key factor in assay development. The scale down of this assay to microfluidics is to be assessed to look at increase in throughput and decrease in scale was also determined.

Work in this chapter was carried out in collaboration with Matthieu Gaudet of the London Centre for Nanotechnology (LCN) as part of the associated BRIC project supported by the BBSRC.

4.2. Feasibility of microfluidic protein detection

Microfluidic systems use volumes of fluid that can range from nanolitres to picolitres of detection volume. Due to this decreased volume, sensitivity of detection must be increased. It is important to assess the feasibility of using these small detection volumes to accurately detect protein concentration and stability. If fluorescence is undetectable as volume is reduced, sample concentration can be increased. However one of the principal aims of this thesis is to reduce reagent consumption therefore increasing the concentration of the protein solution may counteract this aim. For this reason the concentration (number of molecules per volume) to create a detectable fluorescence must be calculated. It is important to

consider that the detection of protein denaturation may not be possible using natural fluorescence due to the low quantum efficiency of tryptophan residues. For this reason feasibility was assessed using both internal and external fluorophores to increase both the quantum efficiency and the wavelength at which detection is carried out.

Feasibility was assessed by comparison to 96 microwell plate format and previously published microfluidic data (Ocvirk et al, 1998) for the detection limit of fluorescein. Comparison to microwells was carried out by assessing the amount of fluorophore (fluorescein) to internal (BSA) and external (BSA/ANS) fluorescence needed to detect a given fluorescence. The detection volume at which the plate reader reads was determined experimentally, allowing calculation of the number of molecules needed to produce this specific fluorescence. This allows the calculation of the feasible scale down ratio for detection of fluorescence at microscale. Internal and external fluorescence concentration, and hence number of molecules for this fluorescence were determined using the 96 well microplate method. Using the feasible scale down ratio from the fluorescein experiment, the equivalent fluorescence signal detectable can be scaled to calculate the required concentrations for both the internal and external fluorophores in microfluidics in a specific volume. If a high concentration is required to detect at microfluidic scale, the microfluidic system development is determined as unfeasible as high concentrations of protein are not available in some processes. If this is the case an external fluorophore (ANS) with a higher emission and excitation wavelength as well as higher quantum efficiency was tested.

4.2.1. Minimum volume detectable in microwells

To ensure the accuracy of the microplate reader and to avoid artefacts being present on the data, we assessed performance at a range of volumes. Detection was carried out with excitation and detection from the bottom of UV transparent plates. Signal in the microplate reader was detected using BSA samples of 20mg/ml (30μM). Samples were used in decreasing volumes from 10 to 280μL to determine the minimum well volume detectable. The fluorescence signal decreased when the signal detection volume is reached. In Figure 4.1, the fluorescence signal remains constant upon reaching the volume of 40μL. Below 40μL the volume of liquid in each well was too low for detection and signal decreased to the baseline value. Standard error also dramatically increases on volumes under 40μL indicating that the minimum detectable volume is 40μL and this value is used in further calculations. This result assumes that there is a full coverage of liquid on the well bottom with no meniscus affecting the reading.

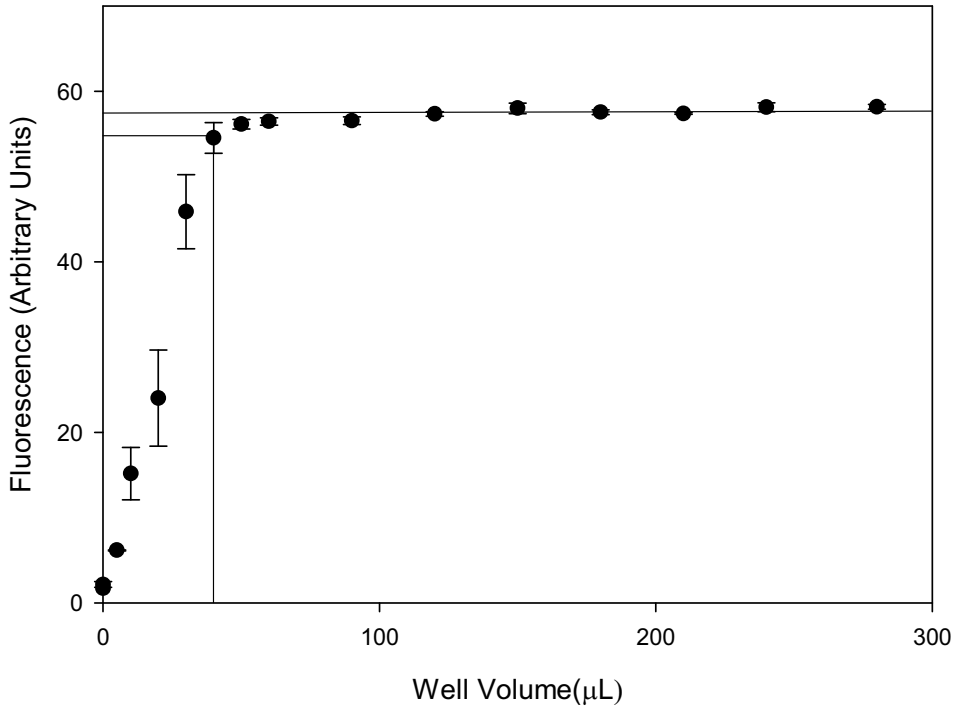

Figure 4.1. Variation of fluorescence signal with well volume
Fluorescence of BSA at 20mg/ml (30μM) in sodium phosphate buffer 7.4 in 96 well microplates using the BMG FLUOstar plate reader. Samples were read using various volumes ranging from 10 to 280μL. Fluorescence remains constant down to 40μL (indicated by the upper baseline). Fluorescence decreases dramatically after this value down to the background value. Standard error also appears to increase after 40μL.

4.2.2. Feasibility study

.

From literature it is known that 225 molecules of fluorescence can be detected in 1 picolitre of fluid (Ocvirk et al, 1998). For these calculations it is assumed that the area of detection for BSA and ANS in microfluidics is also 1ρL of fluid to assume use of similar equipment for detection. Three fluorophores ANS, BSA and fluorescein were tested at various concentrations to determine concentration against fluorescence signal for each fluorophore (Figure 4.2). From this graph values of concentration for equivalent fluorescence were

found. The number of molecules in the detected volume (assumed to be 40μL from Figure 4.1) were calculated. This was compared to the 225 molecules of fluorescein measurable at microfluidic scale to assess the feasibility of protein measurement at microfluidic scale using tryptophan fluorescence and ANS fluorescence.

Fluorescein concentration (5 to 50nM) results were in a detectable range of the plate reader and results were plotted as a function of fluorescence. As expected this gave a linear relationship with a good R^2 value of 0.994. Fluorescence of BSA/ANS also appears to increase linearly with concentration however BSA fluorescence against concentration appear to be linear for initial values however at higher concentrations there appears a decrease of fluorescence in relation to that expected. This maybe due to saturation of samples causing a decrease in detected fluorescence of the plate reader as the full fluorescence signal could not be measured.

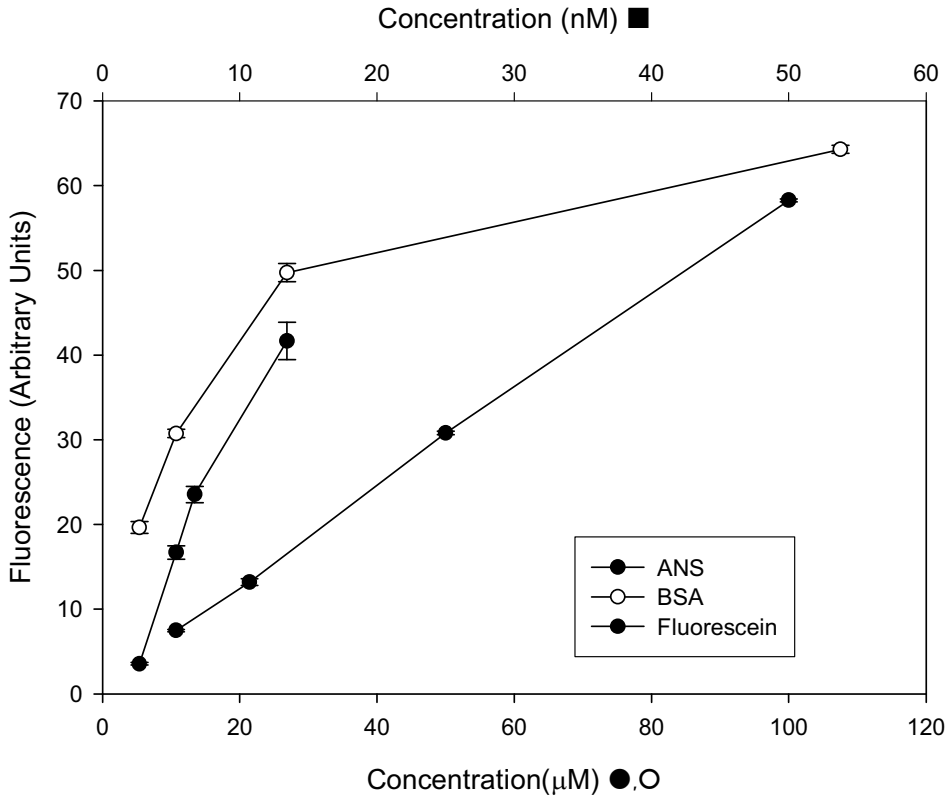

Figure 4.2. Comparison of standard curves for various fluorescent molecules
Fluorescein, ANS and BSA were assessed in sodium phosphate buffer pH 7.4 to assess the variation of fluorescence of internal and external fluorophores with concentration. It is seen that 25nM fluorescein, 13.4μM BSA/ANS and 10.8μM BSA have an equivalent fluorescence value. These values were used to assess feasibility of using microfluidics. Saturation is seen in higher concentrations of BSA. Standard deviation of each sample is also plotted.

4.2.3. Calculation to determine minimum molecules of detection

From the results in Figure 4.2 it can be seen that the concentrations of equivalent fluorescence in microwells are BSA (10.75μM), ANS (13.44μM) and fluorescein (25nM). If we use the previously determined 40μL detection volume (Figure 4.1), number of molecules detected in microwell can be calculated as BSA (2.58×10^{14} molecules), ANS (3.23×10^{14} molecules) and fluorescein (6.00×10^{11} molecules). If at microfluidic scale 225 molecules can be detected (Ocvirk et al, 1998) it can be calculated that for an equivalent fluorescence measured in 1ρL, the BSA concentration would be 0.16μM (0.011mg/ml) and the BSA/ANS concentration would be 0.20μM (0.013mg/ml). This limit of detection is feasible for the use of microfluidics as a tool for protein fluorescence detection and infers the possibility of scale down. A reduction in volume from 40μL to 1ρL indicating a scale down potential of 10^{-6} in volume and 10^{-10} molecules of reagent.

4.3. Confocal microscopy detection of capillary fluorescence

To practically assess the feasibility of using natural tryptophan fluorescence for protein stability detection in capillaries, a confocal microscope was used to detect tryptophan fluorescence signal. Confocal microscopy was carried out on a TCS SP confocal microscope, which is a 3 colour UV and visible microscope in one system using fiber coupled UV VIS IR laser. Excitation and emission were detected using a filter for wavelengths 190 to 370nm specialised for use with a commonly used dye, 4',6-diamidino-2-phenylindole (DAPI) stain. A capillary was stripped of outer coating and filled with 200mg/ml of BSA in 60mM sodium phosphate buffer (pH 7.4). It was then fixed to a microscope slide to inhibit movement. Using the confocal microscope at pinhole aperture

of 1.4a and a PMT gain of 124V, UV fluorescence can be detected at very low levels (Figure 4.3a). Fluorescence detected was inconsistent throughout the capillary (in Figure 4.3b). Although fluorescence was detected at this high concentration of BSA, no consistent results for total fluorescence in each confocal slice could be determined. There was also seen to be a high background signal due to the high gain and aperture.

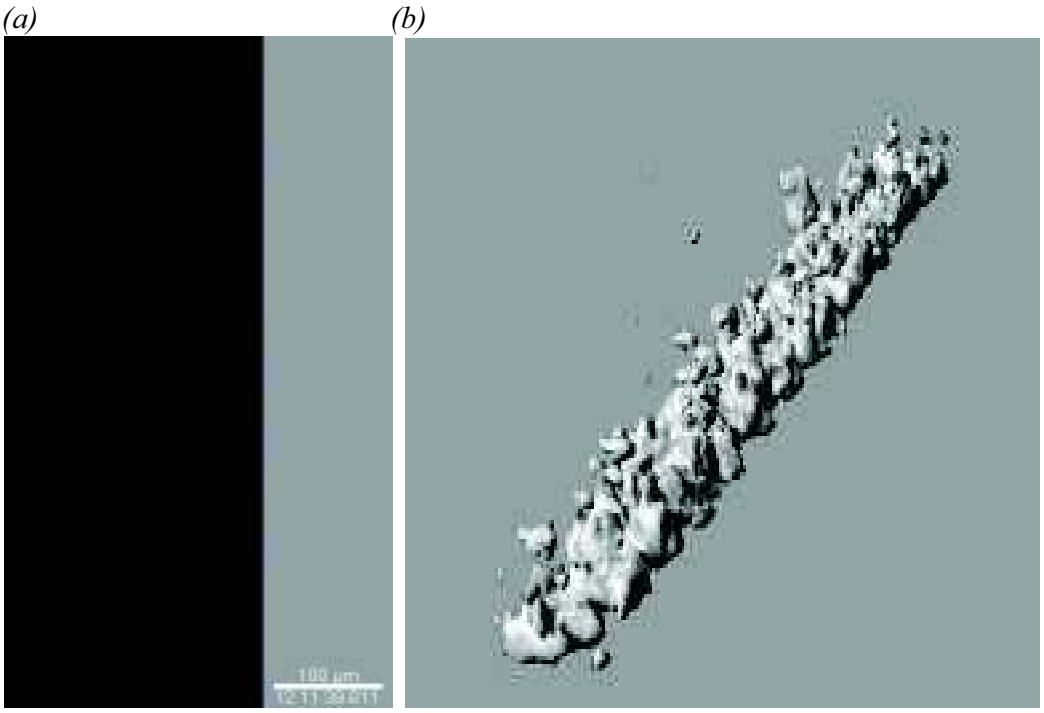

Figure 4.3. Confocal detection of tryptophan fluorescence in a capillary
Capillary was filled with BSA 200mg/ml (3mM) in 60mM sodium phosphate buffer pH 7.4 and detected using confocal microscopy. Filters used were optimized for DAPI stain. (a) shows the visual results with a z stack of slices shown in b. Fluorescence is detected but could not be quantified due to inconsistency in detection. System was determined not optimized for detection of protein stability.

This result was seen using a high gain and width of aperture hence indicating that this system is inadequate for protein stability studies. The system is not optimized for detection of the maximum emission and excitation related to the tryptophan residues. This is due to the filter and optics used, which are optimized for much stronger UV stain (DAPI). It is possible to detect tryptophan fluorescence indicating feasibility at this scale although detection is not adequate for quantification of protein stability studies. This shows the need for a microfluidic scale detection system for protein stability studies.

4.4. Concentration viscosity investigation

Due to the small dimensions of microfluidic systems, it can be possible for high pressures to occur. A high pressure in a microfluidic system can be detrimental to the system itself due to the small radius of the capillary. This in turn can cause to leaking, air in the system or detection variability as seals in the system may be compromised. As viscosity and pressure are related by Poiseulle's Law *(Equation 4.1)*, viscosity can be measured to investigate pressure in the system.

$$\Delta \boldsymbol{P} = \frac{\boldsymbol{8\mu LQ}}{\boldsymbol{\pi r^4}} \qquad \textit{Equation 4.1}$$

Where **ΔP** is the pressure drop, **L** is the length of tubing, **μ** is the dynamic viscosity, **Q** is the volumetric flow rate, **r** is the radius of the tubing, **d** is the diameter. As viscosity of a liquid increases flow pressure will increase. Samples of BSA were prepared at concentrations 0.1 to 500mg/ml in 60mM sodium phosphate buffer pH 7.4. Viscosity was measured using a rheomat rotational viscometer to determine the shear stress and shear rate

of the liquid. The viscometer uses a cylinder rotated at a specific speed to measure shear rate by measuring the torque the liquid exerts on the cylinder. When viscosity is plotted as a function of concentration (Figure 4.4), it can be seen that viscosity increases slowly up to a concentration of 200mg/ml. After 200mg/ml viscosity begins to increase dramatically with concentration. The maximum concentration of protein tested should hence not exceed 200mg/ml to keep viscosity and pressure at a constant level to reduce damage to the system.

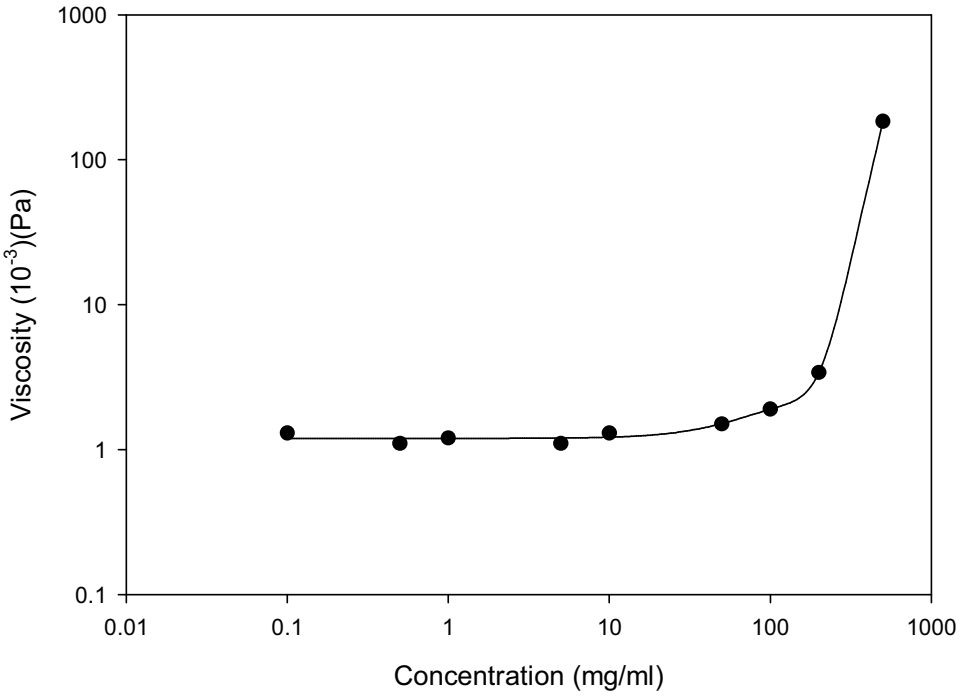

Figure 4.4. Viscosity as a function of albumin concentration
BSA solutions were prepared in 60mM sodium phosphate buffer pH 7.4 (0.1 to 500mg/ml). Solutions were tested using a rotational rheometer to determine the associated viscosity. As concentration increased above 200mg/m, viscosity increases dramatically. This signifies an increase in pressure inferring that concentration should be kept below 200mg/ml.

4.5. Microfluidic optical detection system

When configuring an experimental system to detect fluorescence in a microfluidic capillary each component should be carefully chosen to optimise sensitivity of detection in the UV range. It is important to consider what components are needed for this system and how to optimise configuration for the highest signal to noise ratio. This system should include a high-powered emission source with a single wavelength emission of between 260 to 290nm to allow optimal excitation of tryptophan residues (Figure 4.5). Optimum emission is seen at between 340 to 350nm after excitation at 280nm however other excitation wavelength can be used with reduced emission. The excitation source should be focusable to a small beam on a microfluidic flow vessel. Beam power should be monitored so as not to allow heating of the sample, which may affect signal and cause denaturation of the sample. Excitation signal should be stable after warm up period decreasing variance in signal.

Flow cell must be UV transparent with little or no fluorescence itself and be made of a material that does not promote protein adhesion to surfaces leading to fouling. Adequate excitation and emission of the sample should be allowed with minimal interference by the flow vessel itself.

Detector should be able to detect sample emission at 320 to 380nm in the UV range while not detecting the incident beam or scattering effects that may occur from the flow cell. The detector should be sensitive enough to detect small changes in fluorescence as seen in urea denaturation (Figure 4.6) at the require wavelength. Detector output should allow easy facilitation for the user and should be capable of fast data collection and analysis.

To reduce interaction of the light from the atmosphere all experiments should be carried out in the dark. This will help to reduce the background noise and scattering from the flow capillary. All components should be secured to reduce vibration and movement.

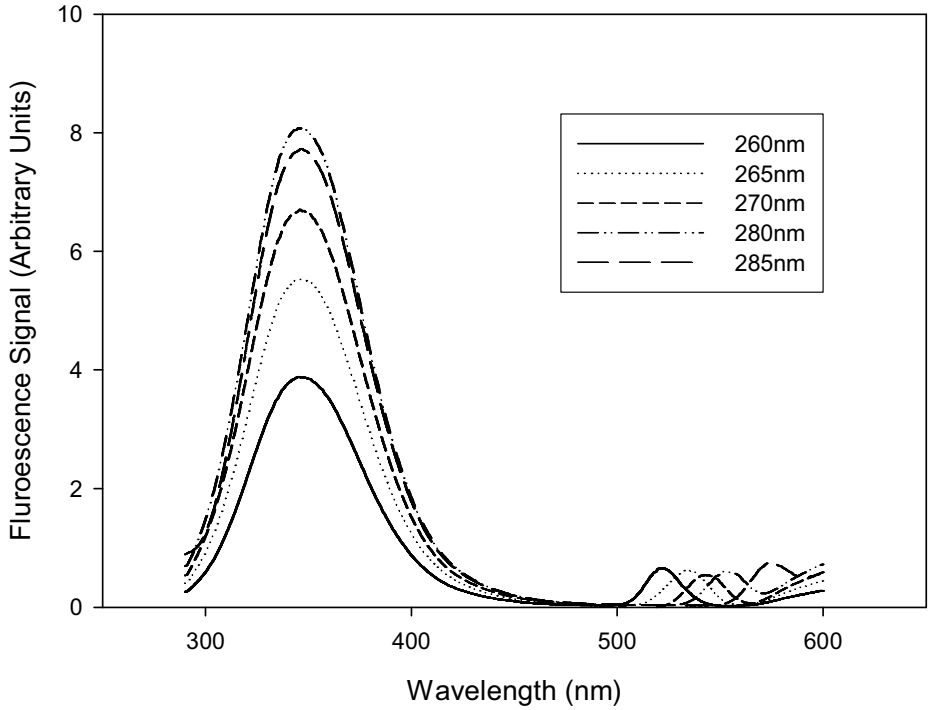

Figure 4.5. Wavelength dependency of emission spectrum of tryptophan residues
Spectral scan of emission of tryptophan residues when excited between 260 to 290nm. BSA 20mg/ml (0.3mM) in 60mM sodium phosphate buffer pH 7.4 was scanned using ***a*** *luminescence spectrophotometer. Emission maxima seen between 340 to 350nm for all excitation wavelength. Maximum emission can be seen at excitation wavelength of 280nm. 50% reduction in intensity seen at 260nm.*

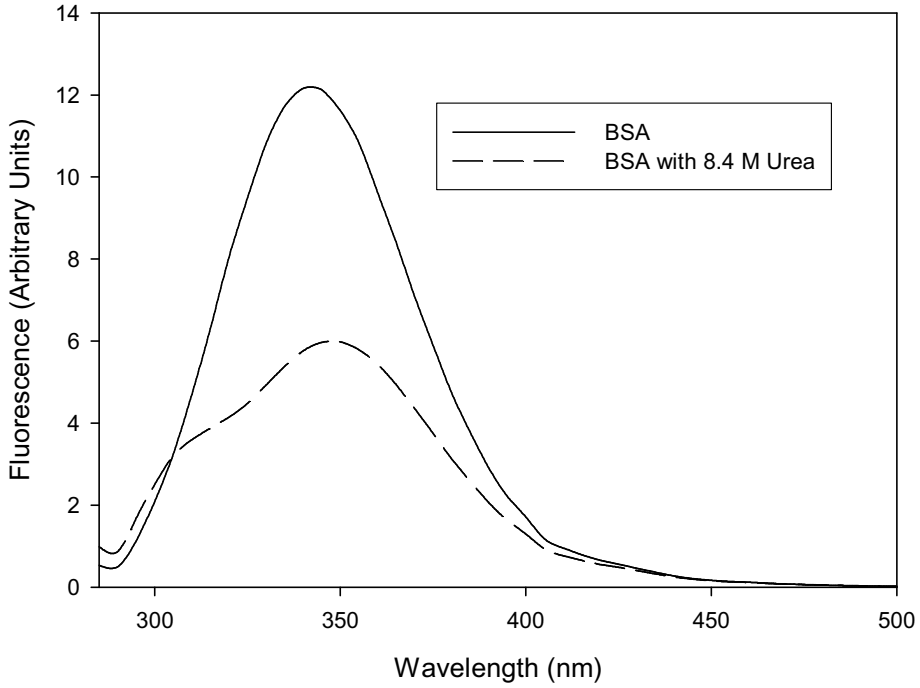

Figure 4.6. Spectral scan of BSA with urea
BSA 10mg/ml (0.15µM) in sodium phosphate buffer (pH 7.4) with and without urea (8.4M) scanned using the microwell plate reader (Tecan). Samples were excited at 280nm and a spectral scan of emission taken. With addition of urea a 50% reduction is seen at 340nm as expected. Profile is characteristic of the protein state and type.

4.5.1. Flow vessel

For the initial design of the optical detection system, a capillary was used as the flow vessel instead of a chip system. There are many advantages to using microfluidic chips such as parallelisation of a series of chips or a series of channels on one chip. They also allow the integration of several laboratory functions on chip such as mixers. The design of a microfluidic chip can sometimes be laborious however upon completion mass production can occur quickly and easily. Due to the large task of chip design and optimisation, capillary flow vessel was used in this project as a first generation microfluidic device. This capillary is prefabricated and commercially available allowing the design and optimisation

of the optical detection equipment to be decided. However the optical detection system was designed to allow the capillary flow vessel to be replaced with a chip design in the future. The scale of this capillary was larger (inner diameter (ID) of 100μM) than the conventional chip channel to allow optimisation of the system with a high level of fluorescence allowing the potential for further scale down.

4.5.2. Laser

The laser used was a diode pumped compact Q switched CrystaLaser® emitting in the UV range via a Nd:YAG (neodymium-doped yyttrium aluminium garnet) crystal. The Nd:YAG crystal typically emits at 1064nm in the infrared (IR) range. This high intensity pulse is frequency doubled using non linear optical methods to produce a 532nm green light which is frequency doubled again to produce a 266nm UV laser light. The wavelength emitted should be assessed to ensure that the 266nm wavelength is the only wavelength present. All harmonics should be filtered to ensure the protein is only excited at 266nm to not contaminate the emission signal. Through the use of filters it was found that the laser was displaying the 532nm harmonics as well as the 266nm. This will be discussed further in the filters section. Although the wavelength of the laser was not at the optimum excitation wavelength of 280nm, the 266nm laser beam still provided an emission at the desired wavelength however with a lower efficiency (Figure 4.5). Heating of the protein can be minimised by reducing the power to produce the laser beam. The laser signal has a manufacturer specified root mean squared (rms) of 5% after 3 minutes at a repetition rate of 1kHz. Pulse width is between 10 to 20 nanoseconds with a beam divergence of 3 to 4 mrad and beam point stability of 0.02mrad. The laser is triggered externally allowing control and

synchronisation with detection system. No cooling system is required other than the internal cooling, reducing vibrations of the system. Laser beam emission dimensions were 500μM by 200μM illuminating the entire capillary.

4.5.3. Photomultiplier tube (PMT)

A photomultiplier tube (PMT) was chosen instead of a charge coupled device (CCD) camera due to the high sensitivity and low noise offered by a PMT. The PMT was powered by a high voltage power supply at 1000V. This voltage allowed a high detection signal without a high associated noise. Voltage can be used to determine amplification of signal and is equivalent to gain on the BMG FLUOstar plate reader (Figure 4.7). Fluorescence signal was seen to exponentially increase with voltage. By increasing the voltage of the PMT to 1300V noise and background is increased as well as sensitivity. For this reason it was decided to use 1000V so as not to saturate the PMT and reduce background noise.

The PMT was sensitive to UV fluorescence in the range of 300-650nm. A custom made cone was placed on the PMT to reduce scattering detection. PMT was placed 5mm from capillary and positioned at 135 degrees to the incident beam to reduce detection of scatter and incident light from the laser. Neutral density filters were used to reduce PMT saturation and determine the optimum laser beam excitation strength for detection of emission by the PMT (further discussed in filters section). Saturation may cause damage to the PMT.

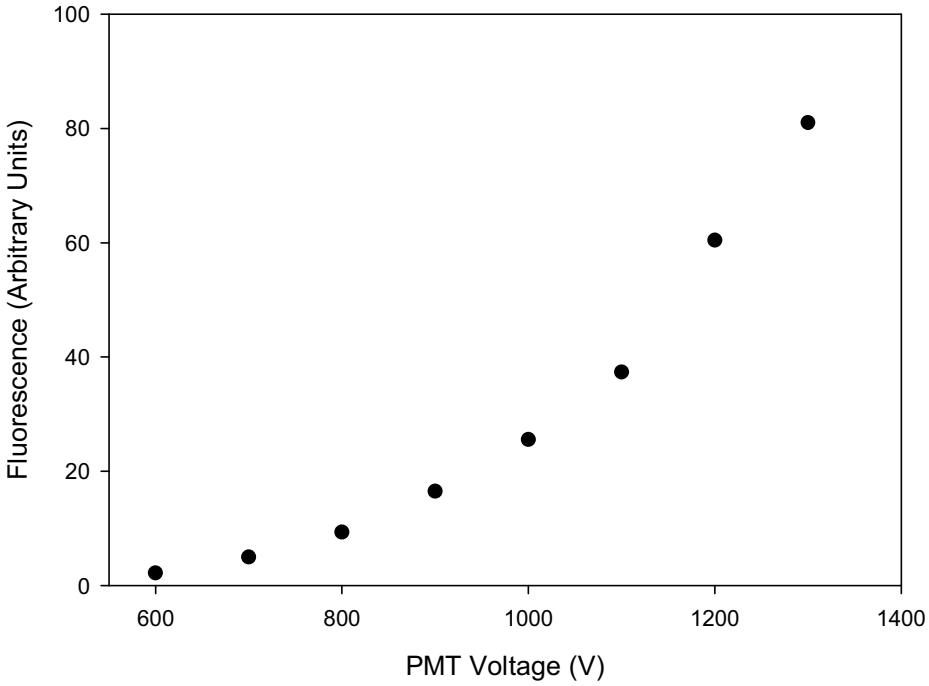

Figure 4.7. Fluorescence variation with PMT voltage
60mM sodium phosphate buffer pH 7.4 was measured in a capillary using various PMT voltages (600 to 1300V). Fluorescence exponentially increases due to PMT voltage. Voltage acts as a sensitivity gain for the equipment. 1000V was decided as an optimum for detection of sample and blank. Voltage can be increased for sensitivity however noise will also be increased.

4.5.4. Filters

Although manufacturer specifications indicated that the laser was 266nm specific, it was found that harmonics were also displayed. Initially the optical detection system did not filter the laser beam before interaction with the flow vessel however the detection of the 532nm harmonic of the laser beam indicated that a filter must be used. The 532nm harmonic is caused by inefficient doubling of the incident laser beam within the laser. The power of the laser beam and proximity of the filters caused burning and alteration of many

filters, transmission gratings and their coatings. A filter that was resistant to a high laser power and specific to 266nm allowing 97% signal transmission at 266nm (UG5, Schott).

BSA samples of 10 and 100mg/ml in 60mM sodium phosphate buffer pH 7.4 were flowed through the capillary. The empty capillary and sodium phosphate buffer was used as blanks. Optical density filters were used to reduce laser beam intensity allowing various percentages of the beam to encounter the capillary flow vessel ranging from 10 to 100%. 100% of the laser beam caused heating within the capillary and saturation of the PMT. This can be seen as a reduction in sample fluorescence of 10 and 100mg/ml samples. A 90% reduction in signal was found to still be detectable above the background level (Figure 4.8). There is the potential to increase the sensitivity of the system however heating and saturation should be avoided.

A lens was used to focus the laser beam onto the capillary. It was found that the use of a lens caused heating within the capillary. Due to the 360μM outer diameter of the capillary, the entire capillary was illuminated by the unfocussed laser beam, providing optimum signal excitation without sample heating.

The cylindrical shape of the capillary scattered the emission in 360˚. Detection of this scattering was reduced by design of a cone to cover the entrance to the PMT (Figure 4.12). The cone was placed adjacent to the capillary so signal was detected directly from the capillary and scattering was reduced. The distance between the capillary and the PMT was kept constant. Signal was filtered using a Nd:YAG, high energy laser mirror to reflect high intensity 266nm wavelengths and 340 ±2 nm biomedical band pass filter to remove the incident beam. The use of both filters for signal allowed only the tryptophan emission to be

detected. To reduce background noise from atmospheric light, detection apparatus was placed inside a custom made black matt box.

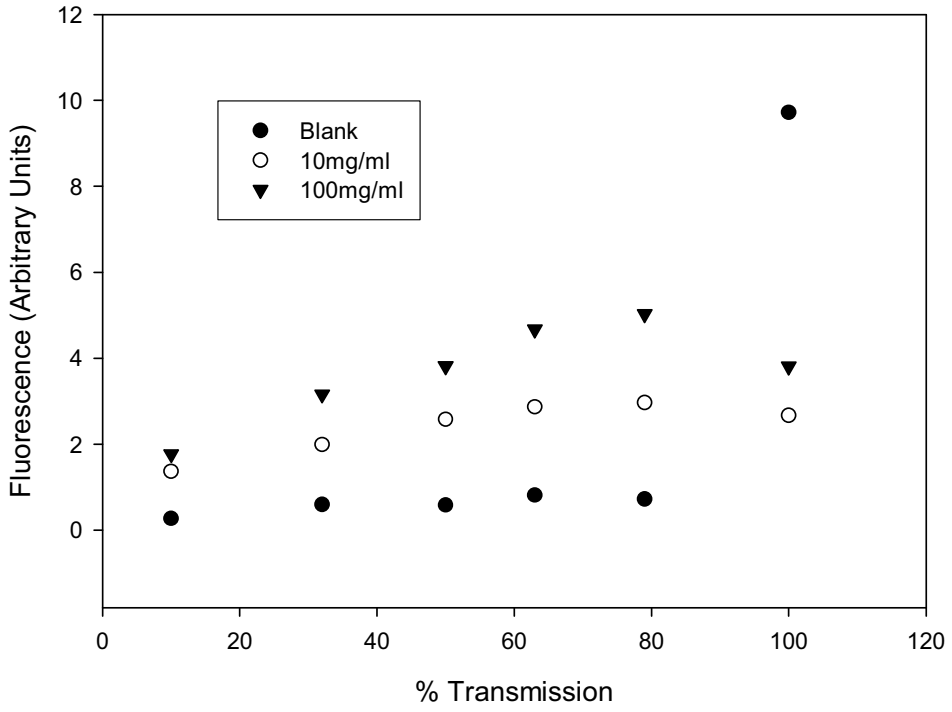

Figure 4.8. Fluorescence variation with optical density filters
Effect of optical density filters to reduce laser beam intensity. Percentage transmission ranged from 10 to 100%. Samples of 10 and 100mg/ml of BSA in 60mM sodium phosphate buffer pH 7.4 were flowed through a capillary for each percentage transmission. Background noise was determined using buffer and blank capillary. Saturation of the PMT occurs at 100% transmission for both BSA samples seen by a reduction in fluorescence. 10% transmission was chosen for optimum detection.

4.5.5. PMT signal analysis

PMT signal analysis was initially carried out using an oscilloscope to view signals however this was found to be labour intensive. LabVIEW was used to create an automated analysis system to log data results from the flow vessel emission detected by the PMT. 200 data points were measured on each signal curve and the area under each curve was calculated indicating average fluorescence for each sample. Signals were averaged over one minute to reduce the sample standard deviation. The trace of the signal could also be recorded, as the shape of the fluorescence curve is characteristic of protein denaturation (Figure 4.9).

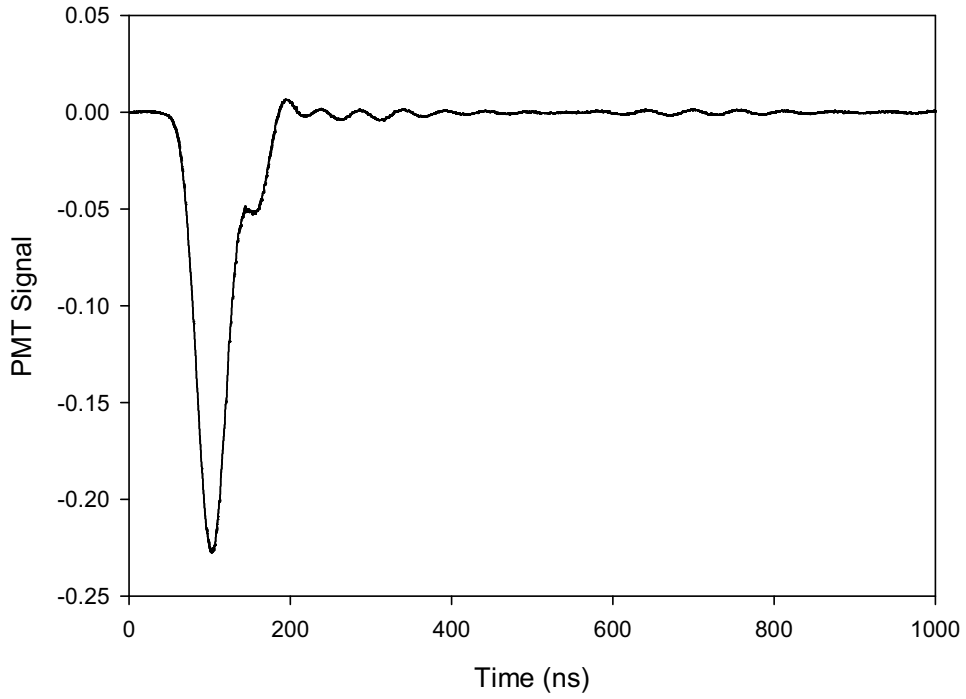

Figure 4.9. Fluorescence decay from albumin resulting from 266nm laser pulse
Fluorescence decay detected using a PMT to detect signal intensity as a function of time (ns). Decay curves are characteristic of protein denaturation. Average fluorescence is calculated by taking the area under signal using an average of 200 points. Trace profile is detected using National Instruments LabVIEW program to calculate area and standard deviation. Trace of BSA 5mg/ml (75μM) in 60mM sodium phosphate buffer pH 7.4. Excitation at 266nm with emission detected at 340nm.

4.5.6. Capillary dimensions

The 100μm internal diameter capillary was used for the optimisation of this system. For further scale down capillary is available with outer diameters of 10, 25, 50μm. It is important to ensure that the full diameter of the capillary is illuminated and that the beam is focussed on the capillary. By using a 20cm capillary length, the capillary volume is 1.6 x 10^{-3}μL. At a flow rate of 20μL/min, this equals a linear velocity of 0.04 m/s. If an averaging time of 1 minute is required per reading this means that a total consumption of 20μL per

sample is needed to read. This is 14 times less than the volume used in each well of a 96 well microplate.

4.5.7. Capillary preparations

To reduce background signal the fluorescent polyimide coating of the capillary was removed. The coating was heated in a blue flame until all the outer coating was removed. Capillary was piranha cleaned (see materials and methods) to remove any residues from the outside and inside of the capillary. This involved the use of SEM to check this procedure and it was seen that the coating was fully removed (Figure 4.10). This process reduced background noise and fouling of the capillary however, the capillary was left brittle and delicate but still useable.

(a) *(b)*

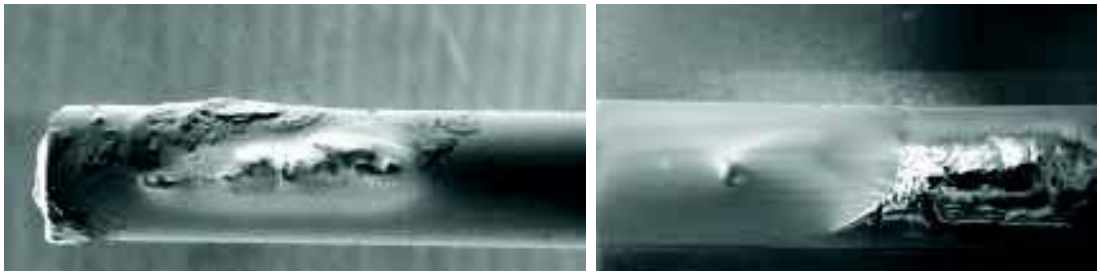

(c)

Figure 4.10. SEM pictures of stripped capillaries
SEM pictures of fluorescent polyimide coated capillaries stripped by burning (a), piranha cleaning (b) and both (c). It can be seen that both burning and piranha cleaning alone leave residues on the capillary. Using both methods cleans the capillary both inside and outside.

4.5.8. Capillary contamination

Due to the concentrations of protein used it is important to control the amount of contamination in the capillary system. All components of the system were kept unbonded allowing the system to be dismantled for cleaning. All connectors and syringes were washed with water and 2% detergent (Helmanex) to decontaminate equipment after use. Capillary was rinsed thoroughly with water at high flow rates to ensure all remnants of protein and detergent were removed. If there is any uncertainty of contamination especially

at higher concentrations of protein, capillary should be replaced and connectors and syringes thoroughly washed again.

4.5.9. Syringe pumps

KD Scientific 210 syringe pumps were daisy chained using an RS232 interface. Using LabVIEW these syringe pumps were programmed to create a controlled automated flow with an accuracy of ±1% and a reproducibility of ±0.1% as quoted in manufacturer's specifications. The use of syringe pumps allowed high pressure syringes containing various solutions to create a concentration gradient for denaturation allowing full analysis of protein stability to be carried out within minutes. This KDS210p allows integration with LabVIEW to control two daisy chained pumps that can create a number of denaturant or concentration gradients.

4.5.10. Nanomixer

To allow the automated formation of gradients two laminar flow streams must be mixed. A Nanomixer (Figure 4.11) was used to mix with low turbulence by hyper diffusion between flow laminae on an internal silicon chip via an internal silicon chip. It is ideal for applications whereby 2 flows must be combined into one mixed output. The Nanomixer can be used for high or low flow rates of under 1μL/min or up to 500μL/min to produce a homogenous output and can easily be connected to a capillary making it ideal for use in this system.

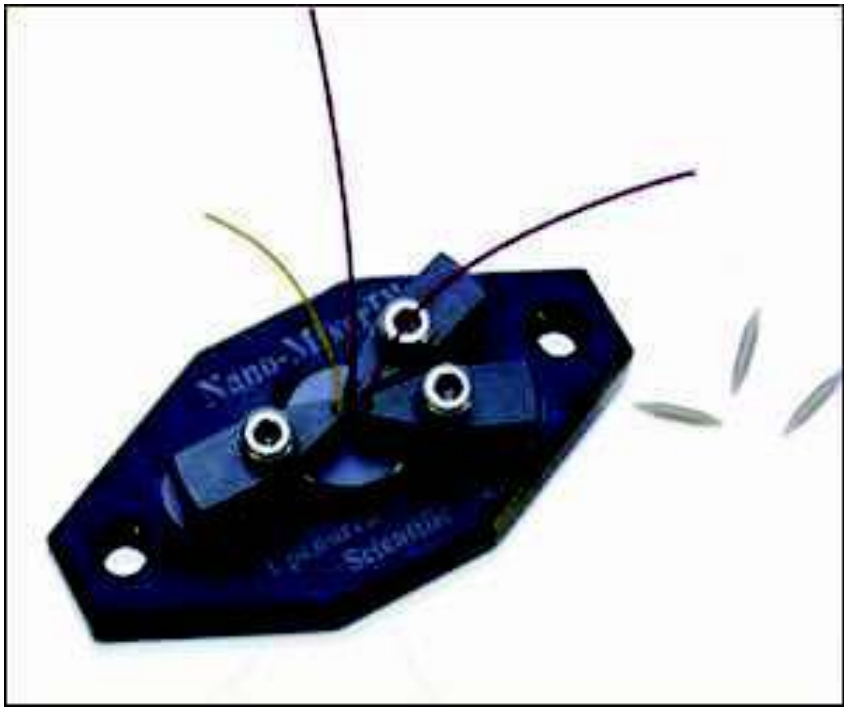

Figure 4.11. Upchurch Scientific Nanomixer
Device to allow mixing of two individual flows to produce one even output flow. Mixing carried out by internal silicon chip which allows turbulence at microfluidic scale. (Adapted from UpChurch Scientific). This will be used to mix the syringe pump outputs to create gradients to produce the required environment for a protein.

4.6. Optical detection system

Figure 4.12 shows a schematic of the designed optical detection system. Figure 4.12a shows the orientation of the basic components of the initial optical detection system. Capillary is placed vertically in PEEK tubing sleeves held by a specially designed holder to allow connection and flow from syringe pumps. Capillary and filters can be moved using xyz platforms to optimise and fix positioning of components. This component can be adapted for chip use for further scale down. PMT was placed at 135º to the laser so as not to experience the incident beam. All objects were fixed to an optical bench to reduce vibration and movement and placed in a black box to reduce background noise.

Modifications were made to include a cone in front of the PMT to reduce background noise associated with readings. Figure 4.12b shows the final optical detection system with all optimisation components.

(a)

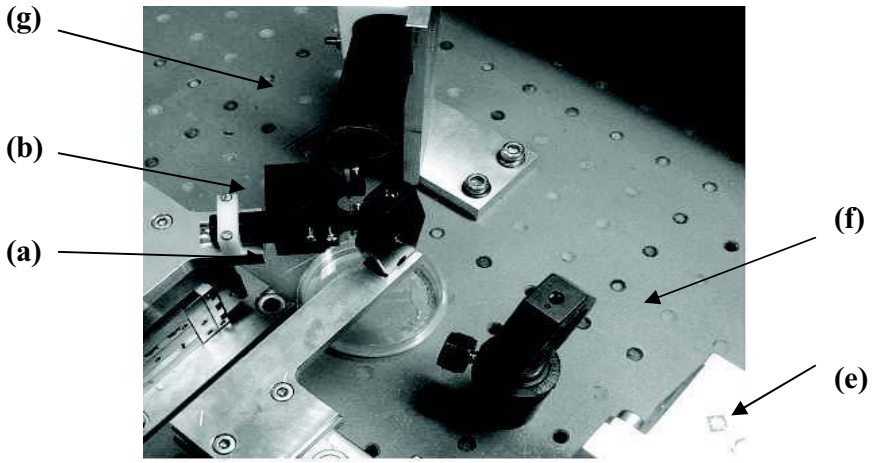

(b)

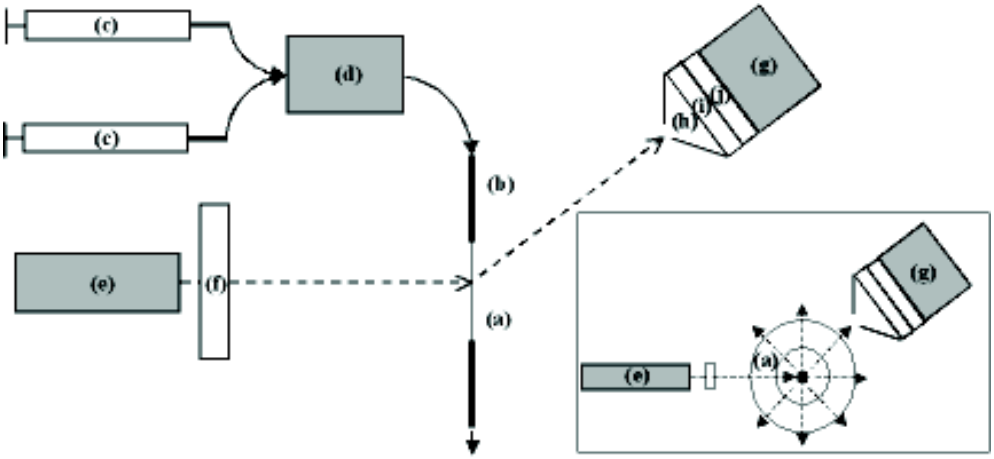

Figure 4.12. Fluorescence detection system

Capillary flow cell (a) of 100μm inner diameter and 360μm outer diameter held horizontally by PEEK tubing sleeves (b). Samples are pumped into the capillary using syringe pumps (c) through a Nanomixer (d) to produce homogenously mixed samples to visualise using the system. Capillary is illuminated using a 266nm laser (e) to excite tryptophan residues in sample. Laser light is filtered and reduced (f) using a filter and neutral density filter. Laser spot of illumination is 500μm by 200μm. Emission signal at 340nm is detected by UV sensitive PMT (g) at 135 degrees to the laser. Background light scattering is reducing using a conical cover (h). Emission signal is also filtered (i,j) to specify wavelength. Data acquisition carried out by National Instruments card to give fluorescence signal area. Initial optical equipment showing laser, PMT, lens, capillary and filter (4.12a). Schematic of final system (4.12b) showing all components of the final detection system. Inset picture shows the optical schematic not to scale detailing cross section through capillary.

4.6.1. Signal to noise

Signal to noise ratio of the capillary detection system must be assessed to determine sensitivity. This can be done by using a comparison of background noise or "blank" to a value of fluorescence for a sample of protein. Baseline was assessed by flowing 60mM sodium phosphate buffer pH 7.4 through the capillary at a flowrate of 20μL/min. Baseline variation was seen to be low with a fluorescence value of 2.9 with a signal to noise ratio percentage (SNR %) of 1.02%. 10mg/ml of BSA in 60mM sodium phosphate buffer was seen to show an increase in fluorescence with a fluorescence reading of 16.4 and a SNR % of 0.65. This value is approximately the standard deviation of the noise hence it can be determined that the optical detection equipment can detect both a stable baseline value and can detect fluorescence with BSA.

4.6.2. Initial protein denaturation data

As a signal change is detectable between the protein sample and the blank, the system was tested to investigate ability to detect protein denaturation curves. Premixed BSA samples at 20mg/ml with various concentrations of urea (0 to 7M) in 60mM sodium phosphate buffer pH 7.4 were used. This allowed the initial detection of protein denaturation, to determine feasibility. Data was analysed and compared to unfolding curves obtained from microwells (Figure 4.14).

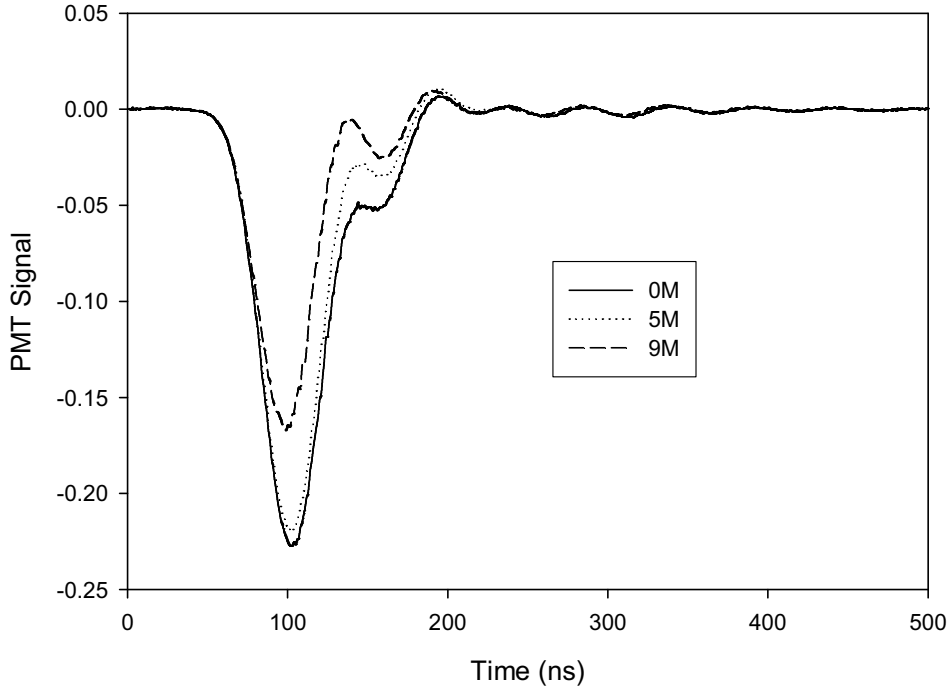

Figure 4.13. Effect of urea on protein signal trace
Trace signal of BSA 5mg/ml (75μM) in 60mM sodium phosphate pH 7.4 with various amount of urea 0 to 9M. Traces are characteristic of protein condition. A change can be seen in trace between 0M and 9M. This shows that the optical detection system can detect a change in protein fluorescence with addition of urea.

Signal traces were detected using the optical detection system, 5mg/ml BSA (75μM) in 60mM sodium phosphate buffer pH 7.4 with various concentrations of urea (0 to 9M). It can be seen that as urea concentration increases there is a decrease in fluorescence maxima as expected (Figure 4.13). Denaturation was carried out with BSA samples at 20 mg/ml (0.3mM) in 60mM sodium phosphate buffer pH 7.4 with 0 to 8.4M urea. Average fluorescence values were taken and plotted against urea concentration (Figure 4.14).

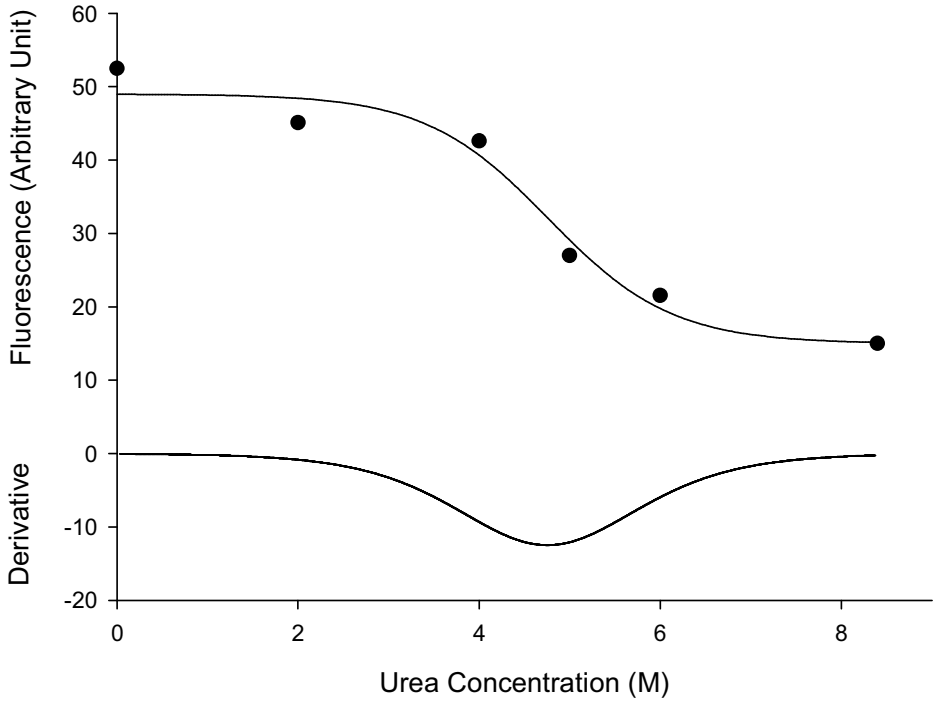

Figure 4.14. Initial denaturation data for microfluidic detection system
Microfluidic production of fluorescence denaturation profile with addition of urea denaturant (0 to 8.4M). BSA 20mg/ml (0.3mM) in 60mM sodium phosphate buffer (pH 7.4). Data was fitted using non linear least squares regression. Lower graph shows the derivative of the fitted plot to indicate the maximum denaturation point believed to occur at $C_{(1/2)}$ *(4.77M).*

Protein denaturation parameters in both systems are consistent with parameters calculated in microwells, falling within 3% error for both methods (Table 4.1). All three values of $C_{1/2}$, m_G and ΔG_{H2O} show similar results in microfluidics and microwell assays implying that this system can be used to monitor protein stability. It was thought that the scale down to this size might cause irregularities in stability parameters however it can be seen that this is not the case. A low number of points are recorded in the initial data, which should be increased to improve accuracy of parameter determination and decrease error associated with these values. Samples were premixed in this initial denaturation to allow configuration

of the basic optical components. The process should be automated to increase throughput and decrease handling. Further investigations were carried out to characterise protein stability curves using the microfluidic detection system.

	$C_{1/2}$ (M)	m_G (kcal $mol^{-1}M^{-1}$)	ΔG_{H2O} (kcal mol^{-1})
Microfluidic	4.77	0.86	4.28
Microwell	4.88	0.89	4.36

Table 4.1. Summary of microfluidic and microwell denaturation data
$C_{1/2}$, m_G and ΔG_{H2O} were calculated from preliminary data of the optical detection system. BSA (20mg/ml) was pre mixed with various concentrations (0 to 7M) urea in sodium phosphate buffer (pH 7.4). This was compared to detection in microwells. Microfluidic data appears comparable to microwell data however number of points on graph is low.

4.6.3. Limits of detection

When developing a system it is important to know the range of detection offered to allow assessment of scale down. This allows assessment of optimisation and comparison to other traditional methods, such as microwell, to determine the effect of concentration on fluorescence. For each model proteins (BSA, RNase A and chymotrypsin) a concentration range of detection of the optimised system was characterised (Figure 4.15). This range however is not equivalent to the range of detection of denaturation curves as fluorescence varies throughout these profiles. Although protein signal can be detected, this does not necessarily mean that the stability curve of the protein can be detected at this concentration. Samples of BSA, RNase A and chymotrypsin were prepared in 60mM sodium phosphate buffer (pH 7.4). Microwells detection was carried out in 96 well format in UV transparent plates with a final well volume of 280µL. Capillary set up detection was carried out using a

PMT voltage of 1000V and with laser power at 1.1kHz. Flow rate through the capillary flow vessel was kept at 20μL/min.

(a) *(b)*

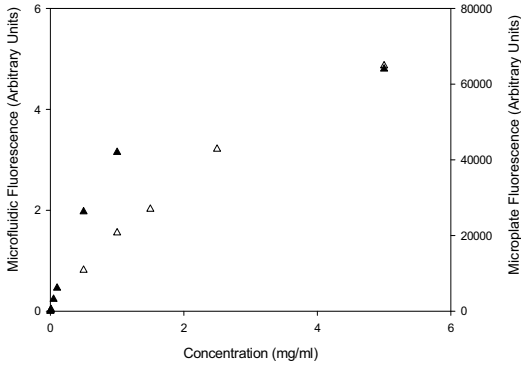

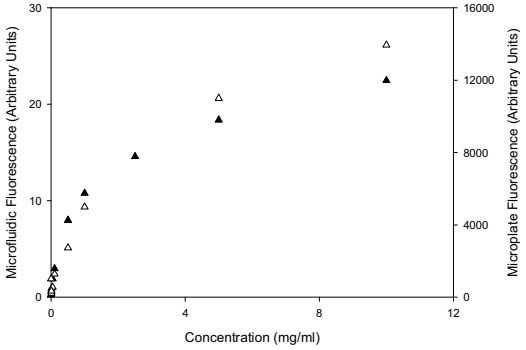

(c)

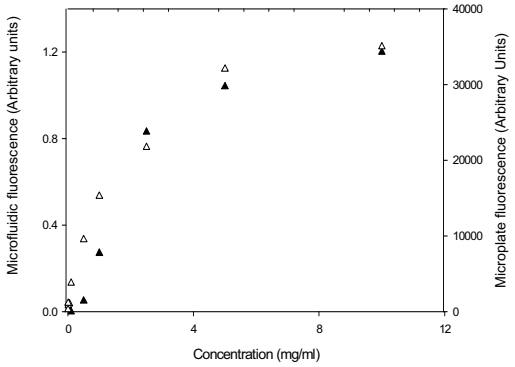

Figure 4.15. Minimum detection concentrations for capillary and microplate set ups
Comparability of capillary detection to microwell detection. Capillary optical detection was carried out using a PMT voltage of 1100V and with laser power at 1.1kHz (Δ). Microwell detection was carried out using UV transparent plates with a well volume of 280μL(▲). Comparable concentrations of each protein can be detected in each system. Molecules of protein detected are summarised in Table 4.2. BSA (Figure 4.15a), RNase A (Figure 4.15b) and chymotrypsin (Figure 4.15c) were prepared at varying concentrations in 60mM sodium phosphate buffer pH 7.4.

Method	Minimum Conc detectable (mg/ml)	Volume (L)	Protein Molecules
Microplate			
BSA	0.005	4.00×10^{-5}	1.81×10^{12}
RNase A	0.0001	4.00×10^{-5}	1.75×10^{11}
Chymotrypsin	0.001	4.00×10^{-5}	1.11×10^{13}
Microfluidics			
BSA	0.50	1.50×10^{-11}	6.75×10^{7}
RNase A	0.10	1.50×10^{-11}	6.57×10^{7}
Chymotrypsin	0.01	1.50×10^{-11}	4.17×10^{6}

Table 4.2. Summary table of data collected from minimum concentration experiment
Ranges of detection for the microfluidic system developed. It can be seen in this table that the overall molecules of sample used to detect protein concentration in the microfluidic system is less than that of the microplate reader.

In the microfluidic system, these samples were not produced using the Nanomixer before detection using the capillary system. It can be seen that there was an increase in fluorescence with concentration (Figure 4.15) consistently between microfluidics and microwell. At low concentration the relationship appear to be linear however this is no longer the case as saturation occurs at higher concentrations. From these graphs, the lowest concentration of proteins detectable can be determined. Signal concentrations were deemed detectable when fluorescence values are one standard deviation above the noise of the blank. Low concentrations have a low signal to noise ratio making detection less reliable. This data can also be used to look at the extent of scale down possible using this scale of capillary. It can be seen in the summary table (Table 4.2) that the minimum concentration detectable for the microplate (for each protein) is of up to three magnitudes lower than that of the microfluidic system. However upon looking at the scale of the volumes used in both scales it can be seen that the volume used in the microfluidic capillary system is seven orders of magnitude smaller than that of the volume of the microfluidic well. This is

important for reagent consumption as in process development product is very scare and expensive in preliminary stages. Calculating the number of molecules allows the minimum proportion of molecules that can be detected by each of the systems to be assessed. In each well of the 96 well plate, the number of molecules of protein used in the lowest concentration reading is of the order of 10^{11} molecules however for the capillary system the number of molecules detectable are in the order of 10^{6}. It is seen that the capillary system can detect 10^{5} less molecules than the microwell system. Although the experimental scale down is reduced in comparison to calculated scale down, there is still a significant scale down from microwell to microfluidic scale. Readings can be taken over a longer time, producing an average over a larger number of readings rather than a small number of samples as in a microwell. This will increase the accuracy and reliability of the reading while still reducing the amount of protein used.

4.6.4. Limits of detection using denaturation profiles

BSA and RNase A solutions were prepared in 60mM sodium phosphate buffer pH 7.4 with urea (0 to 8.4M) to produce denaturation curves. BSA sample concentrations were reduced until the limits of detection were reached testing optimisation and automation of the optical detection system. BSA and RNase A denaturation was carried out in both the microfluidic system and the conventional microwell assay (Figure 4.16). Parameters from these experiments are summarised in Table 4.3. Upon addition of the denaturants the samples were equilibrated for 15 minutes during flow through a long length of capillary (640cm) to reach equilibrium. It can be seen here that the denaturation in both the microwell and microfluidic system seem comparable from the denaturation curves plotted using raw

fluorescence values (Figure 4.16). Data is compared as percentage unfolded to correct for varying scale of data collection. This consistency is seen in both RNase A and BSA analysis, showing that this method is reproducible and consistent between methods. Denaturation profiles were deemed undetectable when the denaturated and native fluorescence were within one standard deviation of each other. It can be seen that for RNase A and BSA denaturation profiles could not be seen at 0.5mg/ml for microfluidics hence parameters were determined on 1mg/ml. BSA $C_{½}$ can be determined for both methods to within 0.08M of denaturant. This does not fall between the 0.09% coefficients of variance values of the error.

(a) *(b)*

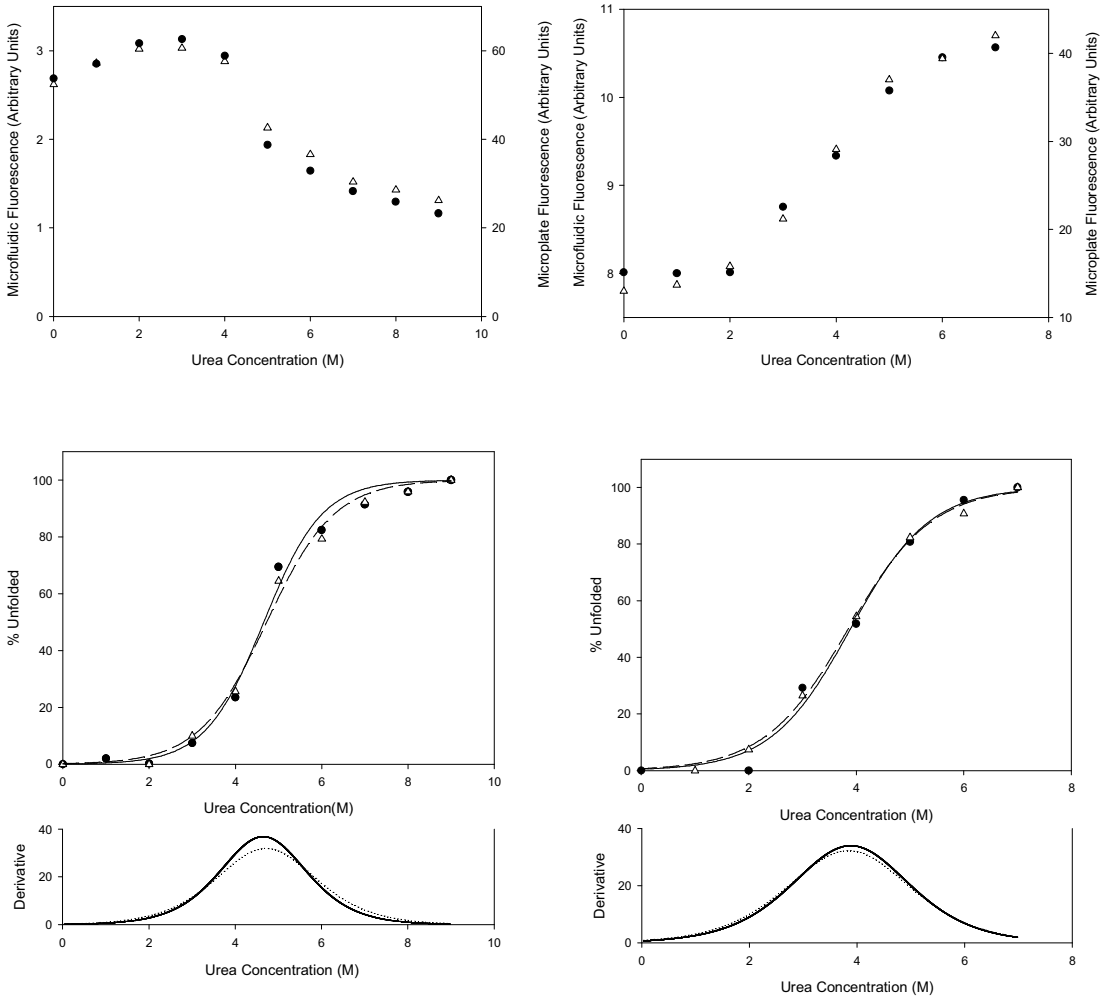

Figure 4.16. Limit of denaturation detection using BSA and RNase A using microfluidic and microwell

*BSA (a) and RNase A (b) compared to microplate and microwell denaturation at low concentrations. The lowest concentration denaturation detection possible using capillary system (**Δ**) is plotted above. It can be seen here that denaturation profiles between the microplate and microwell were comparable when plotted as percentage unfolded. At 0.5mg/ml however a denaturation curve could not be seen hence 1mg/ml is the denaturation detection limitation of the capillary system. Errors were kept to below 0.8% of the signal in each case. Figures consist of raw denaturation profiles of fluorescence detection signal versus urea concentration. This is then followed by data represented as percentage unfolded with linear regression fitting of graphs to produce an unfolding transition profile and derivative of fit that can be used to determine parameters for unfolding.*

				%CV		
Method	**$C_{1/2}$** (M)	**m_G** (kcal mol^{-1} M^{-1})	**ΔG_{H2O}** (kcal mol^{-1})	**$C_{1/2}$** (M)	**m_G** (kcal mol^{-1} M^{-1})	**ΔG_{H2O}** (kcal mol^{-1})
Microplate						
BSA	4.85	0.88	4.27	0.09	0.41	0.36
RNase A	3.89	0.72	2.80	0.09	0.35	0.51
Microfluidics						
BSA	4.80	0.9	4.32	0.07	0.26	0.30
RNase A	3.85	0.78	2.97	0.05	0.19	0.43

Table 4.3. Parameters determined from microfluidic and microplate denaturation *Parameters determined from linear regression fitting of denaturation curves produced by both microfluidic and microwell methods with RNase A and BSA. Samples at 1mg/ml in sodium phosphate buffer pH 7.4 with urea (0 to 8.4M).*

4.6.5. Increase in throughput

One important advantage of microfluidics is the potential for an increase in throughput due to continuous flow and automation. By the use of syringe pumps to produce a gradient of buffer and concentration via LabVIEW programming and mixing using a Nanomixer a fully automated system can be used to produce a denaturation curve to examine protein stability. Multiple syringe pumps can be used with multiple Nanomixers to produce an array of conditions to assess protein stability in one experiment. Throughput is inevitably determined by incubation time of a protein, however, if results are take over an average of one minute for each sample condition there is the potential to assess more than 1400 samples per day. This is also the potential to parallelise this method with various capillary systems increasing throughput even further. As previously mentioned MALDI/MS methods (Ghaemmaghami et al. 2000) can analyse 1000 samples per day however this equipment is

expensive and specialised. The traditional microwell method has increase throughput cheaply however it is prone to errors via pippetting and evaporation. With the use of microfluidics this throughput has the potential to be greatly increased without an increase in expenditure.

4.7. Conclusion

Automated robotic microwell systems have become commonplace during the analysis and production of proteins. These systems have been optimised to produce a small scale high throughput alternative to traditional spectroscopic methods. However the demands of the process industry have exceeded the potential of this system for further scale down and throughput. For this reason there is an opening in the market for a microfluidic system with the potential for full automation.

The aim of this chapter was to develop a microfluidic system able to detect protein stability using a previously optimised UV fluorescence assay to produce a scaled down high throughput protein stability screening system. This will allow automated high throughput analysis in formulation and process design. A study was initially carried out to investigate feasibility of this scale down to microfluidic. By comparison to microwell it was calculated that it is feasible to detect protein ultraviolet tryptophan fluorescence and external fluorophore fluorescence at this scale despite low quantum efficiency and volumes at this level. These results lead to the development of an optical detection system using a capillary flow system to analyse protein denaturation. The optical detection apparatus was constructed allowing excitation of the capillary flow vessel using a UV laser with emissions detected by a UV sensitive PMT. Flow was controlled and automated using syringe pumps,

used to produce gradients making concentration control automated. Automated samples were mixed using a Nanomixer. It was also found that for BSA viscosity increases dramatically above 200 mg/ml hence increasing pressure in the system. To assess feasibility of detection, confocal microscopy was tested to see if this optical system could detect this low tryptophan fluorescence. This was found that quantification was not possible however this system was not optimised for use of tryptophan detection but for DAPI detection. Initially the capillary detection system was found to be able to detect baseline variability, protein concentration and denaturation accurately. When the system was optimised it was found that a minimum concentration of 0.5, 0.1, 0.01mg/ml of BSA, RNase A and chymotrypsin respectively were detected. This however differs from the minimum concentration of denatured protein detectable. Denaturation curves of RNase A and BSA each were detectable at 1mg/ml in the optical detection system. Data was found comparable to previously assessed microwell system in both accuracy and reproducibility with scale down of 10^5 molecules. This system also allows the increase in throughput by 1.5 times with the potential for further increase.

As can be seen from this chapter, microfluidics can be used to increase throughput and scale down of the tryptophan fluorescence assay that has previously been optimised in microwells. This allows the rapid production of protein stability data to produce a 3D landscape of stability for each protein. This in turn can be used to optimise conditions in processing. Production use and analysis of these 3D graphs is shown in the next chapter.

Chapter 5:

Fluorescence determination of protein stability: Construction and analysis of protein stability maps

5.1. Introduction

During process development and manufacturing, there are a large number of conditions that can vary from stage to stage. These variations can compromise the quality and stability of the end product, highlighting the importance of monitoring protein condition as a function of these changes. As established in previous chapters, protein stability can be evaluated with a UV fluorescence assay that can be used at microfluidic scale. The use of automation and high throughput microfluidics offers the opportunity to increase data acquisition rate, creating detailed protein profiles. It is important to understand how this data can be used to gain the most information about a protein's stability, for the determination of optimum process and formulation conditions. This increase in data acquisition can allow multiple parameters such as pH and temperature to be tested at once to gain more information regarding the protein. The interaction of multiple parameters may cause a variation in stability that might not be seen when parameters are monitored separately.

The aim of this chapter is to create and assess multidimensional plots of protein stability. Plots can be used indicate optimum formulation and storage conditions as well as provide information for process design. Data was experimentally determined to investigate the effects of pH, chemical and thermal denaturation on the stability of various proteins. Plots were analysed by both surface fitting and calculation of thermodynamic parameters to assess the stability of the protein. Assessment of surface fits was carried out by comparison to published and experimental data. Work in this chapter was carried out in collaboration with Simon Edwards-Parton of the Biochemical Engineering Department, UCL.

5.2. 3D plot production

In Chapter 3, stability was measurable as a function of one denaturant condition such as temperature, pH or chemical denaturation. However by combining these parameters, a more detailed picture of protein stability can be determined. Multivariant analysis was carried out in the fixed volume 96 microwell plate method as used in Chapter 3 (Aucamp et al. 2005). Samples were denatured using a variety of conditions (pH, thermal and chemical denaturation) and fluorescence read using the BMG FLUOstar plate reader. BSA, chymotrypsin, RNase A were screened using various conditions to determine protein stability maps across this range of process relevant conditions.

5.2.1. BSA thermal and pH denaturation

BSA was tested to assess the effect of temperate and pH denaturation on the fluorescence and stability of the protein. BSA samples were made up in pH range of 6 to 10 and heated using the BMG FLUOstar thermal heating plates as previously described in Section 3.5.2. Samples were treated over a range of temperatures from 24.7 to 57.4˚C as profiled in Figure 3.9 and fluorescence signal monitored over time. Figure 5.1 shows an unfitted mesh plot of fluorescence as a function of pH and temperature. Mesh plot and experimental data are both displayed.

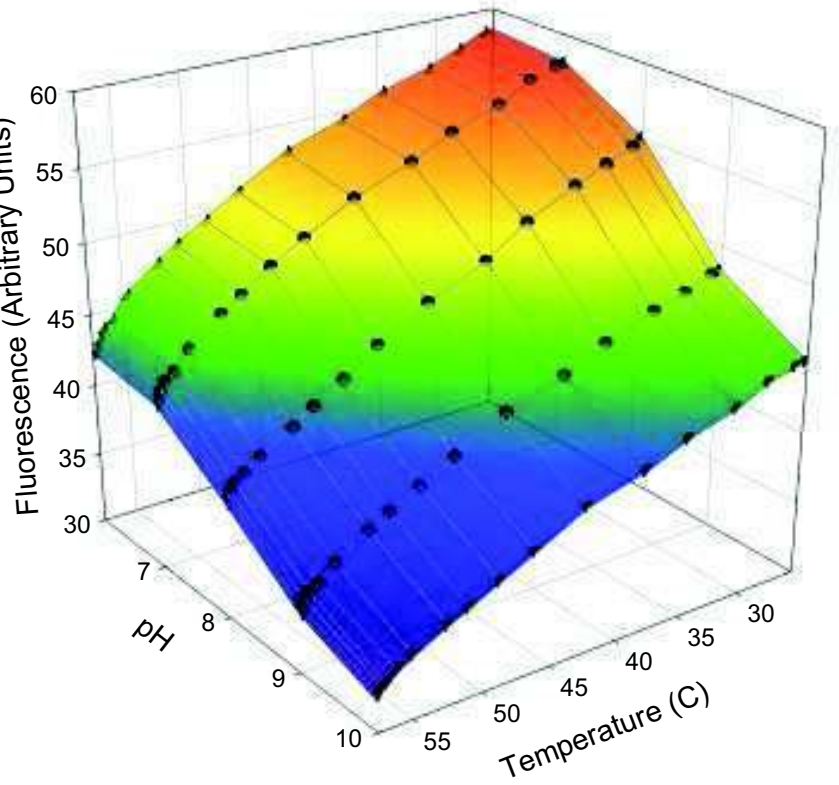

Figure 5.1. pH and thermal denaturation of BSA

BSA formulated in pH 6 to 10 in 50mM TRIS buffer at concentration 1.43mg/ml (21µM). Samples were heated to a maximum temperature of 57.4˚C using thermal heating plates in the BMG FLUOstar plate reader. Mesh plot is overlayed on experimental data (●) Increasing pH and temperature causes a decrease in fluorescence indicating a decrease of BSA stability. Melting temperature could not be determined due to the limited experimental temperature range. Temperature range of 37˚C shows a 28% decrease in fluorescence at pH 6 and pH 10. Initial and final fluorescence is lower at pH 10 than at pH 6.

In Figure 5.1 an increase in pH causes a decrease in fluorescence at 25˚C as previously seen in Figure 3.11. There is seen to be a 23% decrease in fluorescence signal as pH increases at both 24.7˚C and 57.4˚C. As temperature increases, fluorescence also decreases. It is known that thermal denaturation of a protein should be a sigmoidal decrease in fluorescence with a similar profile to chemical denaturation (Kuhlman et al. 1998; Fersht 1999). Thermal

denaturation in Figure 5.1 is not complete for the entire thermal denaturation profile, with range of detection limited by the range of the BMG FLUOstar heating plates. Melting temperature is the midpoint of thermal denaturation in the sigmoidal thermal denaturation curve as the $C_{1/2}$ is the midpoint of the chemical denaturation. These values occur when $\Delta G=0$ and $K=1$. It is known that the melting temperature of BSA of 59˚C (Arakawa et al. 2000) indicating that the testing range is not large enough for a full thermal denaturation to be seen. In Figure 5.1 BSA appears most stable at pH 6 and 7 at 24.7˚C with minimum stability seen at pH 10 at 57.4˚C. Although this profile is not able to confer thermodynamics stability parameters, it does give an indication of the stability of the protein with changes in condition. This plot can be used for comparison when a protein has been treated or engineered. Proteins can be compared using this multivariant plots to calculate percentage unfolded in comparison to the native to allow quantification of stability changes in the protein. There is the potential to use microfluidics for heating in capillaries to induce thermal denaturation profiles (discussed later) with the potential to increase the range of heating as well as throughput.

5.2.2. pH and chemical denaturation of BSA

As can be seen above, a change in pH affects the stability of BSA. To quantify this effect, chemical denaturation can be carried out at each pH to confer parameters related to the stability as pH changes. BSA 1.43mg/ml (21μM) samples prepared at pH 6 to 10 were chemically denatured using urea (0 to 8M). Fluorescence of each sample was read as a function of pH and chemical denaturant (Figure 5.2). For each pH, chemical denaturant was fitted to normalised data of percentage unfolded. Fits of each plot are shown in Figure 5.2a. Parameters determined from these fits are displayed in Table 5.1. Derivative of fits are shown to simplify depiction of the plot (Figure 5.2b).

(a)

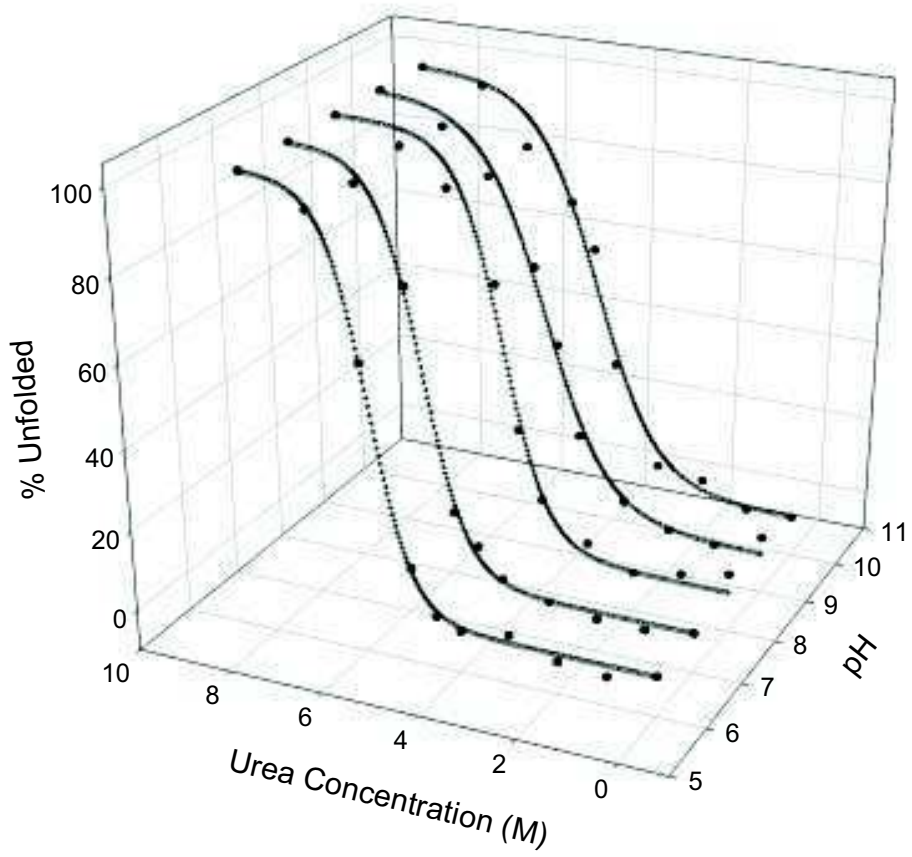

Figure 5.2a. pH and chemical denaturation of BSA

Protein response curves produced to determine the stability of a protein when subjected to various conditions such as urea denaturation and pH. In this graph (a) BSA at 1.43mg/ml (21μM) was denatured using pH and urea (0 to 8.4M) in 50mM TRIS buffer. Fitted data of denaturant concentration and pH are plotted against percentage unfolded. Overlayed experimental data is also seen (●). Parameters are summarized in Table 5.1.

(b)

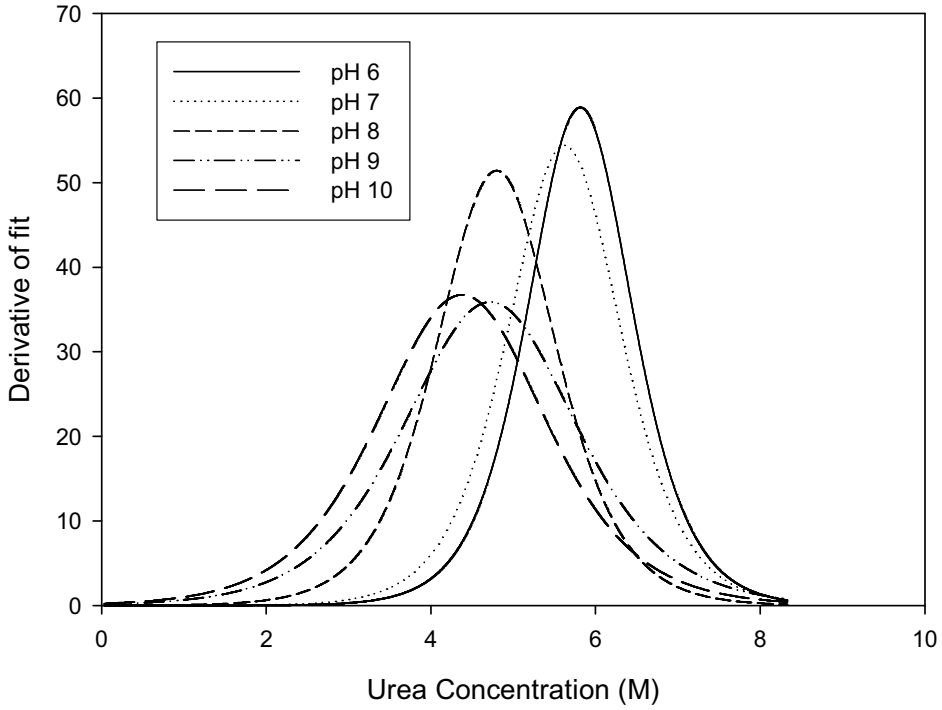

Figure 5.2b. pH and chemical denaturation of BSA

Protein response curve produced to determine the protein stability when subjected to various conditions such as urea denaturation and pH. In this graph (a) BSA at 1.43mg/ml (21μM) was denatured using pH and urea (0 to 8.4M) in 50mM TRIS buffer. Denaturant was plotted against derivative of fit (b). Denaturation from pH 6 occurs at a higher rate than at any other pH as seen in the derivative of the plot. There is a gradual decrease in derivative maximum to pH 10. Parameters are summarised in Table 5.1.

A reduction in fluorescence indicates that BSA becomes less stable as pH increases as previously seen (Figure 3.11). It can be seen that there is a 23% decrease in initial fluorescence of BSA as pH increases from 6 to 10. In Table 5.1 it is indicated that as pH increases, $C_{1/2}$ and ΔG decrease indicating a decrease in stability. However the magnitude of derivative plots and m_G (indicative to the speed of the denaturation) show that denaturation occurs more rapidly at lower pHs. This implies that as pH increases,

denaturation occurs over a larger range of chemical denaturant. At lower pHs, BSA is resistant to protein denaturant at lower concentrations. Once denaturant is increased to higher concentrations, denaturation occurs rapidly. These terms can be used for comparison to BSA when treated or engineered as assess stability over a number of parameters.

pH	$C_{1/2}$ (M)	m_G (kcal $mol^{-1}M^{-1}$)	ΔG_{H2O} (kcal mol^{-1})	Derivative maximum
6	5.75	1.44	8.47	58.8
7	5.60	1.26	7.00	54.3
8	4.79	0.85	4.07	51.4
9	4.73	0.80	3.90	35.9
10	4.39	0.8	3.5	36.4

Table 5.1. Summary of parameters determined from pH and urea denaturation

Parameters determined using the linear extrapolation method to determine $C_{1/2}$, m_G and ΔG of data depicted in Figure 5.2. As pH increases, $C_{1/2}$ and derivative maximum decrease indicating a decrease in stability. Δ G and m_G both decrease with an increase in pH indicating that although the protein is more stable at lower pHs chemical denaturation occurs at a fast rate at a higher concentration of denaturant.

5.2.3. pH and thermal denaturation of RNase A

RNase A was used at a concentration of 1.43mg/ml (0.1mM) in 50mM TRIS buffer at various pHs in a range of 6 to 10. RNase A was heated to a maximum temperature of 57.4°C as shown in Figure 3.9. It is known from chemical denaturation that a decrease in stability of RNase A shows an increase in fluorescence unlike BSA and chymotrypsin. This is due to the local environment of the fluorescent tryptophan residues. There is seen to be a decrease in fluorescence signal of 20% when heating between the ranges of 24.7 to 57.4°C at pH 6, with pH 10 resulting in a decrease of 23% as temperature is increased. At pH 10, initial fluorescence is lower than at lower pHs. It is known that the isoelectric point of RNase A is 9.6 (Sigma) above which the protein is negatively charged. A change to a net

positive charge may cause a structural change itself and maybe the reason for the decreased fluorescence at pH 10. As RNase A was heated, a 20% decrease in fluorescence is seen, decreasing to 12.5% at pH 10. As the initial fluorescence at pH 10 was lower that that of pH 6 it is thought that the protein is partially unfolded before thermal denaturation. At pH 6, the protein maybe more susceptible to denaturation due to pH treatment. As the pH is increased past the isoelectric point a dramatic change is stability profile is seen upon thermal heating. From this plot it can be determined that the protein is most stable at 57.4°C at pH 10. To ensure there was no degradation in the range of pH, an SDS-PAGE gel was run of RNase A at pH 6 and pH 10 (Figure 5.4) (Navon 2001).

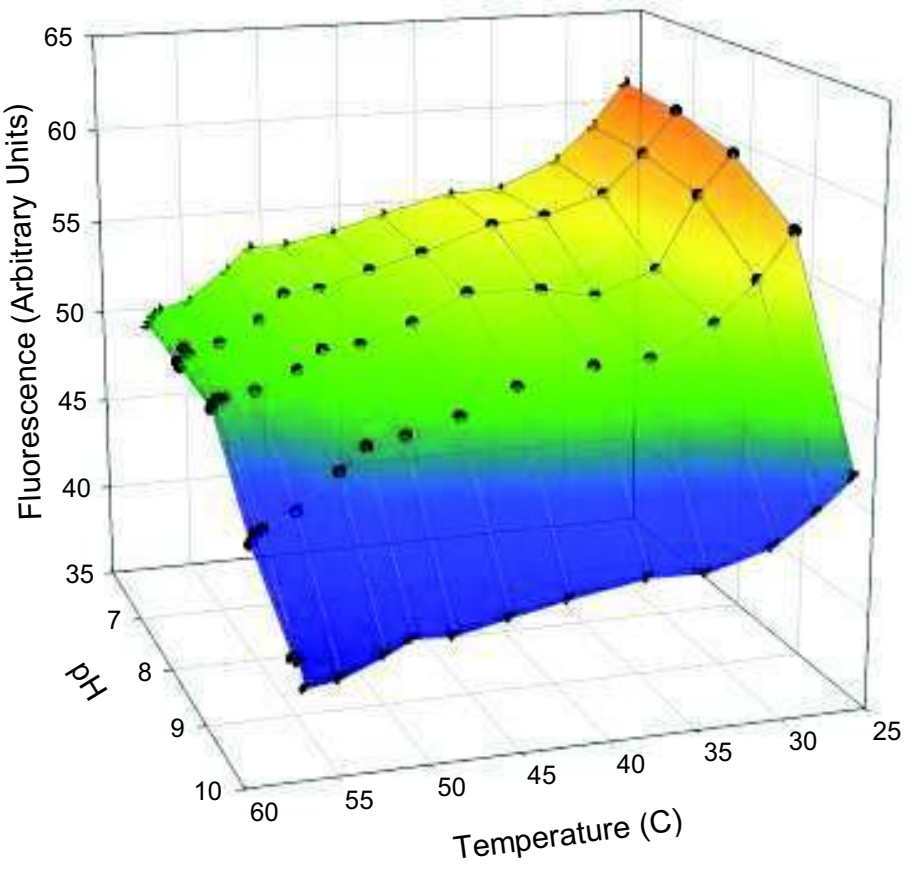

Figure 5.3. pH and thermal denaturation of RNase A
Graph of heating of RNase A 1.43mg/ml (0.1mM) in 50mM TRIS buffer at various pHs (6 to 10). Fluorescence is plotted as a function of pH and temperature (24.7 to 57.4°C). There is a decrease in fluorescence with an increase in temperature (20%) at pH 6 that decreases to 12.5% at pH 10. As pH increases above the isoelectric point (9.6) the effect of temperature is less due to the increase in stability of the protein due to pH treatment. (Navon 2001)

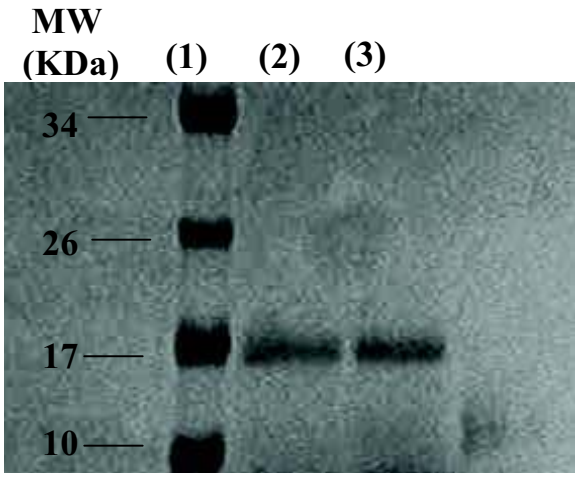

Figure 5.4. SDS-PAGE of RNase A

SDS-PAGE gel of RNase A. Lane 1 is a molecular marker with lanes 2 and 3 showing RNase A at pH 6 and pH 10 respectively. It can be seen that there is only one band in each lane signifying at both pHs RNase A has not been degraded

Heated RNase A samples at pH 6 and 10 were run on an SDS-PAGE gel to determine if degradation has occurred. In this gel it can be seen that both samples have the same molecular weight showing no degradation when heated. This attributes the decrease in fluorescence to an increase in stability and not degradation. It is known that for RNase A the temperature at which optimum activity occurs is 60˚C according to manufacturers' specifications (Sigma). Previous studies on RNase A have shown an increase in melting temperature with a increase in pH implying that the protein becomes more stable as pH increases (Barone 1997 et al; Knapp et al. 1999). Although the melting temperature of RNase A is quoted as 41˚C (Wang 1999) at pH 2.8 it is seen that at pH 6.7 this has increased to 64˚C indicating that as pH increases, the stability of the protein also increases (Poklar et al, 1999). It is suggested however that as pH increases to pH 10 the thermal denaturation of a protein no longer becomes a two state denaturation with intermediates (Navon et al. 2001). For this reason the thermal denaturation of RNase A can no longer be assessed by classical two states thermodynamics due to the increase past the isoelectric

point at pH 9.6. RNase A is further assessed using pH and chemical denaturation to quantify the effect of pH on RNase A.

5.2.4. pH and chemical denaturation of RNase A

It can be seen above that pH affects RNase A stability. To assess this change in stability, RNase A was tested at various pHs using chemical denaturant to determine stability parameters. RNase A samples at 1.43mg/ml (0.1mM) in 50mM TRIS buffer at pHs 6 to 10 were treated with GdHCl. GdHCl was made up in a range of concentrations between 0 to 6.5M. Fluorescence was measured in microwell and percentage unfolded plotted (Figure 5.5a). Percentage unfolded was plotted as a function of pH and GdHCl concentration and fitted using non-linear least squares regression (Figure 5.5b). Parameters determinable from these fits are summarised in Table 5.2. It can be seen that as pH increases, derivative maximum increases.

(a)

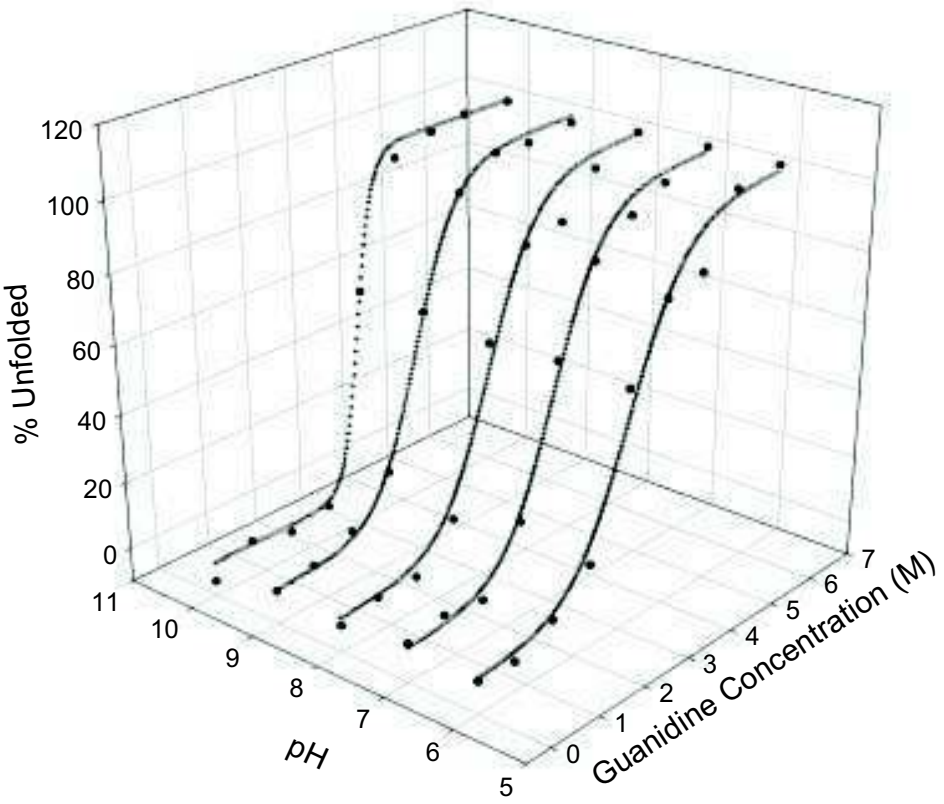

Figure 5.5a. pH and chemical denaturation of RNase A

Protein response curve produced to determine the stability of a protein when subjected to GdHCl and pH denaturation. RNase A at 1.43mg/ml (0.1mM) was denatured using pH and GdHCl in TRIS buffer at pHs 6 to 10. Percentage unfolded was calculated and plotted as a function of GdHCl and pH (a). Experimental data(●) sets are shown with fits overlayed. Parameters are summarized in Table 5.2.

(b)

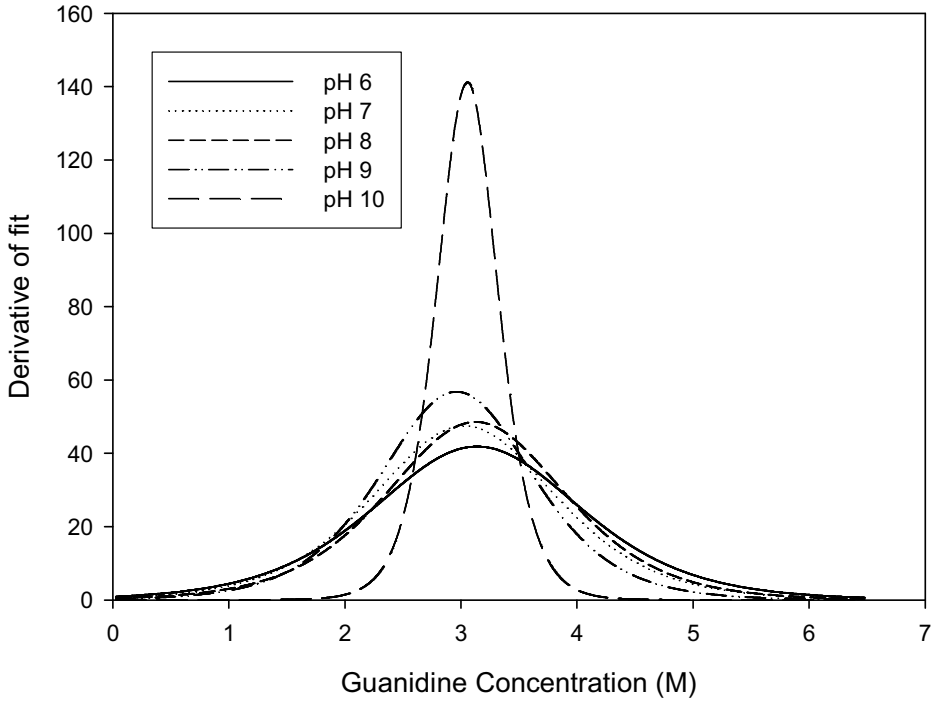

Figure 5.5b. pH and chemical denaturation of RNase A

Protein response curve produced to determine the stability of a protein when subjected to GdHCl and pH denaturation. RNase A at 1.43mg/ml (0.1mM) was denatured using pH and GdHCl in TRIS buffer at pHs 6 to 10. Derivative of protein denaturation fits are shown (b). Rate of denaturation increases as pH increases with a dramatic increase seen at pH 10.

pH	$C_{1/2}$ (M)	m_G (kcal $mol^{-1}M^{-1}$)	ΔG_{H2O} (kcal mol^{-1})	Derivative Maximum
6	3.14	1.00	3.14	41.8
7	3.05	1.10	3.36	47.5
8	3.13	1.15	3.60	48.5
9	2.97	1.35	4.00	56.8
10	3.07	3.34	10.25	141

Table 5.2. Summary of parameters determined from pH and guanidine denaturation

Parameters were determined using the non linear least squares extrapolation method to determine $C_{1/2}$, m_G and ΔG. As pH increases there appears to be no trend in $C_{1/2}$ however derivative maximum, m_G *and ΔG_{H2O} increase with an increase in pH indicating denaturation occurs at a faster rate with a higher initial stability of the protein in water.*

As pH increases it can be seen that there is no trend in $C_{1/2}$. There is an increase in m_G, ΔG_{H20} and derivative maximum indicating that the protein is more readily denatured at high pHs particularly pH 10. There is, however, also an increase in associated ΔG_{H20} indicating that the protein is most stable at pH 10. The dramatic increase in both m_G and ΔG_{H20} at pH 10 may be due the denaturation of the protein no longer being a two state denaturation due to the pH increasing above the isoelectric point of the protein 9.6 (Tanford 1956). This indicates that the protein is most stable at pH 10 as previously seen. However the assumption of the two state model for fitting the parameters may not be accurate for pH 10. This additional stability may be caused by the pH increasing to above the isoelectric point, hence protein configuration may be altered due to a change in overall charge distribution. This data can be used to confer optimum process conditions of RNase A

5.2.5. pH and heating of chymotrypsin

Chymotrypsin was treated using pH and thermal denaturation. Chymotrypsin 0.71mg/ml (0.29μM) was heated to a maximum temperature of 57.4°C as shown in Figure 5.6. Chymotrypsin samples were prepared in 50mM TRIS buffer at various pHs to investigate the affects of both aggregation and denaturation. Absorbance was measured at 600nm to detect aggregation within the sample when treated with both pH and thermal denaturation. Fluorescence was monitored with excitation at 280nm and emission at 340nm.

(a)

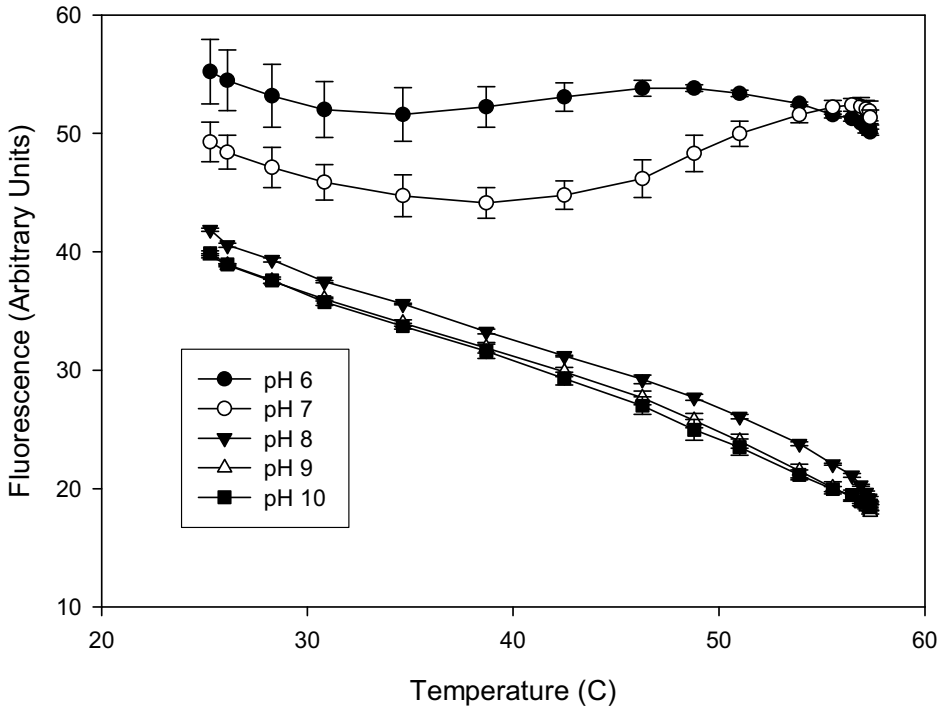

Figure 5.6a. Fluorescence measurements of thermal denaturation of chymotrypsin
Heating of chymotrypsin 0.71mg/ml (0.29μM) in 50mM TRIS buffer at various pH (6 to 10). Fluorescence readings were measured in triplicate and plotted as a function of temperature with standard deviation. pHs 8,9,10 show a decrease in fluorescence as temperature increases. pHs 6 and 7 show an initial decrease in fluorescence which increases again as temperature increases. Fluorescence measurements at these pHs appear higher at room temperature than at higher pHs.

(b)

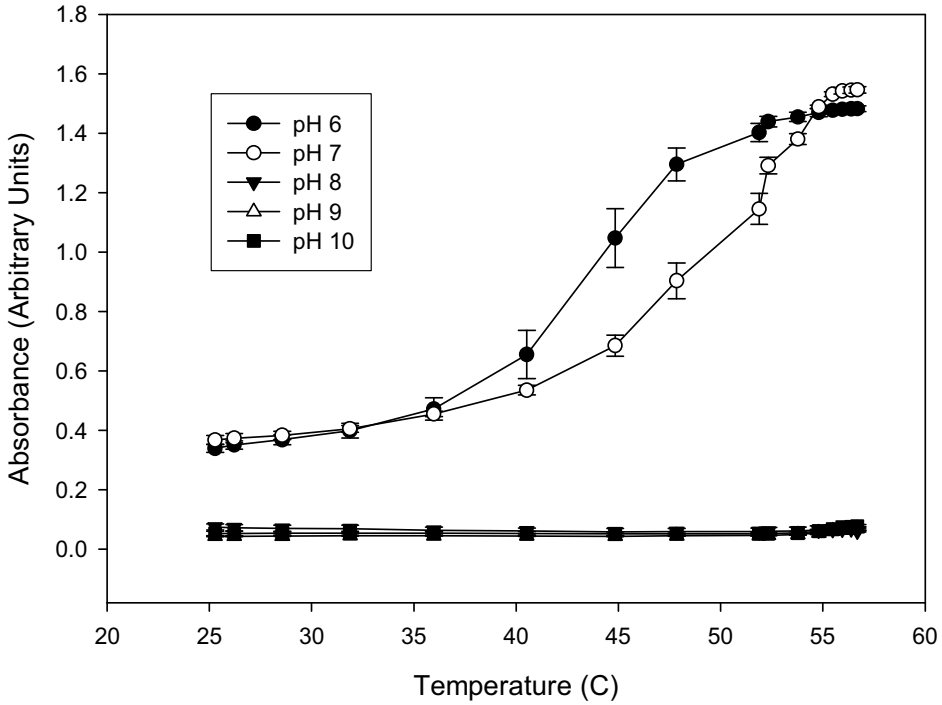

Figure 5.6b. Absorbance measurements of chymotrypsin heating.
Heating of chymotrypsin 0.71mg/ml (0.29μM) in 50mM TRIS buffer at various pH (6 to 10). Absorbance at 600nm was measured in triplicate and plotted with standard deviation. At pH 6, 7 absorbance increases (due to aggregation) with temperature, affecting fluorescence signals (a). pH 8, 9 and 10 show decrease in fluorescence with no increase in absorbance as temperature increases.

In fluorescence detection of chymotrypsin (Figure 5.6a) it appears that there is a decrease in fluorescence signal of over 50% when heated between the range of 24.7 to 57.4°C at pHs 8 to 10. At pH 6 and 7 fluorescence at room temperature is much higher than at pHs 8 to 10. There is a decrease in fluorescence with heating at pHs 8 to 10 however an increase is seen with pH 6 and 7. This indicates an anomaly at lower pHs. For this reason absorbance was tested. At pHs 8 to 10 there appears to be no increase in absorbance however at pH 6 and7 there appear to be a rapid increase in absorbance with heating with absorbance increasing by a factor of 4. This increase in absorbance can be attributed to aggregation of the protein.

It is known that the isoelectric point of the protein is 7.4. Under this point the protein becomes net positively charged and above this point carries a net negative charge. This may be the reason for the aggregation and hence change in fluorescence profile seen when heated at lower pHs. Aggregation appears to dramatically occur around the melting temperature of chymotrypsin (42 to 47˚C) for both pH 6 and 7 (Lozano et al. 1997; Wang 1999) This is also seen below where samples of chymotrypsin in TRIS buffer, pH 6 and 10 were run on SDS-PAGE to determine molecular weights of species involved when heating occurs (Figure 5.7). It is thought aggregates are seen on this gel due to the sample not being fully reduced by the SDS.

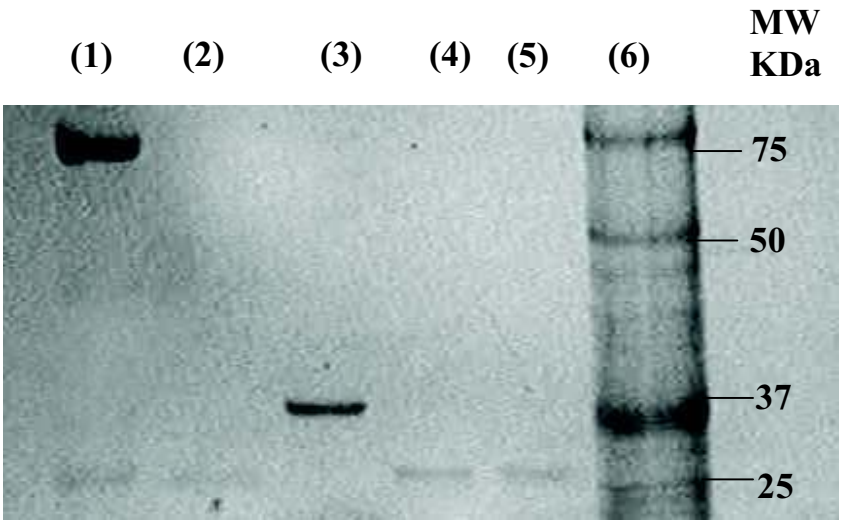

Figure 5.7. SDS-PAGE of chymotrypsin

Lanes 1 and 2 showing pH 6 and pH 10 chymotrypsin after heating. Lane 6 contains molecular weight marker. In Lane 1 it can be seen that there are two bands signifying both the native chymotrypsin (25kDa) and aggregated chymotrypsin in the trimer form (75kDa) In Lane 2 there appears to be only one band of 25kDa.

In Figure 5.7 it can be seen that in the heated protein at pH 10 (Lane 2) there is no aggregation. In Lane 1 containing heated chymotrypsin at pH 6 there appears to be two bands, the native protein and the aggregate. This indicates that the protein is aggregating at lower pHs when heated. In the paper by, Rezaei-Ghaleh et al, (2008) it is seen that at higher pHs, aggregation of α-chymotrypsin does not occur with thermal denaturation. However at lower pHs, the activity of the chymotrypsin itself stops aggregation at room temperature. As temperature increases, the activity of chymotrypsin is decreased causing aggregation. The fluorescence assay can hence detect that there is a change in the protein structure by showing an irregularity in protein fluorescence profile. However no information is given regarding the structural change. For this reason it is beneficial to use fluorescence detection in conjunction with other more detailed analysis techniques. This method can be used as a

warning of protein structural and stability changes. Due to the aggregation seen in chymotrypsin, the protein was not tested with pH and chemical denaturation, only with chemical and thermal denaturation at pH 8.

5.2.6. Thermal and chemical denaturation of RNase A

To quantify the extent of RNase A thermal denaturation, chemical denaturation was carried out simultaneously. By using multiple denaturants, parameters could be quantified that could not be calculated from one dimensional analysis of thermal denaturation. RNase A samples were chemically denatured using GdHCl in a concentration range of 0 to 6.5M. The protein was thermally heated using the BMG FLUOstar heating plates and fluorescence was monitored over a range of 27.4 to 54.7˚C (Figure 5.8).

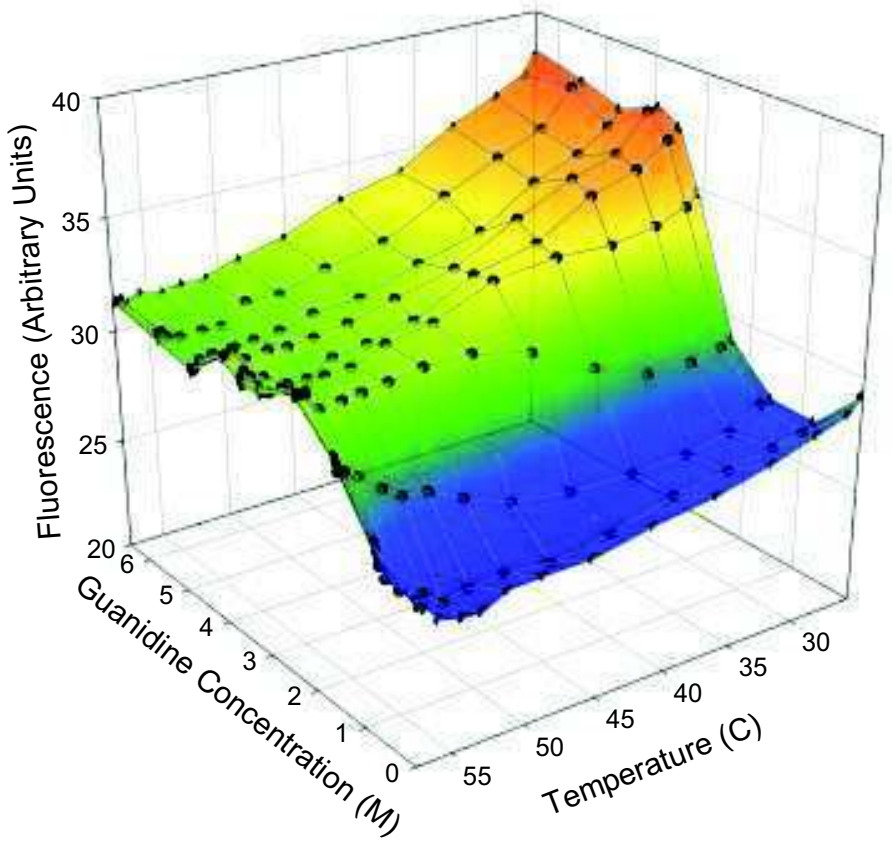

Figure 5.8. Thermal and chemical denaturation of RNase A

RNase A 1.43mg/ml (0.1mM) was tested in 50mM TRIS buffer at pH 7.4. RNase A was denatured using GdHCl (0 to 6.5M) and thermally denatured over the range 24.7 to 57.4˚C. A mesh plot is plotted with experimental data points shown (●). RNase A shows an increase in fluorescence as stability is decreased. It is seen that the protein is most stable at 0M GdHCl at 54.7˚C. A greater denaturation effect is seen at 24.7˚C than at 57.4˚C.

From this plot it can be seen that RNase A is most stable at 54.7˚C at 0M GdHCl as expected. Chemical denaturation can be seen at 24.7˚C with a 24% decrease in fluorescence. This is reduced at 57.4˚C to 14.7% indicating that the protein is more stable at this temperature due to the lesser extent of denaturation (Jones 2006). This variation is summarised in Table 5.3. It can be seen that $C_{1/2}$ decreases as temperature increases.

Although this can be calculated from individual one dimensional plots there can be inaccuracies in baseline determination as temperature increases due to the profile of denaturation becomes less defined. This may be the reason for the decrease in $C_{1/2}$ as temperature increase. From Figure 5.8 it can be seen that fluorescence is lowest at 0M guanidine at 55 ˚C. From profiles of thermal and pH denaturation it can be determined that RNase A is most stable at 55˚C at pH 9 and 10. More accurate parameters may be determined using a surface fit to account for the decrease in effect of chemical denaturant.

Temperature (C)	**24.7**	**36.1**	**40.9**	**45.2**	**57.4**
$C_{1/2}$(M)	2.97	2.32	2.32	2.10	N/A

Table 5.3. Variation of $C_{1/2}$ with temperature for RNase A

$C_{1/2}$ is seen to decrease with an increase in temperature determined from Figure 5.8. Parameters are determined from non linear least squares regression of data.

It can be seen that as temperature increases the $C_{1/2}$ decreases. This is not consistent with previous data indicating an increase in stability with temperature. It is thought this may be to do with the loss of profile as temperature increases indicating that multivariant surface analysis may offer more information on the stability of chemical and thermal denaturation of RNase A. It can be seen from this plot that denaturation occurs to a greater extent at 24.7˚C seen by the higher fluorescence signal seen at 6M GdHCl at this temperature.

5.3. Surface fitting to confer stability parameters

Although this method of testing protein denaturation using multiple parameters can measure the protein stability as a function of denaturant it is often important to quantify changes in stability (Kuhlman et al. 1998; Dimitriadis et al. 2004). Although the method described above can confer parameters in the case of chemical denaturant analysis, this can be laborious. The production of multivariant curves allows data analysis with multiple parameters by surface fitting to identify parameters available (Denisov et al. 1998). This can confer more information about the protein as parameters regarding both denaturants can be established quickly. It is known that both thermal and chemical denaturation can be fitted using least squares non linear regression to model certain parameters that indicate protein stability. Both denaturant parameters show a sigmoidal denaturation that can be fitted as described below.

5.3.1. Thermal denaturation stability calculations

As previous mentioned in Chapter 3 that the free energy of a protein **ΔG** is a linear function of the denaturant **[D]** in the following equation

$$\mathbf{\Delta G_{obs} = \Delta G_{H20} - m_G [D]} \qquad \textit{Equation 5.1}$$

where $\mathbf{\Delta G_{H20}}$ is the free energy of the protein at 0M denaturant and $\boldsymbol{m_G}$ is determined by the change in free energy with addition of denaturant. According to classical thermodynamics it is known that enthalpy of unfolding changes with temperature.

Assuming the two state model of protein is valid the denaturation enthalpy $\Delta H_{D\text{-}N(T)}$ at a specific temperature **T** is related to $\Delta H_{D\text{-}N(To)}$ at another temperature by this equation

$$\Delta H_{D\text{-}N(T)} = \Delta H_{D\text{-}N(T0)} + \Delta Cp(T - T_0) \qquad \textit{Equation 5.2}$$

Entropy is related to **Cp** by the relationship (Fersht 1999; Prabhu et al. 2005)

$$\delta S = Cp \frac{\delta T}{T} \qquad \textit{Equation 5.3}$$

This can then be translated to

$$\Delta S_{D-N(T)} = \Delta S_{D-N(T0)} + \Delta Cp \ln \frac{T}{T_0} \qquad \textit{Equation 5.4}$$

Using the equation

$$\Delta G_{D-N} = \Delta H_{D-N} - T\Delta S_{D-N} \qquad \textit{Equation 5.5}$$

Equations 5.2, 5.4 and 5.5 can be combined to form

$$\Delta G(T) = \Delta H^{o}_{To} - T\Delta S(T_o) + \Delta Cp(T - T_o + T(\ln(\frac{T_o}{T})) \qquad \textit{Equation 5.6}$$

Where **T** is the temperature, $\mathbf{T_o}$ is a reference temperature $\mathbf{\Delta H(T_o)}$ is the change in denaturation enthalpy at the reference temperature, $\mathbf{\Delta S(T_o)}$ is the change in denaturation entropy at the reference temperature, **ΔCp** is the change in heat capacity. This assumes **ΔCp** and **m** are independent of temperature and denaturation concentration (Freire 1995; Poklar 1999). *Equations 5.1 and 5.6* can be combined to form the equation

$$\mathbf{\Delta G = \Delta H(T_o) - T\Delta S(T_o) + \Delta Cp(T - T_o + T(In\frac{T_o}{T})) - m[D]}$$

Equation 5.7

Protein stability was monitored as a function of UV fluorescence. As previously described the observed fluorescence can be fitted using the below equation.

$$\boldsymbol{F}_{obs} = \frac{(\mathbf{F^\circ_N}) + e^{\left(\frac{-G}{RT}\right)}(\mathbf{F^\circ_U})}{e^{\left(\frac{-G}{RT}\right)} + 1} \qquad \textit{Equation 5.8}$$

Where $\mathbf{F_{obs}}$ is the observed fluorescence signal, $\mathbf{F^\circ_N}$ is the fluorescence signal for the native state at 0M denaturant, $\boldsymbol{F^\circ_U}$ is the fluorescence signal for the denatured state at 0M denaturant, **G** is the free energy and **R** is a gas constant. The values for F°_N and F°_U are defined as a function of both temperature and denaturant concentration. For multivariant plots these determine the baselines for the entire plot to allow non linear regression fitting.

$$\mathbf{F^o_N = a + bT + c[D]} \qquad \textit{Equation 5.9}$$

$$F^{o}_{u} = d + eT + fT^{2} + g[D] \qquad \textit{Equation 5.10}$$

a,b,c,d,e,f,g, are constants used to describe the fluorescence of baseline at denatured and native states. For F°_{U} there is seen to be some non linearity hence f*T2 is added as seen in (Kuhlman et al. 1998). Using non linear least squares regression to fit to determine eleven parameters including ΔH, ΔS, ΔCp and m as well as constants a-g. This can be compared to previously determined parameters (Navon et al. 2001; Okajima, Kawata et al. 1990; Pace et al. 1999)

5.3.2. BSA thermal and chemical denaturation

BSA was thermally and chemically denatured at 1.43mg/ml (21μM) in 60mM sodium phosphate buffer (pH 7). BSA was treated using GdHCl in a concentration range of 0 to 6.5M. The protein was thermally heated using the BMG FLUOstar heating plates and fluorescence was monitored over a range of 24.7 to 57.4˚C (Figure 5.9).

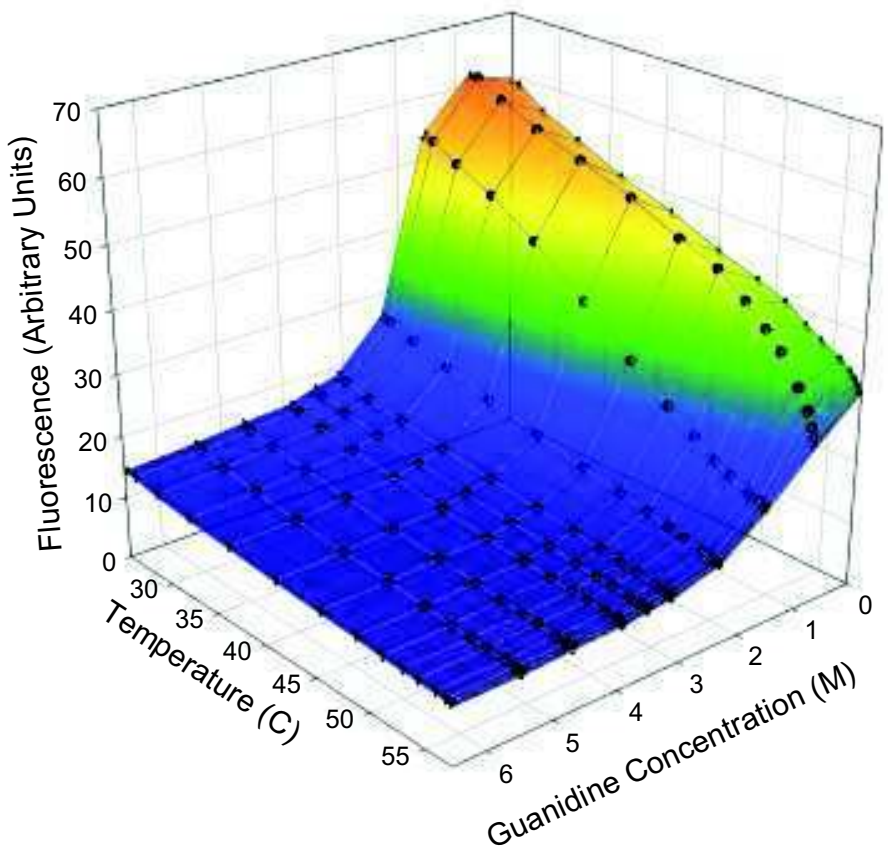

Figure 5.9. Thermal and chemical denaturation of BSA

Thermal and chemical denaturation on BSA 1.43mg/ml (0.1mM) in 60mM sodium phosphate buffer. BSA was heated using thermal heating plates and fluorescence was monitored over a range of 24.7 to 57.4˚C using BMG FLUOstar. A mesh plot is plotted with experimental data points shown (●). Protein appears most stable at 24.7˚C as judged by the high fluorescence. Chemical denaturation is complete at this temperature. As temperature increases, a sigmoidal decrease is not seen indicating an incomplete denaturation range.

It can be seen in Figure 5.9 that fluorescence decreases as a function of both chemical and thermal denaturant. BSA appears most stable at 0M GdHCl at 24.7˚C. A sigmoidal decrease is seen with an increase in GdHCl concentration at this temperature. As temperature increases, this chemical denaturation becomes linear. This may be caused by

the thermal denaturation decreasing the initial fluorescence, and hence the stability of the protein without chemical denaturant. This may be due to the effect of both parameters on the protein. It is seen that there is a 76% decrease in fluorescence at 24.7˚C with chemical denaturant. This is decreased to 65% at 54.7˚C. At 0M denaturant it is seen that there is a 48.2% decrease in fluorescence with thermal denaturation, which is decreased at 6.5M GdHCl to 36%. This is due to the initial stability of the protein being affected by the denaturant concentration. It can be seen however that the decrease in temperature is not sigmoidal indicating that the limitation of temperature range in the thermal denaturation analysis using one dimensional plots due to the difficulty of determination of upper and lower baselines for two state analyses. It is thought that surface fitting can allow determination of parameters associated with thermal denaturation by extrapolation of the upper and lower baselines.

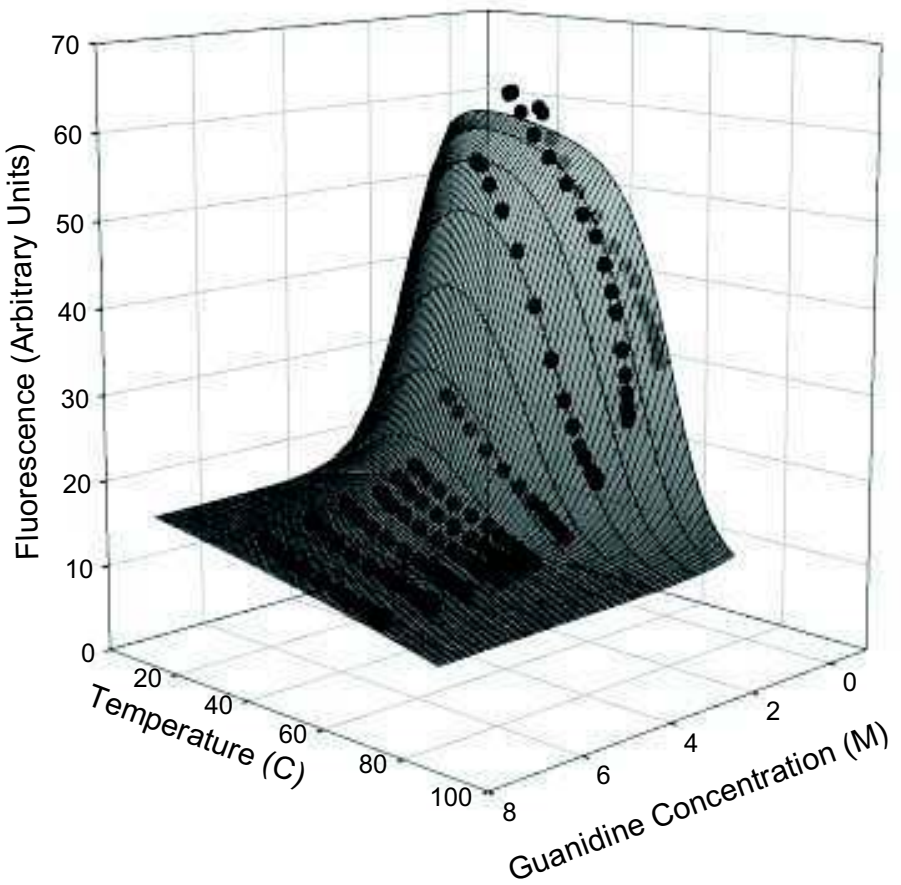

Figure 5.10. Surface fitting of multivariant BSA plot

Surface fitting of chemical and thermal denaturation data for BSA 1.43mg/ml (21μM) in 60mM sodium phosphate buffer pH 7. Experimental temperature range did not show entire thermal denaturation of protein. Fit allows extrapolation of data to high and low denaturation ranges by non linear least squares regression by determination of upper and lower baselines. Mesh depicts the fitted surface with experiment data shown (●). Mesh calculations carried out using MATLAB.

Surface fitting was carried out in MATLAB to extrapolate data to the upper and lower range of thermal denaturation allowing determination of parameters characteristic to the protein (Figure 5.10). Surface was fitted to *Equation 5.8* with baselines determined using *Equations 5.9 and 5.10* to give basic thermodynamics parameters for unfolding. Surface with overlayed experimental data can be seen in Figure 5.9. R^2 value can be defined using a parity plot with the linear fit of 0.96 (Figure 5.11). The results from the fit are listed in Table 5.4, it can be seen that BSA has a maximum stability can be calculated from the surface fitting as 2.13kcal mol^{-1} at 25˚C. The temperature at which ΔH for unfolding is equal to zero is 22˚C. Although the term fT_2 was added to the equation for the denatured baseline it was seen that the associated term (f) was small indicating a small non linear trend in the lower baseline. The term was added to allow for baseline variation, which was unknown due to the small data range used for this fitting.

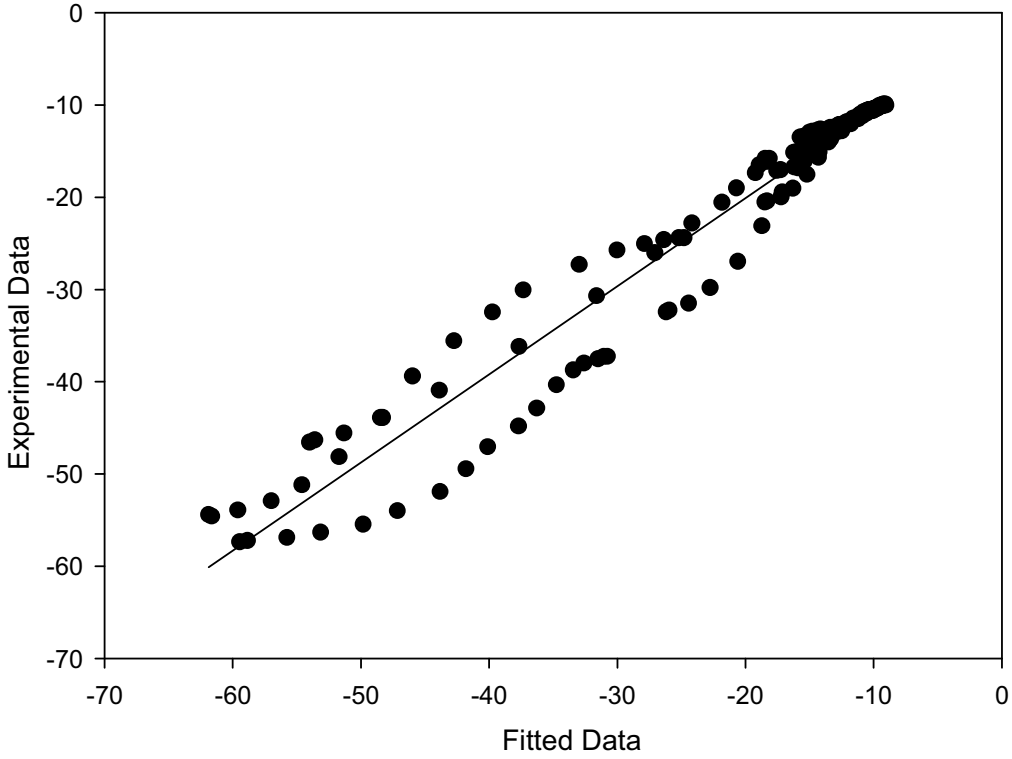

Figure 5.11. Parity plot of BSA fitted and experimental data.
Fitted and experimental data of surface fitting of BSA denaturation with temperature and guanindine plotted to determine the accuracy of fit. R^2 value of the linear fit was 0.96.

	Tm ˚C	Δ G$^{(a)}$ (kcal mol^{-1})	Δ H$^{(a)}$ (kcal mol^{-1})	T Δ S$^{(a)}$ (kcal mol^{-1} K)	m$_G$$^{(a)}$ (kcal mol^{-1} M)	Δ Cp (kcal mol^{-1}K)
Global Analysis	59.5	2.17	3.39	1.12	1.01	1.05
Experimental data		3.21			1.60	
Literature	59 [(b)]					

Table 5.4. Parameters determined from surface fitting of BSA chemical and thermal denaturation

Parameters determined using surface fitting of experimental data of thermal and chemical denaturation of BSA. Experimental data was obtained from analysis of one dimensional chemical denaturation. There is some discrepancy between experimentally obtained m_G and ΔG_{H20}, which may due to determination of upper and lower baselines.
[(a)] At 25 ˚C [(b)] (Arakawa et al. 2000)

From Table 5.4 it can be seen that Tm can be accurately calculated using the surface plotting. There is a discrepancy in calculation of m_G of the plot where by the m_G is detected as too low in comparison to experimental data. Experimental data values were calculated from one dimensional analysis. This inaccuracy of fitting may be due to the underestimation of baselines due to the small data set of thermal denaturation making upper and lower baseline determination difficult. By estimating the baselines on the given data, the extent to which denaturation occurs was inaccurately determined. Baselines of the surface fit are seen in Figure 5.12. Due to the incomplete data set, the surface fit has calculated the upper baseline of the fit as lower than the maximum value of denaturation (0M, 24.7˚C) This may account for the reduction in m_G, which is a measure of speed of denaturation hence by under estimation of the upper baseline decreases estimation of this rate. This in turn decreases the ΔG fitted.

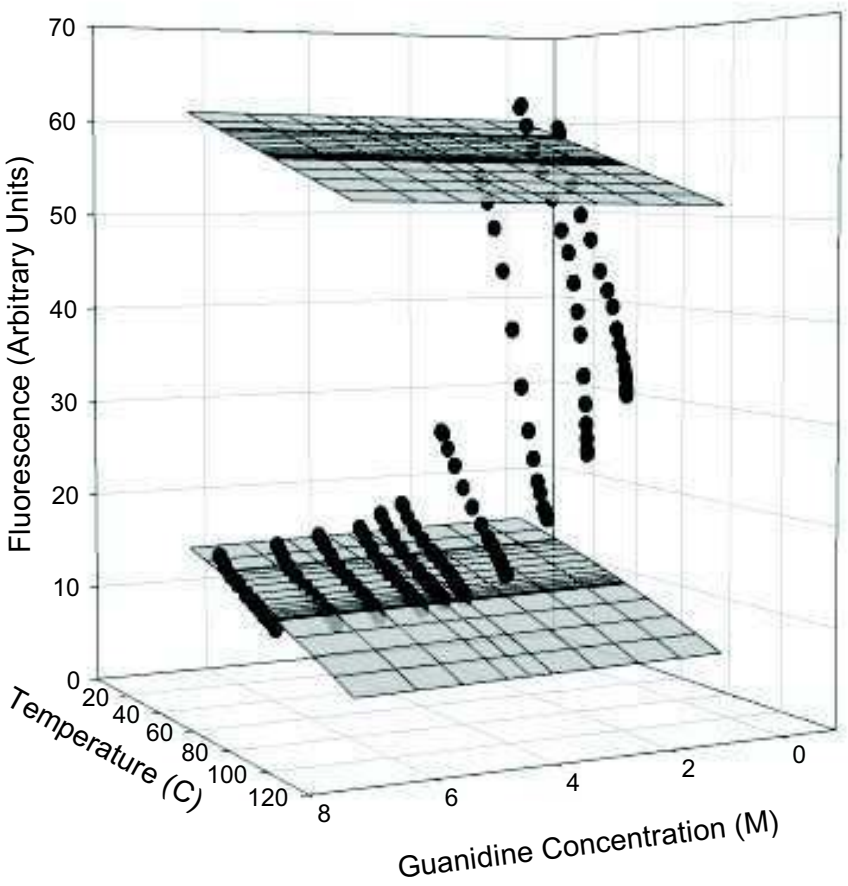

Figure 5.12. BSA thermal and chemical denaturation with experimental data and determined baselines of fitting

Baselines determined by the surface fit plotted with mesh and experimental data. Experimental data (●) with baselines plotted in grey as a function of temperature. Experimental data appears higher than the upper baseline indicating incorrect fitting.

By plotting the ΔG for each denaturant concentration with parameters determined by the surface fit Tm can also be seen (Figure 5.13). The temperature at which ΔG=0, is the melting temperature. Plots appear elliptical due to the potential of cold unfolding. It can also be seen in this plot that as denaturant increases past the $C_{1/2,}$ Δ G does not become positive. Tm is seen to reduce with denaturant concentration indicating a decrease in stability as denaturant concentration increases.

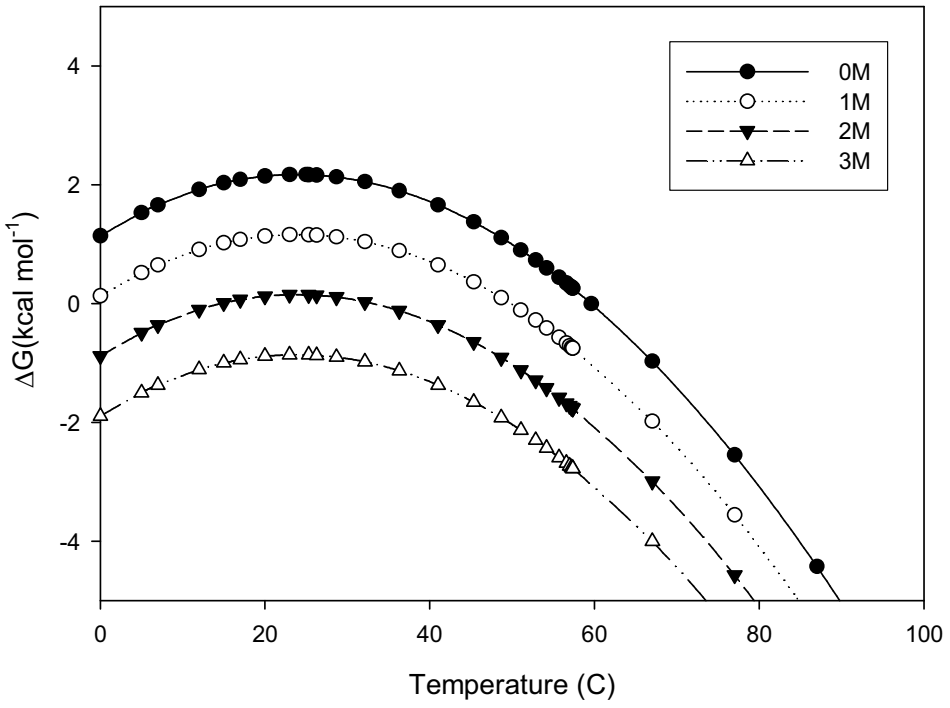

Figure 5.13. Variation of Δ G with temperature and denaturant

ΔG calculated from the fitted surface is plotted as a function of temperature. The melting temperature occurs when Δ G =0. This occurs at 59.5˚C, which is comparable to the literature value of 59˚C at 0M denaturant. Tm decrease as denaturant increases indicated by the various plots. Below the $C_{1/2}$ ΔG does not become positive. Plots appear elliptical due to the potential of cold unfolding.

It can be seen that the melting temperature decreases with denaturation concentration. Below the $C_{1/2}$ the melting temperature cannot be determined, as ΔG does not become positive. Variation of melting temperature with chemical denaturant is summarised in Table 5.5. Melting temperature decreases dramatically with denaturant concentration to a low value of 33.1˚C at 2M denaturant.

Guanidine Concentration (M)	0	1	2	3
Tm (˚C)	59.5	49.8	33.1	N/A

Table 5.5. Melting temperature variation with denaturant concentration

Melting temperature appears to decrease with denaturant concentration. Below the $C_{1/2}$ melting temperature is undeterminable.

The $C_{1/2}$ can also be plotted as a function of temperature (Figure 5.14). It can be seen that $C_{1/2}$ decreases as temperature increases. It can be seen that $C_{1/2}$ is highest at 24.7˚C. The determination of $C_{1/2}$ from the surface fitting can be compare to that determined by one dimensional analysis (Figure 5.6). However the surface fitting slightly over estimates the decrease in $C_{1/2}$ with temperature. This may once again be due to the over estimation of upper and lower baselines causing inaccuracies in parameters determination. Although the R^2 of the surface plot is 0.96 the estimation of the baseline is not included in this value as no experimental data is available in the upper and lower extremes of the data.

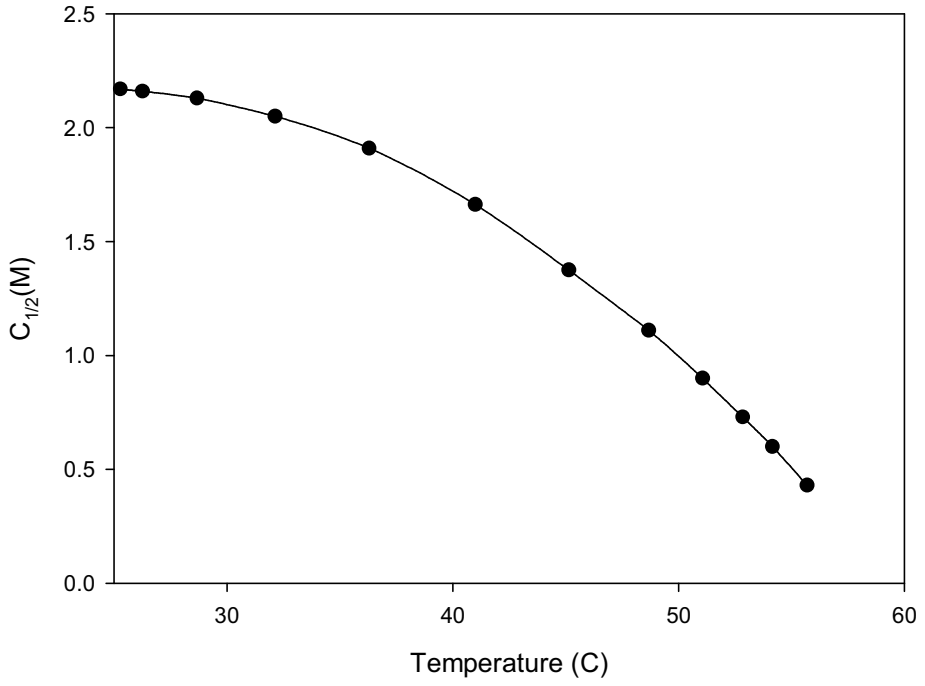

Figure 5.14. $C_{1/2}$ as a function of temperature

$C_{1/2}$ calculated from the surface fit is displayed here as a function of temperature. $C_{1/2}$ decreases exponentially as a function of temperature. As temperature increases stability of the protein decreases.

Temperature (˚C)	**25**	**32**	**36**	**41**
Global analysis ($C_{1/2}$)	2.17	2.02	1.88	1.64
1D analysis ($C_{1/2}$)	2.05	1.95	1.93	1.91

Table 5.6. Comparison of $C_{1/2}$ determined from global analysis and 2D analysis

$C_{1/2}$ values determined from both the surface fitting and 2D analysis are compared over a range of 25 to 41˚C. The surface fit can be seen to overestimate the decrease in $C_{1/2}$ with temperature in comparison to one dimensional analysis

Surface fitting of BSA allowed the determination of parameters that can be related to BSA that would otherwise not be determinable due to the limitations of range of detection. Although in this case the parameters were not accurate it is thought that with more data, surface fitting can be carried to accurately determine protein stability characteristics (Dimitriadis et al. 2004). By using one dimensional analysis the thermal denaturation parameters for this plot were undeterminable. By surface fitting the experimental data this has allowed a greater understanding of the stability of the protein with variation in denaturant due to the many parameters determinable. By using a larger data set in a wider range, the accuracy of fitting can be greatly increased. For this reason it is thought that the use of microfluidics can help to increase this range by increasing throughput and allowing a larger range of thermal denaturation. From this data it can be seen that BSA is most stable at 24.7˚C at pH 6 with no denaturant present.

5.3.3. Thermal and chemical denaturation of chymotrypsin

Thermal denaturation of chymotrypsin was carried out at 0.71mg/ml (28μM) in 60mM TRIS buffer (pH 8). Chymotrypsin was chemical denatured using GdHCl in a concentration range of 0 to 6.5M. The protein was thermally heated using the BMG FLUOstar and fluorescence plotted as a function of both of these denaturants (Figure 5.15). As chemical denaturant concentration and temperature are increased, fluorescence decreases indicating a decrease in stability. This can be assessed by surface fitting using MATLAB (Figure 5.16). It can be seen that a surface can be fitted to experimental data with a R^2 value of 0.97 (Figure 5.17). Experimental data has the limitation of range of thermal denaturation

indicating the need for surface fitting to allow data extrapolation and parameter determination.

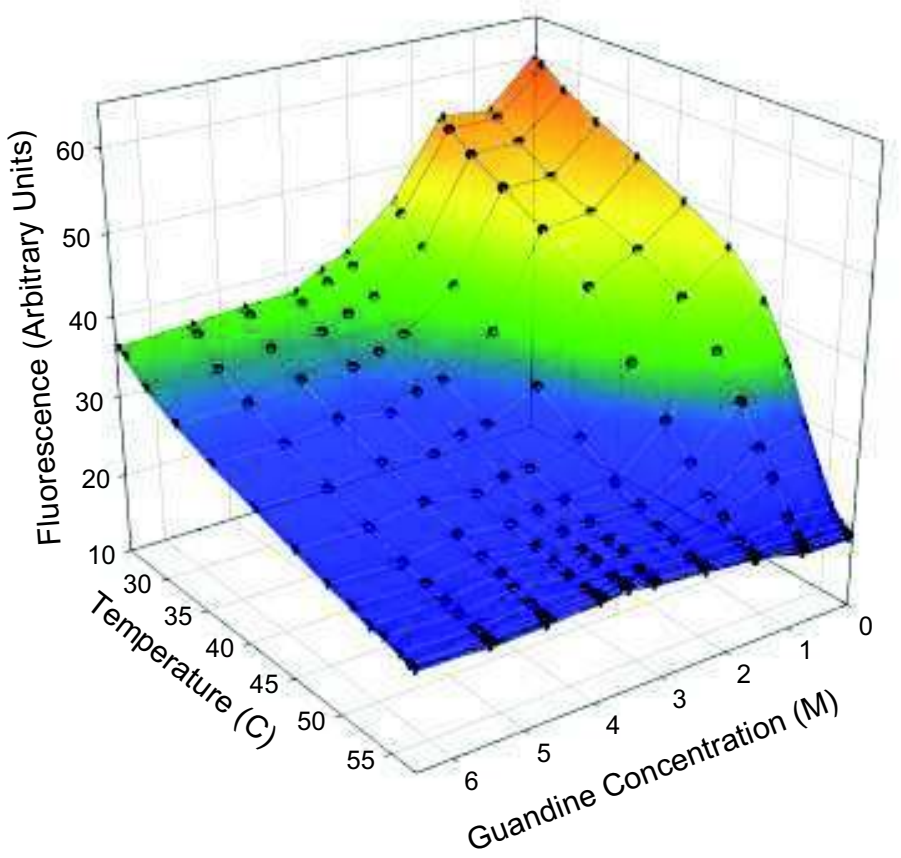

Figure 5.15. Thermal and chemical denaturation of chymotrypsin
Chemical and thermal denaturation data for chymotrypsin 0.71mg/ml (28μM) in 50mM TRIS pH 8. Protein is heated over a temperature range of 24.7 to 57.4˚C. Data is plotted as a function of both temperature(˚C) and guanidine concentration (M). Mesh plot is displayed with experimental data (●). Protein appears most stable at 24.7˚C due to the high fluorescence. Chemical denaturation is complete at this temperature. As temperature increases, a sigmoidal decrease is not seen indicating an incomplete thermal denaturation range.

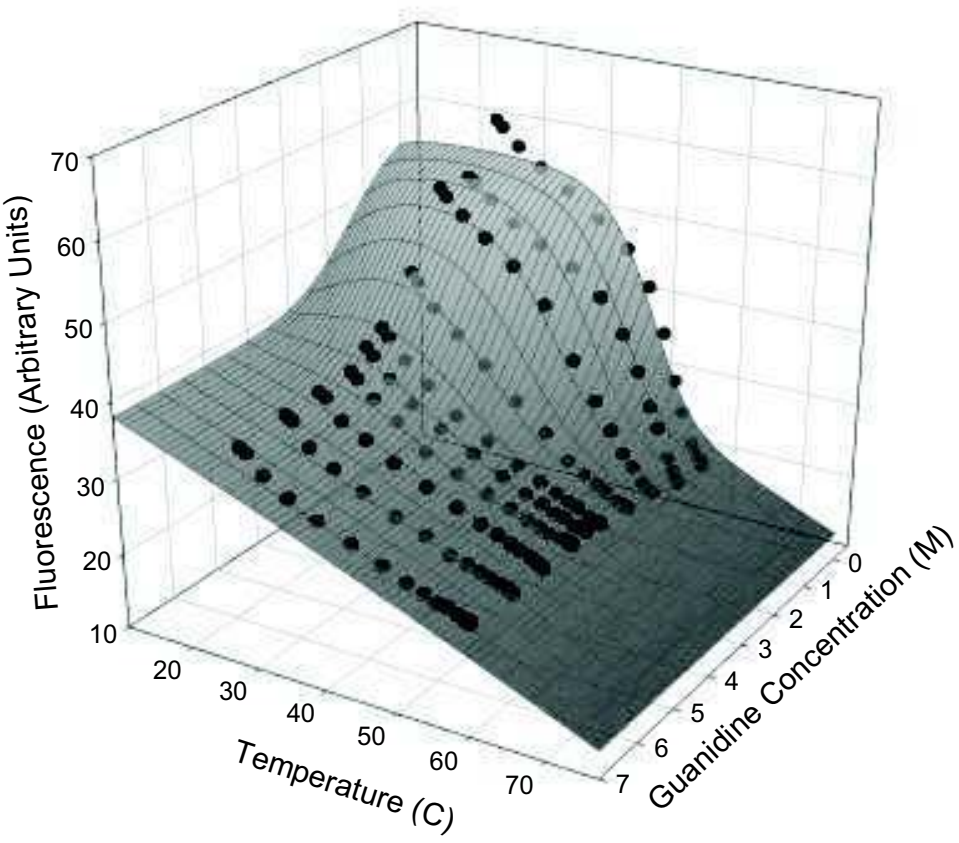

Figure 5.16. Surface fitting of multivariant analysis of chymotrypsin

Surface fitting of chemical and thermal denaturation data for chymotrypsin 0.71mg/ml (28μM) in 50mM TRIS pH 8. Fitting allows the extrapolation of data to high and low denaturation ranges by non linear least squares analysis. Protein is heated over a temperature range of 24.7 ˚C and 57.4˚C. Surface with overlayed experimental data (●). R^2 value can be defined using a parity plot with the linear fit of 0.97.

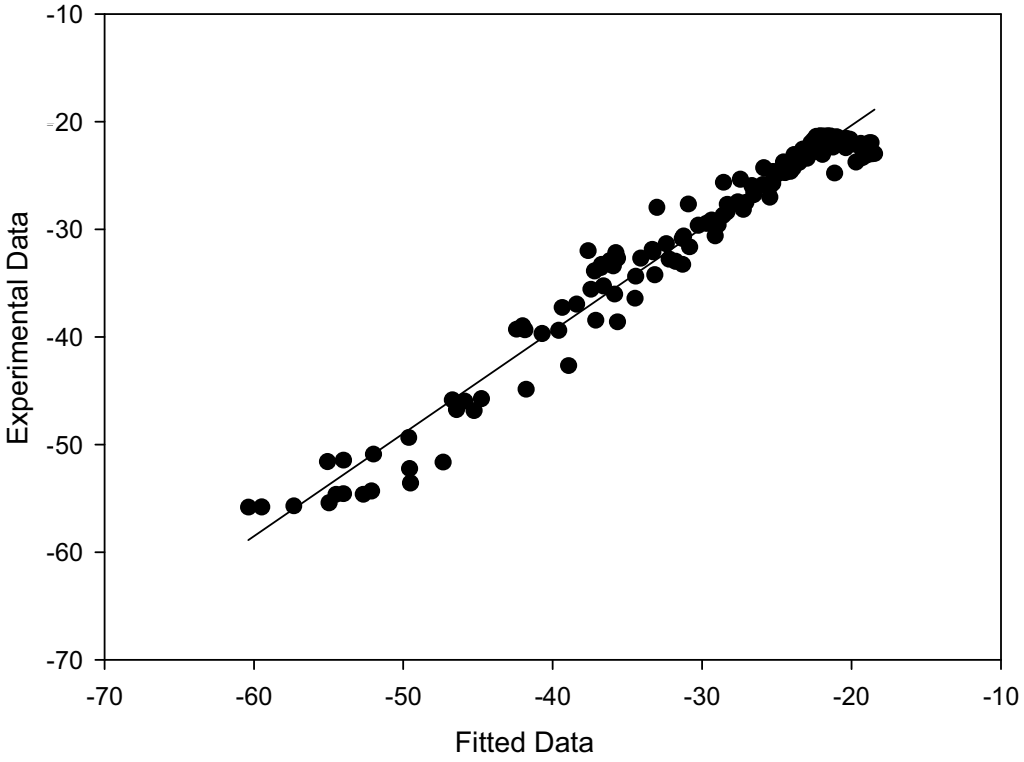

Figure 5.17. Parity plot of chymotrypsin fitted and experimental data.
Fitted and experimental data of surface fitting of chymotrypsin denaturation with temperature and guanindine plotted to determine the accuracy of fit. R^2 value of the linear fit was 0.97.

By using surface fitting, the extrapolation of upper and lower baselines is determined. This allows calculation of parameters to assess stability of the protein as a function of both denaturants. It can be seen that the upper baseline has been underestimated from the surface fit in the low chemical and thermal region. This fit can however be used to determine parameters seen in Table 5.7. The estimation of all parameters is comparable to that in literature and one dimensional analysis. It can once again be attributed to the determination of the baselines as the surface does not encompassing all the experimental data. For this reason estimations may differ slightly. Using a larger data set with a larger range of temperature denaturation can give a better estimation of baselines to confer more accurate parameters however it can be seen that by plotting this data in this way can confer information that cannot be determined using one dimensional analysis. Melting temperature trends can be determined using surface fitting (Figure 5.18).

	Tm (˚C)	Δ G$^{(a)}$ (kcal mol^{-1})	Δ H$^{(a)}$ (kcal mol^{-1})	T Δ S$^{(a)}$ (kcal mol^{-1} K)	$m_G$$^{(a)}$ (kcal mol^{-1} M)	Δ Cp (kcal mol^{-1}K)
Global Analysis	48.1	2.13	2.13	0.0034	0.86	2.43
Experimental data		2.55			1.10	
Literature	42 [(b)]					

Table 5.7. Parameters determined from surface fitting and one dimensional analysis of chymotrypsin thermal and chemical denaturation

Parameters determined using surface fitting of experimental data of thermal and chemical denaturation of chymotrypsin. Experimental data was obtained from analysis of one dimensional chemical denaturation. There is some discrepancy between experimentally and calculated m_G and ΔG_{H20}. This maybe due to the extrapolation of upper and lower baselines due to the limited experimental range of the thermal denaturation however parameter determination is possible by using this method.
[(a)] At 25˚C [(b)] (Wang 1999)

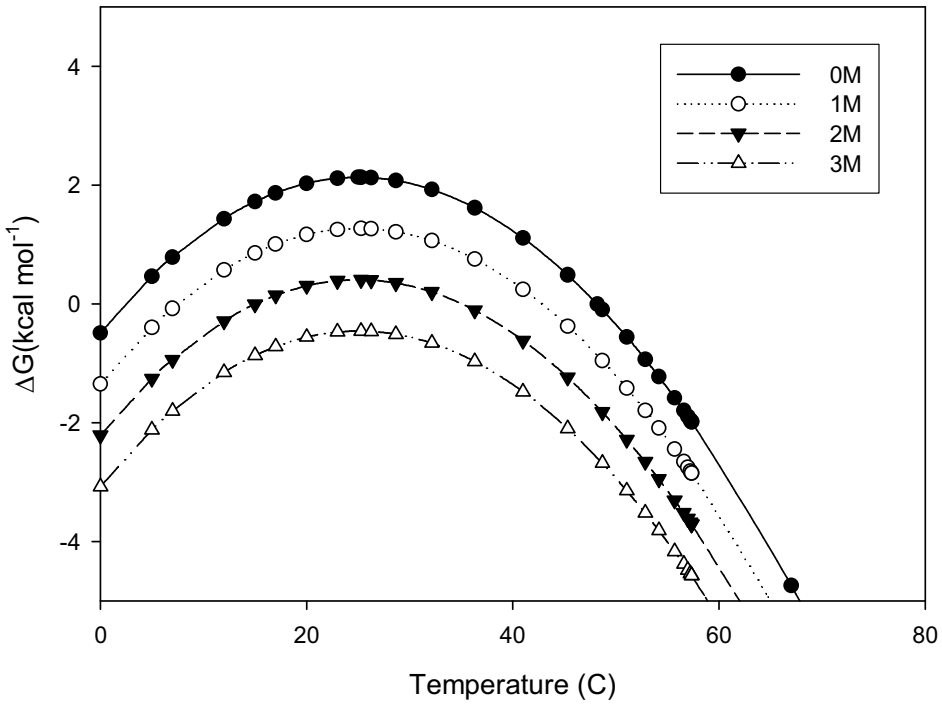

Figure 5.18. ΔG variation with temperature

ΔG of chymotrypsin calculated from the fitted surface plotted as a function of temperature. The melting temperature occurs when Δ G =0. This occurs at 48.1˚C at 0M denaturant. Tm decreases as denaturant increases indicated by the various plots. Plots appear elliptical due to the potential of cold unfolding.

Guanidine Concentration (M)	0	1	2	3
Tm (˚C)	48.1	42.9	35.0	N/A

Table 5.8. Comparison of melting temperature calculated by surface fitting.

Melting temperature of chymotrypsin appears to decrease with denaturant concentration. Below the $C_{1/2}$ melting temperature is undeterminable.

As guanidine concentration increases, melting temperature decreases as displayed in Table 5.8. Above the $C_{1/2,}$ a melting temperature can no longer be determined. From these plots, it can be seen that chymotrypsin is most stable at pH 8, 0M guanidine at 24.7˚C. Due to the thermal experimental range it can be seen that the estimation of the baselines for fitting were inaccurate. Using a larger data set, a more accurate fit can be established. Microfluidics has the potentioal allow data acquisition at in a larger range with a higher throughput while reducing reagent consumption. It is thought that surface fitting is applicable to use with multivariant plot analysis to allow rapid analysis of large amounts of data.

5.4. Conclusion

There is often the need in bioprocessing to determine the optimum working parameters for a protein or drug. Various stages of each process may require varying conditions to achieve the desired outcome. For this reason it is important to determine how the protein stability changes as a function of these parameters. By using multivariant plots, conditions in which the protein is most stable can be determined for various denaturants. These plots can provide information regarding comparison between proteins that have been treated differently. This is seen in the treatment of BSA, RNase A and chymotrypsin with pH,

thermal and chemical denaturant. The assay was found to be able to determine the optimum parameters for denaturation for each of these proteins.

To increase the throughput of data analysis of these multivariant plots surface fitting, using simple thermodynamic principals, was carried out to extrapolate data allowing parameter determination. The experimental denaturation range of the experiment was inadequate to allow analysis of the one dimensional plots due to the limitations of the thermal heating plates in the microplate reader available. Surface fitting was used to extend the profile determined from experimental data to estimate the upper and lower baselines of fit. From these surface fits, the stability parameters could be determined. It was seen that there was some inaccuracy in parameters determined when compared to traditional analysis. It was thought that this was because of the experimental data range of thermal denaturation as the data range was not complete for the upper and lower extremes of thermal denaturation. However surface fitting can be used to estimate parameters associated with stability. Inaccuracies are due to limitations in experimental data and not fitting data.

By using a larger range of thermal heating, accuracy of determination can be increased. Plate readers are not available with integrated thermal heating plates that allow a higher range of thermal denaturation leading back to large scale methods. Microfluidics offer the potential to perform thermal heating in a wider experimental range. This is due the large surface to volume ratio allowing precise thermal control while still reducing reagent consumption. Microfluidics can increase the rate of data acquisition while decreasing reagent consumption. For this reason it is thought that the combination of surface fitting and microfluidic detection could allow a whole new phase of protein stability detection and optimisation of process development.

Chapter 6:

Conclusions

6. Conclusions

Understanding the stability of a protein is paramount in the development of a bioprocess, particularly how the changes in conditions typically encountered during the sequence of operations that constitute the purification process affect a protein's stability. The demands on industry to deliver drugs faster to market and thereby maximise profits, means there is a push to increase the efficiency of this stability assessment. Ideally such measurements need to be carried out in a high throughput manner with minimal reagent consumption. This thesis offers a strategy for the implementation of a fluorescence based protein stability assay on a microfluidic platform to address this issue.

The main aims of this thesis were to determine the performance of a UV fluorescence assay and its application to monitor the stability of a protein during manufacturing, and to scale this down to microfluidics, reducing reagent consumption while increasing throughput. The assay was tested in microwells to determine adaptability of protein stability assessment as a function of various denaturants. It was found that this assay was adaptable to thermal, pH and chemical denaturation, relevant to bioprocessing. This data could be used to assess protein stability variation as a function of one or more denaturants. It was established that a protein could be treated using various process relevant conditions and stability could be assessed using chemical denaturation to determine quantitative stability parameters. In addition the sensitivity of the assay was established to be sufficient that miniaturisation to the microfluidic scale was feasible.

The use of microfluidics to scale down the measurement of protein stability was investigated. An automated optical detection system was constructed to detect UV fluorescence when protein was flowed through a capillary flow cell. This detection system had the capability of detecting changes in protein concentration and also protein denaturation. The system allowed an automated detection of signal with minimal user

interaction. Automation was carried out for mixing, pumping, detection and signal analysis. Development of this system indicated there was the potential for scale down in reagent used of 10^5 molecules from 10^{11} to 10^6 molecules. The results obtained from this system were found comparable to that of data obtained from microwell detection indicating the construction of an accurate and reproducible assay system at microfluidic scale.

Once the feasibility of using microfluidics was assessed, it was deemed important to investigate the use of this data to produce protein stability profiles. It was found that by using multiple parameters to assess protein stability, more information about the protein could be determined. This could allow comparison of processed protein quality and / or provide process understanding of the optimum conditions for stability of the product. Chemical denaturation allowed protein stability parameters in each state to be determined, allowing full assessment of protein stability. Surface fitting of protein stability was also determined for both thermal and chemical denaturation using classical thermodynamics principals. By fitting data in this way, thermal and chemical parameters could be calculated that could not be established using traditional single dimension plots. It was determined to improve the accuracy of this fitting method it would be necessary to increase the range of experimental data gathered. This task of gathering such large datasets to fully understand issues of protein stability is a task the high throughput low sample consumption of microfluidics is well suited for.

The results of this thesis show a potential role for microfluidics in detection of protein stability, particularly in area of bioprocessing where rapid acquisition of such information over a wide range of conditions with minimal material, is critical. Although microfluidics offers many advantages such as increased throughput and data collection, one must consider the potential data interpretation bottleneck this could give rise to. In

this thesis a process is described by which an assay has been scaled to microfluidics allowing the production of a large dataset. It has then been shown how this data can be rapidly analysed to provide a more complete understanding of protein stability for bioprocessing than would have previously be possible in such a period of time. There are many opportunities to take research in this area further depending on the needs of the user. These results indicate that a microfluidic platform can be used as a powerful tool for the generation of protein stability data, offering the possibility to fill a need in the bioprocessing market that is rapidly growing.

References

Ahmad F. 1983. Free energy changes in ribonuclease A denaturation. Effect of urea, guanidine hydrochloride, and lithium salts. J Biol Chem 258(18):11143-6.

Ahmad F, Bigelow CC. 1982. Estimation of the free energy of stabilization of ribonuclease A, lysozyme, alpha-lactalbumin, and myoglobin. J Biol Chem 257(21):12935-8.

Ahmad F, Taneja S, Yadav S, Haque SE. 1994. A new method for testing the functional dependence of unfolding free energy changes on denaturant concentration. J Biochem 115(2):322-7.

Ahmad N, Qasim MA. 1995. Fatty acid binding to bovine serum albumin prevents formation of intermediate during denaturation. Eur J Biochem 227(1-2):563-5.

Arakawa T, Kita Y. 2000. Protection of bovine serum albumin from aggregation by Tween 80. J Pharm Sci 89(5):646-51.

Atencia J, Beebe DJ. 2005. Controlled microfluidic interfaces. Nature 437(7059):648-55.

Aucamp JP, Cosme AM, Lye GJ, Dalby PA. 2005. High-throughput measurement of protein stability in microtiter plates. Biotechnol Bioeng 89(5):599-607.

Baaske P, Duhr, S., Braun, D.,. 2007. Melting curve analysis in a snapshot. Applied Physics Letters 91:133901-133903.

Barone G, Catanzano, F., Vecchio, P. D. 1997. Thermodynamics of protein stability: A family of ribonucleases. Pure and Applied Chem 69(11):2307-2313.

Becker H, Gartner C. 2000. Polymer microfabrication methods for microfluidic analytical applications. Electrophoresis 21(1):12-26.

Biddlecombe JG, Craig AV, Zhang H, Uddin S, Mulot S, Fish BC, Bracewell DG. 2007. Determining antibody stability: creation of solid-liquid interfacial effects within a high shear environment. Biotechnol Prog 23(5):1218-22.

Branden T. 1999. Introduction to Protein Structure: Garland Science. 410 p.

Bru R, Walde P. 1991. Product inhibition of alpha-chymotrypsin in reverse micelles. Eur J Biochem 199(1):95-103.

Burton SG, Cowan DA, Woodley JM. 2002. The search for the ideal biocatalyst. Nat Biotechnol 20(1):37-45.

Carpenter JF, Randolph TW, Jiskoot W, Crommelin DJ, Middaugh CR, Winter G, Fan YX, Kirshner S, Verthelyi D, Kozlowski S and others. 2009. Overlooking subvisible particles in therapeutic protein products: gaps that may compromise product quality. J Pharm Sci 98(4):1201-5.

Carrasquillo KG, Sanchez C, Griebenow K. 2000. Relationship between conformational stability and lyophilization-induced structural changes in chymotrypsin. Biotechnol Appl Biochem 31 (Pt 1):41-53.

Chisti Y. 2001. Hydrodynamic damage to animal cells. Crit Rev Biotechnol 21(2):67-110.

Chovan T, Guttman A. 2002. Microfabricated devices in biotechnology and biochemical processing. Trends Biotechnol 20(3):116-22.

Costin CD, Olund RK, Staggemeier BA, Torgerson AK, Synovec RE. 2003. Diffusion coefficient measurement in a microfluidic analyzer using dual-beam microscale-refractive index gradient detection. Application to on-chip molecular size determination. J Chromatogr A 1013(1-2):77-91.

De Diego T, Lozano P, Gmouh S, Vaultier M, Iborra JL. 2004. Fluorescence and CD spectroscopic analysis of the alpha-chymotrypsin stabilization by the ionic

liquid, 1-ethyl-3-methylimidazolium bis[(trifluoromethyl)sulfonyl]amide. Biotechnol Bioeng 88(7):916-24.

Denisov VP, Halle B. 1998. Thermal denaturation of ribonuclease A characterized by water 17O and 2H magnetic relaxation dispersion. Biochemistry 37(26):9595-604.

DiMasi JA, Hansen RW, Grabowski HG. 2003. The price of innovation: new estimates of drug development costs. J Health Econ 22(2):151-85.

Dimitriadis G, Drysdale A, Myers JK, Arora P, Radford SE, Oas TG, Smith DA. 2004. Microsecond folding dynamics of the F13W G29A mutant of the B domain of staphylococcal protein A by laser-induced temperature jump. Proc Natl Acad Sci U S A 101(11):3809-14.

Dittrich PS, Manz A. 2005. Single-molecule fluorescence detection in microfluidic channels--the Holy Grail in muTAS? Anal Bioanal Chem 382(8):1771-82.

Dittrich PS, Manz A. 2006. Lab-on-a-chip: microfluidics in drug discovery. Nat Rev Drug Discov 5(3):210-8.

Dobson CM. 1999. Protein misfolding, evolution and disease. Trends Biochem Sci 24(9):329-32.

Fersht A. 1999. Structure and Mechanism in Protein Science: A Guide to Enzyme Catalysis and Protein Folding: W.H.Freeman and Company.

Finke JM, Roy M, Zimm BH, Jennings PA. 2000. Aggregation events occur prior to stable intermediate formation during refolding of interleukin 1beta. Biochemistry 39(3):575-83.

Finkelstein A.V. P, O.B. 2002. Protein Physics: A Course of Lectures.

Franks F. 1993. Conformational Stability of Proteins. In: Franks F, editor. Protein Biotechnology: Isolation, Characterization, and Stabilization. Cambridge: Pafra Ltd. p 395-436.

Freire E. 1995. Thermal denaturation methods in the study of protein folding. Methods Enzymol 259:144-68.

Gelamo EL, Tabak M. 2000. Spectroscopic studies on the interaction of bovine (BSA) and human (HSA) serum albumins with ionic surfactants. Spectrochim Acta A Mol Biomol Spectrosc 56A(11):2255-71.

Ghaemmaghami S, Fitzgerald MC, Oas TG. 2000. A quantitative, high-throughput screen for protein stability. Proc Natl Acad Sci U S A 97(15):8296-301.

Giver L, Gershenson A, Freskgard PO, Arnold FH. 1998. Directed evolution of a thermostable esterase. Proc Natl Acad Sci U S A 95(22):12809-13.

Gruebele M. 2002. Protein folding: the free energy surface. Curr Opin Struct Biol 12(2):161-8.

Hadd AG, Raymond DE, Halliwell JW, Jacobson SC, Ramsey JM. 1997. Microchip device for performing enzyme assays. Anal Chem 69(17):3407-12.

Hames BD, Hooper NM. 2000. Instant notes in biochemistry. Ann Biol Clin (Paris) 58(6):767.

Hansen CL, Sommer MO, Quake SR. 2004. Systematic investigation of protein phase behavior with a microfluidic formulator. Proc Natl Acad Sci U S A 101(40):14431-6.

Hatch A, Kamholz AE, Hawkins KR, Munson MS, Schilling EA, Weigl BH, Yager P. 2001. A rapid diffusion immunoassay in a T-sensor. Nat Biotechnol 19(5):461-5.

Huikko K, Kostiainen R, Kotiaho T. 2003. Introduction to micro-analytical systems: bioanalytical and pharmaceutical applications. Eur J Pharm Sci 20(2):149-71.

Jones CL. 2006. Circular Dichroism Method for Heat Capacity Determination of Proteins. Journal of Chemical Education 83(7):1067-1070.

Kang. K. JLL, Koelling, K. 2005. High shear microfluidics and its application in rheological measurement. Experiments in Fluids 38:222-232.

Katakam M, Bell LN, Banga AK. 1995. Effect of surfactants on the physical stability of recombinant human growth hormone. J Pharm Sci 84(6):713-6.

Khandurina J, McKnight TE, Jacobson SC, Waters LC, Foote RS, Ramsey JM. 2000. Integrated system for rapid PCR-based DNA analysis in microfluidic devices. Anal Chem 72(13):2995-3000.

Kim JH, Kang CJ, Kim YS. 2005. Development of a microfabricated disposable microchip with a capillary electrophoresis and integrated three-electrode electrochemical detection. Biosens Bioelectron 20(11):2314-7.

Knapp S, Ladenstein R, Galinski EA. 1999. Extrinsic protein stabilization by the naturally occurring osmolytes beta-hydroxyectoine and betaine. Extremophiles 3(3):191-8.

Kreilgaard L, Frokjaer S, Flink JM, Randolph TW, Carpenter JF. 1998. Effects of additives on the stability of recombinant human factor XIII during freeze-drying and storage in the dried solid. Arch Biochem Biophys 360(1):121-34.

Kuhlman B, Luisi DL, Evans PA, Raleigh DP. 1998. Global analysis of the effects of temperature and denaturant on the folding and unfolding kinetics of the N-terminal domain of the protein L9. J Mol Biol 284(5):1661-70.

Lakowicz JR. 1980. Fluorescence spectroscopic investigations of the dynamic properties of proteins, membranes and nucleic acids. J Biochem Biophys Methods 2(1):91-119.

Lakowicz JR. 1999. Principles of Fluorescence Spectroscopy: Kluwer Academic/Plenum Publisers. 2314-7 p.

Lakowicz JR. 2000. On spectral relaxation in proteins. Photochem Photobiol 72(4):421-37.

Lawrence S, Lahteenmaki R. 2008. Public biotech 2007--the numbers. Nat Biotechnol 26(7):753-62.

Lee J, Tripathi A. 2007. Measurements of label free protein concentration and conformational changes using a microfluidic UV-LED method. Biotechnol Prog 23(6):1506-12.

Lengsfeld CS, Anchordoquy TJ. 2002. Shear-induced degradation of plasmid DNA. J Pharm Sci 91(7):1581-9.

Lesk AM. 2004. Introduction to Protein Science: Oxford University Press.

Lipman EA, Schuler B, Bakajin O, Eaton WA. 2003. Single-molecule measurement of protein folding kinetics. Science 301(5637):1233-5.

Lozano P, De Diego T, Iborra JL. 1997. Dynamic structure/function relationships in the alpha-chymotrypsin deactivation process by heat and pH. Eur J Biochem 248(1):80-5.

Maa YF, Hsu CC. 1996. Effect of high shear on proteins. Biotechnol Bioeng 51(4):458-65.

Maa YF, Hsu CC. 1997. Protein denaturation by combined effect of shear and air-liquid interface. Biotechnol Bioeng 54(6):503-12.

Mach H, Volkin DB, Burke CJ, Middaugh CR. 1995. Ultraviolet absorption spectroscopy. Methods Mol Biol 40:91-114.

Macounova K, Cabrera CR, Holl MR, Yager P. 2000. Generation of natural pH gradients in microfluidic channels for use in isoelectric focusing. Anal Chem 72(16):3745-51.

Macounova K, Cabrera CR, Yager P. 2001. Concentration and separation of proteins in microfluidic channels on the basis of transverse IEF. Anal Chem 73(7):1627-33.

Mannall GJ, Myers JP, Liddell J, Titchener-Hooker NJ, Dalby PA. 2008. Ultra scale-down of protein refold screening in microwells: Challenges, solutions and application. Biotechnol Bioeng.

Matulis D, Baumann CG, Bloomfield VA, Lovrien RE. 1999. 1-anilino-8-naphthalene sulfonate as a protein conformational tightening agent. Biopolymers 49(6):451-8.

Murphy RM, Kendrick BS. 2007. Protein misfolding and aggregation. Biotechnol Prog 23(3):548-52.

Navon A, Ittah V, Laity JH, Scheraga HA, Haas E, Gussakovsky EE. 2001. Local and long-range interactions in the thermal unfolding transition of bovine pancreatic ribonuclease A. Biochemistry 40(1):93-104.

Nguyen HD, Hall CK. 2002. Effect of rate of chemical or thermal renaturation on refolding and aggregation of a simple lattice protein. Biotechnol Bioeng 80(7):823-34.

Nguyen STWN-T. 2002. Fundamental and Applications of Microfluidics. London: Artech House.

NHGRI, N. H. G. R. I. Talking glossary: Protein.

Ocvirk G, Thompson, T., Harrison, J.,. 1998. Optimization of confocal epifluorescence microscopy for microchip-based miniaturized total analysis systems. Analyst 123:1429-1434.

Okajima T, Kawata Y, Hamaguchi K. 1990. Chemical modification of tryptophan residues and stability changes in proteins. Biochemistry 29(39):9168-75.

Oobatake M, Ooi T. 1993. Hydration and heat stability effects on protein unfolding. Prog Biophys Mol Biol 59(3):237-84.

Pace CN. 1986. Determination and analysis of urea and guanidine hydrochloride denaturation curves. Methods Enzymol 131:266-80.

Pace CN, Grimsley GR, Thomas ST, Makhatadze GI. 1999. Heat capacity change for ribonuclease A folding. Protein Sci 8(7):1500-4.

Pace CN, Vajdos F, Fee L, Grimsley G, Gray T. 1995. How to measure and predict the molar absorption coefficient of a protein. Protein Sci 4(11):2411-23.

Patro SY, Freund E, Chang BS. 2002. Protein formulation and fill-finish operations. Biotechnol Annu Rev 8:55-84.

Pihl J, Karlsson M, Chiu DT. 2005. Microfluidic technologies in drug discovery. Drug Discov Today 10(20):1377-83.

Poklar N, Lah, N., Oblak, M.,. 1999. Thermodynamic stability of Ribonuclease A at 25 °C in aqueous solutions of Guanidine Hydrochloride, Urea and Alkylureas. Acta Chim. Slov 46(3):315-322.

Prabhu NV, Sharp KA. 2005. Heat capacity in proteins. Annu Rev Phys Chem 56:521-48.

Rezaei-Ghaleh N, Ramshini, H., Ebrahim-Habibi, A.,. 2008. Thermal aggregation of a-chymotrypsin: Role of hydrophobic and electrostatic interactions. Biophysical Chemistry 132:23-32.

Rosenberg AS. 2006. Effects of protein aggregates: an immunologic perspective. Aaps J 8(3):E501-7.

Royer CA. 1995. Fluorescence spectroscopy. Methods Mol Biol 40:65-89.

Santoro MM, Bolen DW. 1988. Unfolding free energy changes determined by the linear extrapolation method. 1. Unfolding of phenylmethanesulfonyl alpha-chymotrypsin using different denaturants. Biochemistry 27(21):8063-8.

Schapper D, Alam MN, Szita N, Eliasson Lantz A, Gernaey KV. 2009. Application of microbioreactors in fermentation process development: a review. Anal Bioanal Chem.

Schulz S. 1996. Principles of Protein Structure: Springer. 336 p.

Sela M, Anfinsen CB. 1957. Some spectrophotometric and polarimetric experiments with ribonuclease. Biochim Biophys Acta 24(2):229-35.

Shapiro MS, Haswell SJ, Lye GJ, Bracewell DG. 2009. Design and characterization of a microfluidic packed bed system for protein breakthrough and dynamic binding capacity determination. Biotechnol Prog 25(1):277-85.

Shirley BA. 1995. Urea and guanidine hydrochloride denaturation curves. Methods Mol Biol 40:177-90.

Sohn LL, Saleh OA, Facer GR, Beavis AJ, Allan RS, Notterman DA. 2000. Capacitance cytometry: measuring biological cells one by one. Proc Natl Acad Sci U S A 97(20):10687-90.

Soulages JL. 1998. Chemical denaturation: potential impact of undetected intermediates in the free energy of unfolding and m-values obtained from a two-state assumption. Biophys J 75(1):484-92.

Tanford C. 1968. Protein denaturation. Adv Protein Chem 23:121-282.

Tanford CH, J.D. 1956. Hydrogen Ion Equilibria of Ribonuclease. J. Am. Chem 78(20):5287-5291.

Turoverov KK, Kuznetsova IM. 1998. [Intrinsic UV-fluorescence of proteins as a tool for studying their dynamics]. Tsitologiia 40(8-9):735-46.

Uchiyama K, Nakajima H, Hobo T. 2004. Detection method for microchip separations. Anal Bioanal Chem 379(3):375-82.

Vivian JT, Callis PR. 2001. Mechanisms of tryptophan fluorescence shifts in proteins. Biophys J 80(5):2093-109.

Wang W. 1999. Instability, stabilization, and formulation of liquid protein pharmaceuticals. Int J Pharm 185(2):129-88.

Wang W. 2000. Lyophilization and development of solid protein pharmaceuticals. Int J Pharm 203(1-2):1-60.

Wang W. 2005. Protein aggregation and its inhibition in biopharmaceutics. Int J Pharm 289(1-2):1-30.

Weber PC, Salemme FR. 2003. Applications of calorimetric methods to drug discovery and the study of protein interactions. Curr Opin Struct Biol 13(1):115-21.

Wingfield PT, Palmer I, Liang SM. 2001. Folding and purification of insoluble (inclusion body) proteins from Escherichia coli. Curr Protoc Protein Sci Chapter 6:Unit 6 5.

Won. C.M. MTM, McKean. R.E., Spenlehauer. G.A. 1998. Stabilizers against heat-induced aggregation of RPR 114849, an acidic fibroblast growth factor (aFGF). Int J Pharm 167(1-2):25-36.

Wu Z, Nguyen NT. 2005. Rapid mixing using two-phase hydraulic focusing in microchannels. Biomed Microdevices 7(1):13-20.

Yang ZC, Yang L, Zhang YX, Yu HF, An W. 2007. Effect of heat and pH denaturation on the structure and conformation of recombinant human hepatic stimulator substance. Protein J 26(5):303-13.